Serviço Público Federal
Ministério da Educação
Fundação Universidade Federal de Mato Grosso do Sul
Programa de Pós-Graduação em Tecnologias Ambientais

Tiago Souza Mattos

Improving urban flood resilience

Campo Grande, MS
Janeiro, 2021

Fundação Universidade Federal de Mato Grosso do Sul
Faculdade de Engenharias, Arquitetura e Urbanismo e Geografia
Programa de Pós Graduação em Tecnologias Ambientais

Tiago Souza Mattos

IMPROVING URBAN FLOOD RESILIENCE

Tese apresentada para obtenção do grau de Doutor no Programa de Pós-Graduação em Tecnologias Ambientais da Fundação Universidade Federal de Mato Grosso do Sul, área de concentração: *Saneamento Ambiental e Recursos Hídricos*.

Orientador: Prof. Dr. Paulo Tarso Sanches de Oliveira

Aprovada em: 08/12/2020

Banca Examinadora

Prof. Dr. Paulo Tarso Sanches de Oliveira
Presidente

Prof. Dr. Fernando Mainardi Fan
(IPH/UFPR)

Prof. Dr. Murilo Cesar Lucas
(UTFPR)

Prof. Dr. Eduardo Mario Mendiondo
(EESC/USP)

Prof. Dr. José Góes Vasconcelos Neto
(Auburn University, USA)

VERSÃO CORRIGIDA
Campo Grande, MS
Janeiro, 2021

DEDICATION

To my father Manoel da Conceição P. de Mattos (*in memoriam*), who through his character and example of life, taught me the value of honesty, perseverance and hard work in a man's life.

ACKNOWLEDGMENTS

First, I would like to acknowledge GOD to be present in my life, giving me health, wisdom and strength to conclude one more step in my career. My parents, Manoel and Edineide, always present at all times in my life. If I got to where I am today, it is because you have always encouraged me to fight for my dreams, and have given me the conditions to achieve my goals. Thanks!

I am grateful to my advisor, Prof. Dr. Paulo Tarso S. Oliveira, for trusting me and inviting me to do my doctorate, for correcting and praising me when I needed it. I want you to know that you are a great advisor, facilitator, leader and friend. I also thank to Prof. Dr. Dulce Buchala B. Rodrigues, for the advice, incredible classes and long conversations that helped me a lot during my doctorate. I also thank for the Prof. Dr Teodorico Alves Sobrinho, for allowing me to develop my doctoral work in contact with a great group (Laboratório HEROS), that made my workdays much more enjoyable.

I would like to extend my gratitude to my dear friend Prof. Dr. Jhonatan Barbosa da Silva, for sharing an apartment with me during my time in Campo Grande. The coexistence was very good. You are a great engineer and scientist. I wish you much happiness and success.

I am also deeply grateful to the researchers Prof. Dr. Stefan Hagemann, Prof. Dr. Grey S. Nearing, and Prof. Dr. Tirthankar Roy for advice and recommendations. For the Prof. Dr. Jose G. Vasconcelos and Prof. Dr. Murilo C. Lucas for all advices, editions of the papers, and friendship.

This doctoral thesis could not have been done without the generous assistance of engineers Leonardo Bruno and Reinaldo Ossuna, and computer science graduate Leonardo L. Crivellaro who shared their knowledge and expertise in key parts of my doctorate. In addition, I would also like to thank the graduate students at the HEROS (Glauber A. Carvalho, Rodrigo Bahia, Pedro Zamboni, Diego Zanoni) for helping me several times in the field work. The undergraduate student Nilo Diniz for help with climate change data. I also thank to the colleagues, professors, and technical staff of the UFMS, for receiving me so friendly, helping me in every moment.

This doctoral thesis was supported by grants from the Ministry of Science, Technology, Innovation and Communication – MCTIC and National Council for Scientific and Technological Development – CNPq (grants 441289/2017-7 and 306830/2017-5) and Coordenação de Aperfeiçoamento de Pessoal de Nível Superior - Brasil - CAPES (Finance Code 001 and Capes PrInt).

“Now all has been heard; here is the conclusion of the matter: Fear God and keep his commandments, for this is the duty of all mankind.” (*Ecclesiastes 12:13*)

RESUMO

Inundações em áreas urbanas devido a chuvas intensas tem causado perdas materiais, econômicas, ambientais e humanas em vários lugares do mundo. A combinação das mudanças climáticas com o aumento da urbanização traz grandes desafios para o planejamento e gestão das cidades, visto que são considerados os principais responsáveis pelo aumento do risco de inundações nas áreas urbanas. Portanto, é necessário melhorar a resiliência de áreas urbanas a eventos de inundação. Assim, o principal objetivo do estudo apresentado nesta tese de doutorado foi avaliar e desenvolver técnicas para melhorar a resiliências das áreas urbanas a eventos de inundação. Para isso, no capítulo 1, avaliou-se como a utilização de práticas de desenvolvimento urbano de baixo impacto (LIDs) afetam a resiliência do sistema de drenagem de águas pluviais considerando cenários de mudança climática. A resiliência do Sistema de drenagem foi quantificada por meio de um índice de resiliência. Os resultados indicam que o aumento pico de vazão do escoamento pode ser mitigado de forma satisfatória usando combinações de diferentes tipos de LIDs. Em geral, as combinações de LIDs apresentaram redução do pico de escoamento superior a 20%, e a melhor combinação apresentou redução de até 46%. Os dados de radar meteorológico são úteis em modelos chuva-vazão usados em estudos de inundações urbanas. Assim, no capítulo 2, desenvolvemos uma nova abordagem de correção de viés com base no método de correspondência utilizando funções de distribuição Acumulada (CDF) que se concentra em corrigir as estimativas de precipitação do radar considerando eventos diários, horários e sub horários. Os resultados mostraram que o índice de eficiência de Nash-Sutcliffe (NSE) aumentou de 0,11 para 0,63 e o erro médio absoluto (MAE) diminuiu de 11,66 para 6.97 mm após a aplicação do método. Esses resultados indicam que houve uma melhora significativa nas estimativas de precipitação do radar. Além disso, no capítulo 3, um Sistema de Suporte a Decisão acoplado a um aplicativo é usado para desenvolver um sistema de alerta de inundações. O aplicativo foi desenvolvido para permitir a visualização de manchas de inundação, o nível d'água em seções específicas e enviar mensagens de alerta à população. Os resultados encontrados nesta tese de doutorado são informações muito úteis para a tomada de decisão tanto do poder público quanto da população de forma a aumentar a resiliências de áreas urbanas a eventos de inundação.

Palavras-chave: LIDs, correção de viés, CDF, inundações urbanas, alerta de Inundação, radar meteorológico

ABSTRACT

Flooding in urban areas due to extreme stormwater in short time has caused material, economic, environmental and human losses in several places worldwide. The combination of climate change and increasing urbanization brings great challenges to planning and managing cities, because are considered the main responsible for increasing the severe flooding risks in urban areas. Therefore, it is necessary improving the urban flood resilience. Then, the main objective of the study presented in this doctoral thesis was to evaluate and develop techniques to improving the urban flood resilience. To achieve that, in the chapter 1, it was evaluated how Low Impact Development (LID) practices affect the resilience of stormwater drainage system under climate change scenarios. The resilience of the drainage system was quantified by means of a resilience index. The results indicate that the increased runoff peak can be mitigated satisfactory by using combined LID practices. In general, LID combinations showed reduction in runoff peak higher than 20%, and the best LID combination presented reduction up to 46%. The Weather radar data is useful for rainfall-runoff models used in urban flooding studies. Then, In the chapter 2, we developed a new bias correction approach based on Cumulative Distribution Function (CDF) matching method that focuses to correct biased radar rainfall estimates on daily, hour and sub-hour basis. The results showed that Nash-Sutcliffe Efficiency (NSE) index increased from 0.11 to 0.63 and Mean Absolute Error (*MAE*) decreased from 11.66 (biased data) to 6.97 mm (unbiased data) for all rainfall events. These results indicate that there was a significant improvement on the radar rainfall estimates. Additionally, in the chapter 3, a Decision Support System coupled with a mobile application is used to develop a flood alert system. The application based on Progressive Web Application was developed to support the visualization of flood status and to deliver early warning messages to population. The results found in this doctoral thesis is an essential information to decision making by the public authorities as well as to population for improving the urban flood resilience.

Keywords: LIDs, Bias correction, CDF Matching, Quantile Mapping, Urban Flooding, Flood alert

LIST OF FIGURES

LIST OF TABLES

TABLE OF CONTENTS

GENERAL INTRODUCTION

Floods are recognized among the most destructive natural hazards (WMO, 2011), and have created serious threats to human life and social and economic activities (Gain et al., 2015). The combination of climate change and increasing urbanization brings great challenges to planning and managing cities, because they are considered the main responsible for increasing the severe flooding risk over urban areas (Miller; Hutchins, 2017; Zhang et al., 2018).

The increasing in urbanization reduce the natural vegetation cover and increase the amount of impervious areas, reducing the rainfall infiltration capacity and causing increased surface runoff. These runoff amounts increase urban flood risks and lead to economic losses, and human deaths (Hammond et al., 2015; AON, 2019). In the Brazil, some metropolises have experienced unprecedented heavy rainfall events, leading to deadly floods. The city of Sao Paulo (~12.3 million people) received about 114 mm of rainfall on 10 February 2020. It was the second-highest volume in 24 hours (on February) in the last 77 years of weather records. The city of Belo Horizonte (~2.5 million people) received the largest 24-hour rainfall (171.8 mm) in 110 years of rainfall records on January 2020. Since floods represent a significant role in the number of natural disasters globally (Freer et al., 2011), a great effort has been made to assess and predict flood events and their negative impacts.

Traditionally, designing flood control measures starting with hydrological studies, followed by the definition of a design storm, the assessment of its consequent river flow responses, the design and implementation of a hydraulic system cable to comport the design flow (Plate, 2002). However, there is always the residual risk of a hydraulic failure due an event greater than the considered storm (Bertilsson et al., 2019). In addition, current stormwater drainage systems have been designed based on stationary climate data, without considering the changes in the nature of rainfall over time (Milly et al., 2008; Pour et al., 2020).

This scenario indicates the need of improving the urban flood resilience. In general, resilience may be defined as “The ability of an individual, community, city or nation to resist, absorb or recover from a shock (such as an extreme flood), and/or successfully adapt to adversity or a change in conditions (such as climate change or an economic downturn) in a timely and efficient manner” (Sayers et al., 2013).

Urban planners and engineers are now assessing practices which have a potential of mitigation of increased flood risk arising from climate change. Increasing focus has been given on increasing water infiltration using Low Impact Development (LID) practices. Thus, in the

first chapter we evaluate how LID practices affect the resilience of stormwater drainage system under climate change scenarios.

One of the most valuable tools for planning on flood mitigation is rainfall-runoff models. The output of these models can be used to develop flood hazard maps and also flood warning systems for saving lives and property. Despite the many usefulness of hydrological models, accurate models demand for high resolution rainfall data as input for urban hydrology applications (Müller; Haberlandt, 2018). In this context, weather radar provides more accurate the spatial variability of rainfall than conventional rain gauges, and consequently can improve rainfall-runoff model outputs (Abon et al., 2016; Gurung, 2017).

Unfortunately, radar rainfall estimates are still prone to large uncertainties due to random and systematic errors, thereby limiting their hydrological application (Berne; Krajewski, 2013). The uncertainties can be reduced by use of radar bias adjustment based on rain gauge network. Thus, in the **second chapter** we propose a new method for correcting biased radar rainfall against ground-based rain gauge data in daily, hourly, and sub-hourly timescale.

Climate change threats, increasing urbanization, and a poor stormwater drainage network increase the risk of flood disaster if no risk management is done. To prevent the death of people and/or property damage due to floods, it is important to warn people in advance as possible. Hence, in the **third chapter** a Decision Support System coupled with a mobile application is used to develop a flood alert system across the Prosa basin (Brazil) to send early flood warning messages to population.

References

ABON, C. C.; KNEIS, D.; CRISOLOGO, I.; BRONSTERT, A.; DAVID, C. P. C.; HEISTERMANN, M. Evaluating the potential of radar-based rainfall estimates for streamflow and flood simulations in the Philippines. **Geomatics, Natural Hazards and Risk,** v. 7, n. 4, p. 1390-1405, https://doi.org/10.1080/19475705.2015.1058862, 2016.

AON. **Global Catastrophe Recap: March 2019**. AON Empower Results. 2019

BERNE, A.; KRAJEWSKI, W. F. Radar for hydrology: Unfulfilled promise or unrecognized potential? **Advances in Water Resources,** v. 51, p. 357-366, https://doi.org/10.1016/j.advwatres.2012.05.005, 2013.

BERTILSSON, L.; WIKLUND, K.; DE MOURA TEBALDI, I.; REZENDE, O. M.; VERÓL, A. P.; MIGUEZ, M. G. Urban flood resilience – A multi-criteria index to integrate flood resilience into urban planning. **Journal of Hydrology,** v. 573, p. 970-982, https://doi.org/10.1016/j.jhydrol.2018.06.052, 2019.

FREER, J.; BEVEN, K. J.; NEAL, J.; SCHUMANN, G.; HALL, J.; BATES, P. Flood risk and uncertainty. In: (Ed.). **Risk and Uncertainty Assessment for Natural Hazards**: Cambridge University Press, 2011. p.190-233.

GAIN, A. K.; MOJTAHED, V.; BISCARO, C.; BALBI, S.; GIUPPONI, C. An integrated approach of flood risk assessment in the eastern part of Dhaka City. **Natural Hazards,** v. 79, n. 3, p. 1499-1530, 10.1007/s11069-015-1911-7, 2015.

GURUNG, P. Integration of gauge and radar rainfall to enable best simulation of hydrological parameters. **Hydrological Sciences Journal,** v. 62, n. 1, p. 114-123, https://doi.org/10.1080/02626667.2015.1117087, 2017.

HAMMOND, M. J.; CHEN, A. S.; DJORDJEVIĆ, S.; BUTLER, D.; MARK, O. Urban flood impact assessment: A state-of-the-art review. **Urban Water Journal,** v. 12, n. 1, p. 14-29, https://doi.org/10.1080/1573062X.2013.857421, 2015.

MILLER, J. D.; HUTCHINS, M. The impacts of urbanisation and climate change on urban flooding and urban water quality: A review of the evidence concerning the United Kingdom. **Journal of Hydrology: Regional Studies,** v. 12, p. 345-362, https://doi.org/10.1016/j.ejrh.2017.06.006, 2017.

MILLY, P. C. D.; BETANCOURT, J.; FALKENMARK, M.; HIRSCH, R. M.; KUNDZEWICZ, Z. W.; LETTENMAIER, D. P.; STOUFFER, R. J. Stationarity Is Dead: Whither Water Management? **Science,** v. 319, n. 5863, p. 573, https://doi.org/10.1126/science.1151915, 2008.

MÜLLER, H.; HABERLANDT, U. Temporal rainfall disaggregation using a multiplicative cascade model for spatial application in urban hydrology. **Journal of Hydrology,** v. 556, p. 847-864, https://doi.org/10.1016/j.jhydrol.2016.01.031, 2018.

PLATE, E. J. Flood risk and flood management. **Journal of Hydrology,** v. 267, n. 1, p. 2-11, https://doi.org/10.1016/S0022-1694(02)00135-X, 2002.

POUR, S. H.; WAHAB, A. K. A.; SHAHID, S.; ASADUZZAMAN, M.; DEWAN, A. Low impact development techniques to mitigate the impacts of climate-change-induced urban floods: Current trends, issues and challenges. **Sustainable Cities and Society,** v. 62, p. 102373, https://doi.org/10.1016/j.scs.2020.102373, 2020.

SAYERS, P.; YUANYUAN, L.; GALLOWAY, G.; PENNING-ROWSELL, E.; FUXIN, S.; KANG, W.; YIWEI, C.; QUESNE, T. L. **Flood Risk Management: A Strategic Approach**. Asian Development Bank, GIWP, UNESCO and WWF-UK, 2013. ISBN 978-92-3-001159-8.

WMO. **Manual on Flood Forecasting and Warning**. World Meteorological Organization, 2011. ISBN 9789263110725.

ZHANG, W.; VILLARINI, G.; VECCHI, G. A.; SMITH, J. A. Urbanization exacerbated the rainfall and flooding caused by hurricane Harvey in Houston. **Nature,** v. 563, n. 7731, p. 384-388, https://doi.org/10.1038/s41586-018-0676-z, 2018.

OBJECTIVES

General Objective

The main objective of the study presented in this doctoral thesis was to evaluate and develop techniques to improving the urban flood resilience.

Specific objectives

i. To investigate the effect of LIDs as source control solutions at the catchment scale (a few tens of kilometers) to mitigate runoff by implementing a rainfall-runoff simulation for an urban catchment under future rainfall scenario;

ii. To develop a method for correcting biased radar rainfall against ground-based rain gauge data in daily, hourly, and sub-hourly timescale;

iii. To develop a flood alert system in the Prosa basin, and disseminate its warning messages by means of an application for mobile devices.

CHAPTER 1

Improving urban flood resilience under climate change scenarios in a tropical watershed using low impact development practices

Mattos, T. S., Oliveira, P. T. S., Bruno, L. S., Oliveira, N. D., Vasconcelos, J. G., Lucas, M. C. Improving urban flood resilience under climate change scenarios in a tropical watershed using low impact development practices. *Journal of Hydrologic Engineering.* Under Review. (Impact factor, 2020: 1.560; Qualis CAPES: A2)

Abstract

In this paper we present how Low Impact Development (LID) practices affect the resilience of stormwater drainage system under climate change scenarios. We calibrated and evaluated a rainfall-runoff model in a tropical watershed located in Midwestern Brazil. To achieve future climate change scenarios up to 2095, we used an ensemble of 17 General Circulation Models outputs forced by Representative Concentration Pathway (RCP 4.5 and RCP 8.5). Then we evaluated the LID efficiency on the runoff peak reduction and the resilience of stormwater drainage by means of a resilience index. Overall, LID combinations showed a reduction in runoff peak higher than 20%, and the best LID combination presented reduction up to 46%. This represent a significant improvement in the resilience to flooding in the study area. Therefore, our findings contribute to the increase in widespread adoption of LID and can encourage decisionmakers to provide such practices for urban flood management.

Keywords: infiltration trench; permeable pavements; PCSWMM; rain water harvesting; rainfall-runoff modeling; sustainable drainage systems.

1 Introduction

Unplanned populational growth and climate change are mainly responsible for increasing the severe flooding risks in urban areas (Miller; Hutchins, 2017; Zhang et al., 2018). This occurs because impervious surfaces change the hydrological fluxes of (peri) urban watersheds, leading to a decline in evapotranspiration, infiltration and groundwater recharge, and consequently an increase in stormwater runoff (Braud et al., 2013; Miller et al., 2014; Muñoz et al., 2018). Further, in the last three decades the number of rainfall record-breaking events has significantly increased on average globally due to warming of air, and has generated unprecedented surface runoff amounts (Lehmann et al., 2015; Huang et al., 2019). These extreme runoff amounts increase urban flood risks and lead to economic losses, and human deaths (Hammond et al., 2015; AON, 2019). Globally, mainly in low-latitude regions, the future population at risk of flood will increase due to warmer climate (Hirabayashi et al., 2013). For instance, considering a future anthropogenic warming of air (1.5 ◦C), assuming the current vulnerability levels and in the absence of future adaptation, it is estimated that human deaths from flooding could rise by 70–83% and direct flood damage by 160–240% (Dottori et al., 2018).

Stormwater drainage systems have been based on the goal of conveying a runoff associated with a stormwater event of a predetermined return period to prevent urban flooding. Storm inlets allow for the runoff collection its quick discharge to streams through gutters and closed pipe networks. Stormwater drainage system design are often based on rainfall records. As a limitation, this procedure assumes the hypotheses of stationarity, which does not account for climate change (Milly et al., 2008). This scenario indicates the need of improving the urban flood resilience.

The term resilience was at first introduced in the field of ecology by Holling (1973) and has since found popularity in the fields of social science, psychology and disaster management. In relation of flood risk, resilience may be defined as “The ability of an individual, community, city or nation to resist, absorb or recover from a shock (such as an extreme flood), and/or successfully adapt to adversity or a change in conditions (such as climate change or an economic downturn) in a timely and efficient manner” (Sayers et al., 2013). Several quantitative methods have been proposed to assessing resilience (see Owotoki et al. (2006), Mugume et al. (2015), Golz et al. (2015), Birgani and Yazdandoost (2016), Pregnolato et al. (2016), Miguez and Veról (2017), Bertilsson et al. (2019)).

To achieve increased urban resilience due to urbanization and climate change, it has become crucial to reduce the risk of urban flood (Sorensen; Emilsson, 2019). In this context, many solutions have been proposed in the last three decades, such as expanding the drainage system network and storage. Unfortunately, this approach is deemed unsustainable, high costly (Qiu et al., 2019), and increases runoff volume downstream (Abera et al., 2018). On the other hand, Low Impact Development (LID) practices has emerged as alternative sustainable drainage system to decrease runoff (i.e. volume attenuation and peak reduction) in urban environmental (Page et al., 2015; Huang et al., 2016; Zhu et al., 2019).

The LID practices facilitate in-site infiltration, evapotranspiration, water storage, and therefore contributes to the increase in urban resiliency which cannot be fully achieved by traditional stormwater management systems (Sohn et al., 2019). The LID practices, which include permeable pavement, bio-retention, rain gardens, green roofs, swales, rain barrels, and infiltration trench (Rossman, 2015), can mimic natural ecological and hydrological functions in a watershed, as well as improve of stormwater quality (Liu et al., 2015; Wang et al., 2018).

Hydrological benefits of LID systems have been well-documented in previous studies (Dietz, 2007; Ahiablame et al., 2013; Palla; Gnecco, 2015; Wu et al., 2018; Qiu et al., 2019). Ahiablame et al. (2013) evaluated several application levels of barrel/cistern and permeable pavements, and confirm that resulted in 2–12% reduction in runoff and pollutant loads for two watersheds. According to Palla and Gnecco (2015), the combination of green roofs and permeable pavements decreased runoff and flow peak by 23% and 45%, respectively, at the urban catchment scale. Wu et al. (2018) reported that the maximum inundation depth was reduced by 3–29% under eight scenarios of LID combinations with green roofs and/or permeable pavement. Qiu et al. (2019) conducted a simulation and found that the combination of rain garden, green roof, and permeable pavement can reduce runoff volume up to 51% and peak discharge up to 53% in the entire catchment. Damodaram et al. (2010) reported peak flow reduction of about 20–40% using permeable pavement and rainwater harvesting. Khastagir and Jayasuriya (2010) found runoff reduction from 58 to 82% using rainwater harvesting, for tank size from 1 to 5 kL. Goncalves et al. (2018) conducted simulations with infiltration trench and found runoff volume and peak flow reduction of about 55.9% and 53.4%, respectively.

The hydrological impact of climate change on urban environment has been carried out only recently (Hailegeorgis; Alfredsen, 2017; Mishra et al., 2018; Gesualdo et al., 2019; Vemula et al., 2019; Xiong et al., 2019). However, the effects of LID practices in response to the impacts of climate change at catchment scale are still poorly addressed (Sohn et al., 2019). Hence, there is still a need to investigate the effect of LID under future climate change on urban

runoff volume and peak. Here, our goals are to: 1) investigate the effect of LIDs as source control solutions at the catchment scale by implementing a rainfall-runoff simulation for an urban catchment under climate change scenarios (RCP 4.5 and RCP 8.5); 2) evaluate the impact of the rainfall intensity on the streamflow regime; and 3) quantifying stormwater drainage system resilience using a resilience index.

2 Material and Methods

2.1 Study area

This study was conducted in the Prosa Basin (PB), located in the municipality of Campo Grande, MS, Brazil (Figure 1). This basin covers an area of ≃32 km^2, with slope steepness of ranging from 3.8 to 8.0%. The main rivers in the basin are Prosa, Soter, Desbarrancado, Joaquim Portugues, Revellion and Vendas River (PDDU, 2008).

The annual mean ± standard deviation rainfall (between 1992 and 2016) considering the hydrological year (from October to September), is 1,417 ± 203 mm. The monthly minimum and maximum rainfall events occur in winter (34 mm in July) and summer (217 mm in January), respectively. The daily mean air temperature is 24.2 ± 5.2 °C. According to the Köppen climate type, the climate in the PB is Aw type, tropical with dry winter and rainy summer (Alvares et al., 2013).

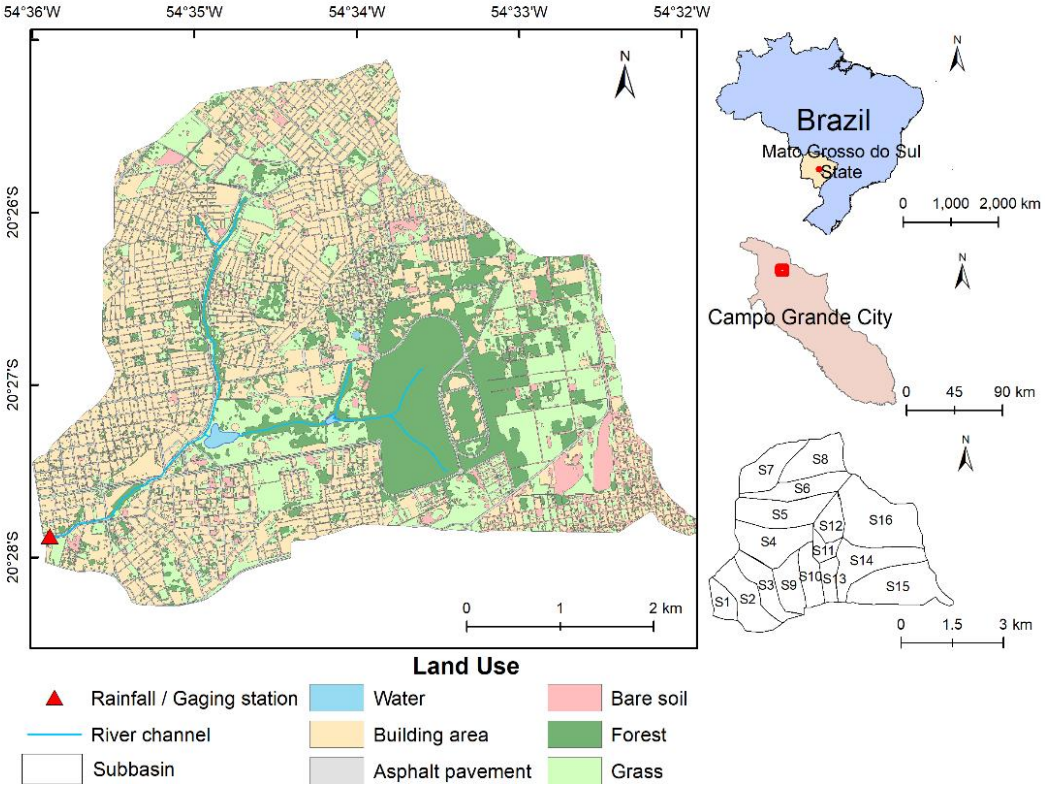

Figure 1 – Location and land cover of study area over the 2016 year.

The PB is characterized by large fraction of impervious surface, mostly commercial and residential areas. The land use types in the region can be classified into five categories: grass (24%), forests (19%), bare soil (6%), asphalt pavement (10%), building area (i.e. residential and commercial areas, 41%). The predominant soil type in the basin has sandy clay loam texture, and constant infiltration rate changes from 10 to 50 mm h^{-1} (Planurb, 1991; Sobrinho, 2015).

This basin has recurrence of flood events and the flow regime is influenced by dams, bridges, holding basins, power dissipation structures and channels with different wear layer. The PB was chosen because historical records of rainfall and flood damage indicate that the region has experienced an increase in flood frequency and magnitude due to urbanization (PDDU, 2008).

2.2 Study delineation

The paper is organized as follows (Figure 2). First, we acquired hydrological data (streamflow and rainfall) and stormwater drainage network characteristics. Second, the rainfall-runoff simulation was performed using Personal Computer Storm Water Management Model (PCSWMM) developed by the Environmental Protection Agency (EPA). The model parameters were calibrated and validated using measured streamflow data in the basin outlet. Third, projected (or future) runoff was generated over the Near future (2020–2045), Middle future (2046–2070) and Far future (2071–2095), using an ensemble of 17 General Circulation Models (GCMs) forced by International Panel on Climate Change (IPCC) Representative Concentration Pathway (RCP 4.5 and RCP 8.5), and scenarios of LID practices. Fourth, we evaluated LID efficiency on the runoff peak reduction and the resilience of stormwater drainage system.

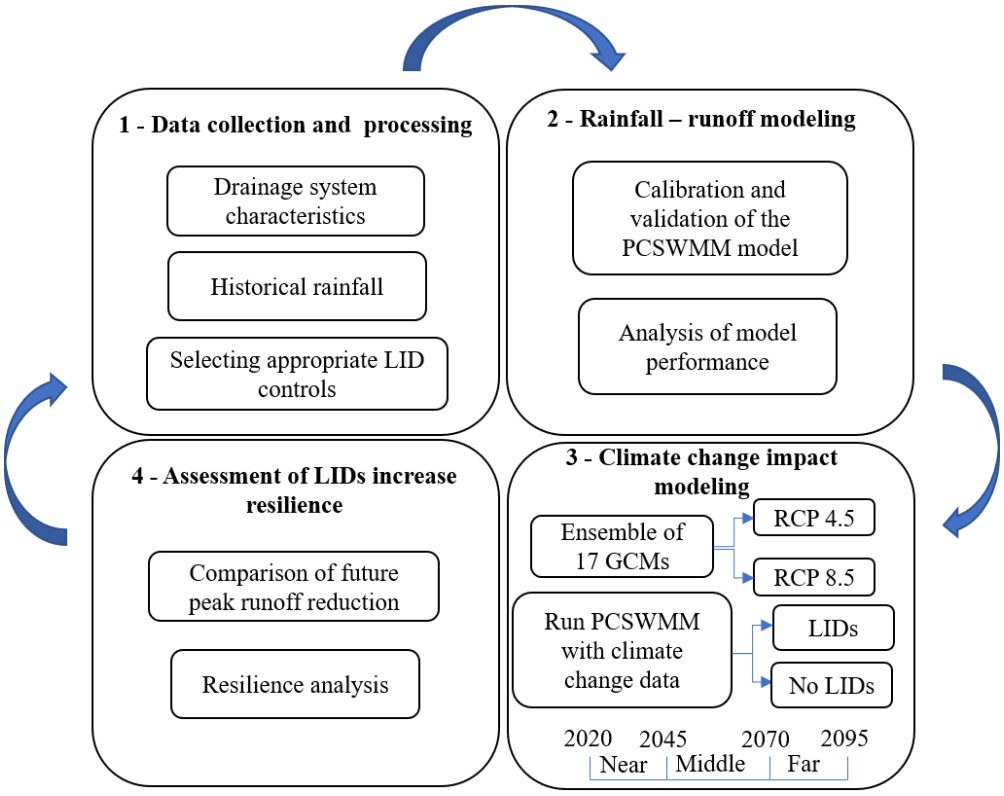

Figure 2 – Study framework of future climate change and Low Impact Development (LID) scenarios for urban stormwater resilience.

2.3 Hydrologic modeling

PCSWMM, a GIS version of the EPA Storm Water Management Model (SWMM 5.1), was adopted for this study to evaluate the effect of LIDs on increased resilience of urban areas

under climate change. The SWMM is a dynamic hydraulic-hydrology model for single or continuous rainfall event for quantity and quality simulation. Several studies have used SWMM for evaluating the effectiveness of LIDs in reducing pollutant loading (Rezaei et al., 2019) or in the context of flood risk (Sorensen; Emilsson, 2019). In addition, the model has been widely used to simulate infiltration and interception of rainfall, as well as routing of surface runoff through LID practices under mitigation and adaptation scenarios (Wu et al., 2018; Sohn et al., 2019).

The hydrological component of SWMM runs on subcatchment areas to generate runoff and requires inputs of rainfall and subcatchment properties such as drainage area, flow length or width, slope, and imperviousness. Each subcatchment surface is treated as a non-linear reservoir, where the inflow comes from rainfall or any upstream subcatchment, and there are several outflows, including infiltration, evaporation and surface runoff. Each "reservoir" has a maximum depression storage (Rossman, 2015). Infiltration can be estimated by Green-Ampt, Soil Conservation Service curve number (SCS-CN), or Horton methods.

The hydraulic component transports this runoff through a system of pipes, channels, bridges, storages, pumps, and regulators. The flow-routing model include steady flow, kinematic, and dynamic wave methods, and both methods employs the Manning's equation to relate flow depth to flow rate (Rossman, 2015).

In this study, the PB was discretized in 16 subcatchments and the initial estimate of the catchments characteristic width was based on the width of the equivalent rectangle, which relates the perimeter and catchment area (Zanandrea; Silveira, 2018). The initial storage height in depressions and roughness coefficient were defined according to the values suggested by Rossman (2015). In addition, the SCS-CN method was used to estimate infiltration processes, runoff was calculated using the Manning's equation, and dynamic wave theory was used for flow routing computation.

2.4 Model calibration and evaluation

The subcatchment model was calibrated and evaluated with rainfall and discharge data measured between May 2015 and February 2016 at the rainfall-gauging station (Figure 1). The permeable area was addressed according to the land cover study performed in the year 2016 because rainfall and flow data monitoring period. The model was calibrated with the following

parameters: subcatchment width; Manning`s roughness coefficient (n); and infiltration parameters (CN), which presented greater sensitivity in SWMM (Rosa et al., 2015).

The model was calibrated for two events and validated for four events, following previous works (Wu et al., 2013; Palla; Gnecco, 2015; Wu et al., 2018; Zanandrea; Silveira, 2018). To assess the performance of model calibration and validation, we applied two set of metrics against streamflow at the PB outlet. The first set comprises errors between the model and measured data: the Relative Percentage Difference (RPD) peak and the RMSE - Observations Standard Deviation Ratio (RSR). The second set corresponds to the agreement between the model and measured data: Nash-Sutcliffe Efficiency (NSE) index and the Coefficient of determination (R^2) (Nash; Sutcliffe, 1970; Moriasi et al., 2007; Palla; Gnecco, 2015).

2.5 Climate change scenarios

Climate projections by ensembles of 17 stochastically downscaled GCM model outputs (BCC-CSM 1.1, BCC-CSM 1.1 m, CSIRO-Mk3.6.0, FIO-ESM, GFDL-CM3, GFDL-ESM2G, GFDL-ESM2M, GISS-E2-H, GISS-E2-R, HadGEM2-ES, IPSLCM5A-LR, IPSLCM5A-MR, MIROC-ESM, MIROC-ESM-CHEM, MIROC5, MRI-CGCM3, and NorESM1-M), from the Coupled Model Intercomparison Project Phase 5 (CMIP5), were used in PCSWMM model to generate streamflow projections over the 2020–2095 period.

We used downscaled daily (future) rainfall using the MarkSim weather generator which comprises 720 classes of weather worldwide to calculate the coefficients of a third order Markov rainfall generator. The MarkSim fits a Markov model to the GCM output and uses it to generate weather data at a daily time step, with a spatial resolution of 30 arc-min (Jones; Thornton, 2013).

We chose an ensemble under two RCPs (RCP 4.5 and RCP 8.5). The RCP 4.5 is an intermediate stabilization pathway in which radiative forcing is stabilized at approximately 4.5 W m^{-2} (~650 ppm CO2 eq) after 2100. In the other hand, the RCP 8.5 is a pessimistic scenario in which radiative forcing reaches greater than 8.5 W m^{-2} (~1370 ppm CO2 eq) by 2100 (van Vuuren et al., 2011). We chose an ensemble because it presents better performance than individual models (Dhakal et al., 2018). That is, the use of ensembles can reduce the GCMs inherent uncertainties and enhance the reliability of climate projection (Knutti et al., 2010;

Salman et al., 2018; Ahmed et al., 2019). We focused on three 25–year time slices: Near future, 2020_2045; Middle future, 2046–2070; and Far future, 2071–2095. Additionally, we used 33 years (1995–2017) of daily rainfall time series as a baseline period to establish a benchmark for climate change scenarios assessment.

The annual maximum rainfall time series were selected taking daily maximum values in each year. The annual maximum rainfall for several return periods was estimated using the Log-normal probability distribution for both baseline and future periods. The statistical Anderson–Darling test was performed to verify the adherence of Log-normal distribution to sample data. The Log-normal distribution was used for each time slices for 6 return periods: 2, 5, 10, 25, 50, and 100 years because they are mostly used in stormwater drainage designs. Further, relationships between rainfall of different durations and alternating block method (Chin, 2013) were used for developing daily rainfall hyetographs with 1 hour duration for each return period at 10 min intervals (Back et al., 2012; Ghazavi et al., 2016). The 1 hour duration was selected based on the time of concentration of the PB, following Chow et al. (2013).

2.6 LID Scenarios

Considering the feasibility of implementing LIDs in the study area, we chose three types of LID practices: Rain Water Harvesting (RWH), Permeable Pavement (PP), and Infiltration Trench (IT), to evaluate their effectiveness for urban flood mitigation under climate change. The surfaces that received PP structures were public areas which are non-main roads of neighborhoods. The quantity of RWH and IT structures was proposed according the rainfall volume to be collected in the impervious area of each block by sub-basin. The rainfall volume was estimated using the urban stormwater master plan of Campo Grande city (PDDU, 2008):

$$V = (Q_u - Q_n).t.k \quad (1)$$

where V is the volume (m^3), Q_n is the pre-development flow ($m^3\ s^{-1}$), Q_u is the flow resulting from urban development ($m^3\ s^{-1}$), and t is the rainfall duration (minutes) and k (-) is the unit conversion factor. Both Q_n and Q_u are estimated for a 10 years design storm of return period. The parameters for RWH, PP, and IT (Table 1) were designed based on PCSWMM

requirements, previous LID literature (Qin et al., 2013; Wu et al., 2018; Zanandrea; Silveira, 2018), and in-situ data carried out in the PB (Sobrinho, 2015). To evaluate future runoff and investigate the effects of LID implementation on watershed runoff reduction, we set a series of proportions from 25% to 50% for different types of LID scenarios, a benchmark (no LID practices) and seven scenarios (Figure 3).

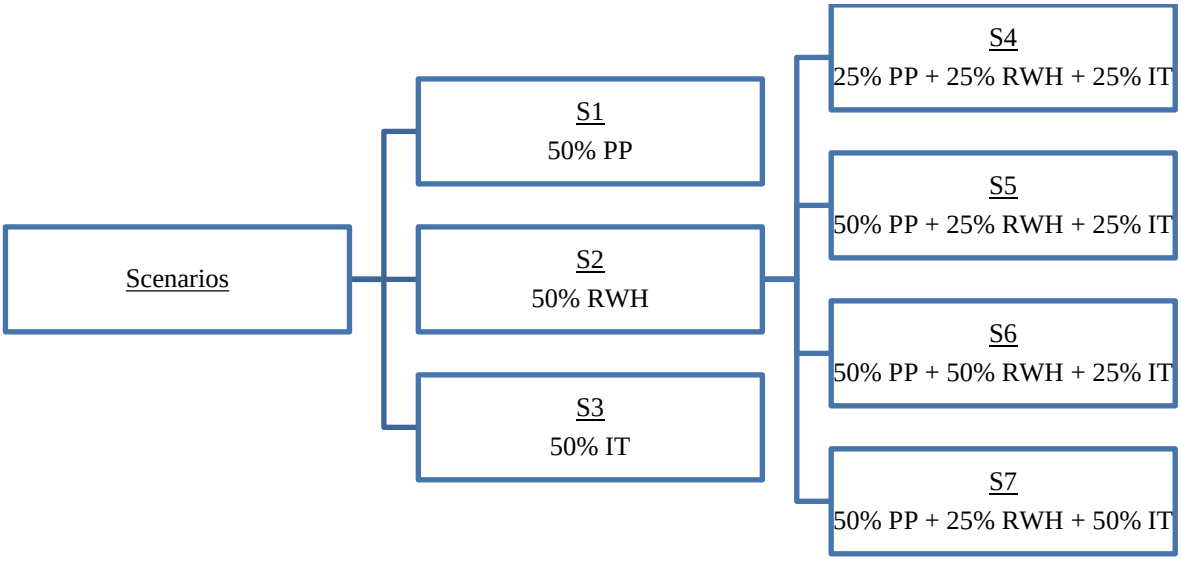

Figure 3 – Seven different types of LID scenarios. PP, RWH and IT is permeable pavement, rain water harvesting and infiltration trench, respectively.

The value of 25 (or 50%) PP is the percent of the roads that received PP, and 25 (or 50%) of RWH (or IT) is the percent of the impervious area of each block in the PCSWMM subcatchment. One should note that we considered that LIDs storage layer was empty as initial condition during simulation scenarios.

It is also important to note that the PB is the most urbanized basin within Campo Grande city. In addition, few non-urbanized areas in this basin are protected green areas (i.e. forest) that cannot be altered (Figure 1). Thus, we kept the current urbanization conditions (2016 year) in the basin for baseline and future scenarios. The current conditions include the existing stormwater management system. The average impervious area per lot is about 65%.

Table 1 – SWMM parameters for LID structures used for rainfall-runoff simulations.

Structure	Parameter	Permeable pavement	Infiltration trench	Rain water harvesting
Surface	Berm height (mm)	2.0	100	-
	Vegetation volume fraction	0	0	-
	Surface roughness (Manning's n)	0.015	0.02	-
	Surface slope (%)	1.0	1.0	-
Pavement	Thickness (mm)	100	-	-
	Void ratio (voids / solids)	0.15	-	-
	Impervious surface fraction	0	-	-
	Permeability (mm h^{-1})	300	-	-
	Clogging factor	0	-	-
Storage	Thickness (mm)	150	1000	-
	Void ratio (voids / solids)	0.75	0.5	-
	Seepage rate (mm h^{-1})	20	5.0	-
	Clogging factor	0	0	-
	Initial saturation (%)	0	0	0
	Height (mm)	-	-	1600
	Area (m^2)	-	-	3.14
Under drain	Drain coefficient (mm h^{-1})	9.0	-	-
	Drain exponent	0.5	-	-
	Drain offset height (mm)	6.0	-	-

- means that the parameter is not applied to the LID practice.

2.7 Resilience index

To quantify of the impact of LIDs on the entire stormwater drainage system, we applied an index of resilience for flood events. The Resilience index (R_h) (Mugume et al., 2015) was used here as:

$$R_h = 1 - \frac{h}{H} \cdot \frac{t_f}{t_n} \quad (2)$$

where h is the maximum depth (m) of water that ponded at the node (stream channel cross section) during the simulation, H is the maximum water depth (m) (i.e. distance from invert of the cross section to ground surface), t_f is the mean duration (minutes) of nodal flooding and t_n the total simulation time (minutes). For a given flood event, R_h quantifies the resilience as function of stream channel flood level and duration. R_h ranges from 0 to 1; with 0 indicating the lowest level of resilience and 1 the highest-level resilience for each scenario.

3 Results and Discussion

3.1 Model performance

Calibrated model parameters (Table S1; Appendix – Chapter 1) were used to generate streamflow at the PB outlet for the calibration and evaluation periods. Figure 4 shows model performance results for two calibration and validation events. The model performance for all events is summarized in Table S2 (Appendix – Chapter 1).

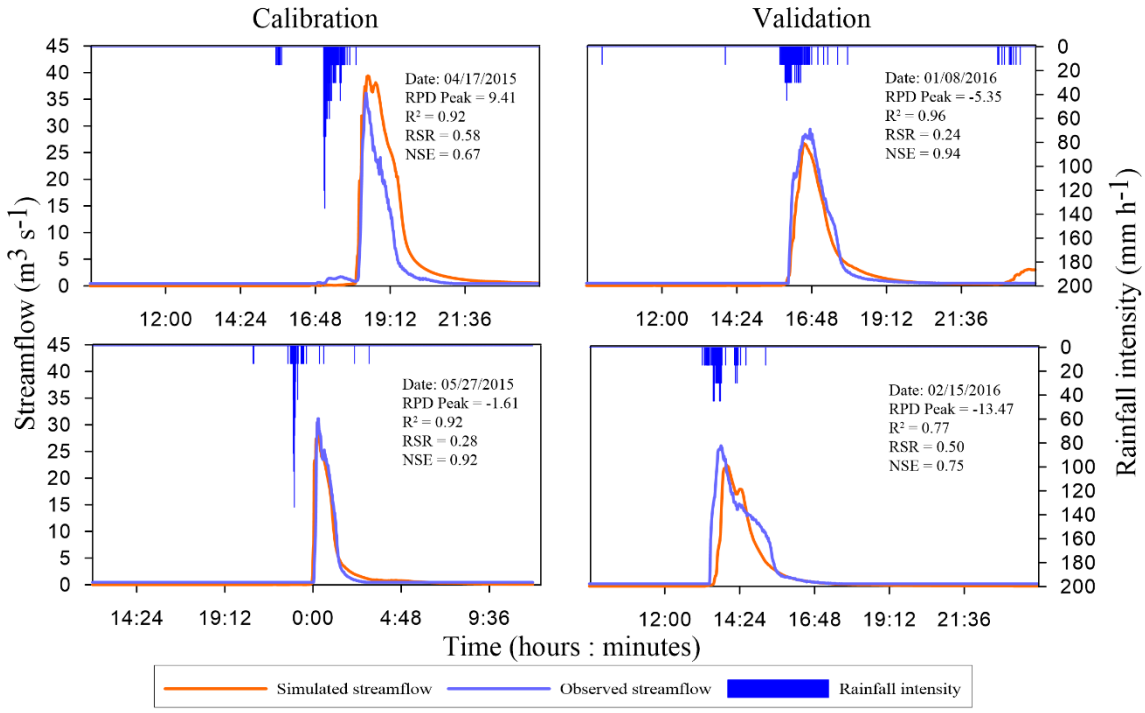

Figure 4 - Comparison between simulated and observed streamflow at the Prosa Basin outlet for two calibration (04/17/2015 and 05/27/2015) and validation (01/08/2016 and 02/15/2016) events. RPD is the Relative Percentage Difference peak, R^2 is the coefficient of determination, RSR is the RMSE - Observations Standard Deviation Ratio, and NSE is the Nash-Sutcliffe Efficiency index.

The model presents good goodness-of-fit for both calibration and validation periods with the mean values of R^2 and NSE higher than 0.80, even during different rainfall events. This indicates the ability of the model to represent the rainfall-runoff process in the PB basin. In general, the model performance can be judged as satisfactory for $R^2 > 0.50$, RSR ≤ 0.70, and NSE > 0.50 (Moriasi et al., 2007). Moreover, the mean value of RPD peak (< 7%) confirms the model reliability in predicting the peak flow during flooding events. These results are vital to establish the performance of LID practices in the PB basin under climate change.

3.2 Projected rainfall assessment

Before evaluating the effectiveness of LIDs to minimize the impacts of climate change on urban floods, we assessed the projected rainfall to determine the impacts of climate change without any adaptation. We found marked differences in rainfall intensity between the baseline period and projected RCPs scenarios for the near, middle and far future (Table 2).

.

Table 2 - Projected changes in rainfall intensity (mm h^{-1}) for rain events with return period ranging from 2 to 100 years under the two RCPs.

Return period (years)	Baseline	RCP 4.5			RCP 8.5		
		Near future	Middle future	Far future	Near future	Middle future	Far future
2	32.48	33.88	43.24	40.95	35.73	34.99	41.12
5	39.23	36.80	45.11	43.30	40.53	42.14	48.83
10	43.30	38.42	46.12	44.59	43.29	46.43	53.42
25	48.11	40.23	47.22	46.00	46.44	51.51	58.78
50	51.50	41.45	47.95	46.94	48.60	55.07	62.54
100	54.75	42.57	48.61	47.79	50.62	58.48	66.11

In general, the mean ± standard deviation rainfall intensity gradually increases in the RCP 8.5 from 44.20 ± 5.51 to about 55.13 ± 9.25 mm h^{-1} in the Near and Far future, respectively. Contrary, the rainfall intensity in the RCP 4.5 increases until the Middle future (from 38.89 ± 3.21 to 46.38 ± 1.98 mm h^{-1}) and decreases slightly until the end of the 21st century (44.93 ± 2.53 mm h^{-1}). In comparison with the baseline period, the highest rainfall intensities were found under RCP 8.5. Thus, we noted a gradual increase in the rainfall intensity during 21st century. This result indicates a potential increase in flooding events over the study area.

Figure 5a shows the runoff peak flow in the outlet of the PB under RCP 8.5, considering the current drainage system, i.e. without climate change adaptation with LIDs, it is characterized by an average increase of about 26% from Near to Far future, respectively. Contrary, the runoff peak under RCP 4.5 increases about 21%, from the Near future to Middle future and decreases ≃3% until Far future. We assign this behavior directly to the variation in rainfall intensity.

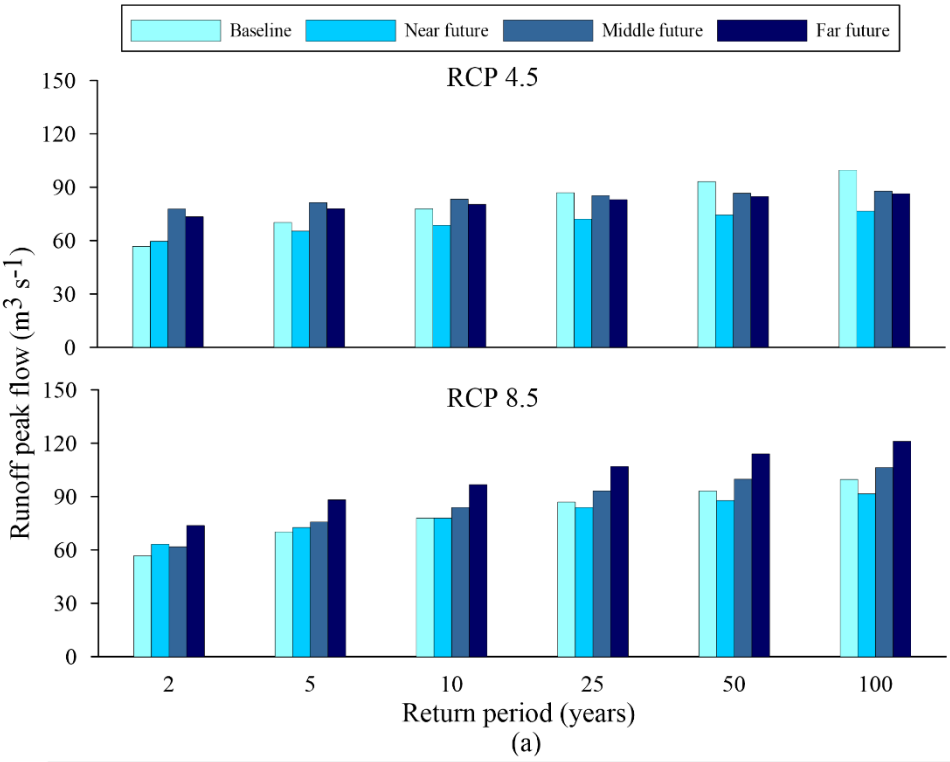

(a)

Return period (years)	RCP 4.5			RCP 8.5		
	Near future	Middle future	Far future	Near future	Middle future	Far future
2	5%	37%	29%	11%	9%	30%
5	-7%	16%	11%	4%	8%	26%
10	-12%	7%	3%	0%	8%	24%
25	-17%	-2%	-4%	-3%	7%	23%
50	-20%	-7%	-9%	-6%	7%	22%
100	-23%	-12%	-13%	-8%	7%	22%

(b)

Figure 5 – (a) Projected runoff peak flow and (b) relative difference between projected and baseline runoff peak given the return period for climate change (RCP 4.5 and RCP 8.5).

Overall, the relative difference in projected runoff peak increases from Near to Far future (Figure 5b). The runoff peak is expected to increase, on average, by 24% until Far future under RCP 8.5. The results corroborate the future increase in flooding risk due to increased extreme rainfall (Marengo et al., 2013; Gesualdo et al., 2019). Thus, we warn that some adaptations are needed to manage future climate change.

3.3 Performance of LID Practices Under Climate Change Scenarios

We adopted LID practices in the PB to mitigate the effects of climate change on urban flood. Hence, we chose the projected runoff peak for each return period under RCP 8.5, which presented the highest positive differences in relation to the baseline period (Figure 5b).

The results show that the S2 (RWH) has larger impact than the S1 (PP) and the S3 (IT) (Figure 6). That is, the S2 is more effective regarding reduce runoff peak, on average, of 30% for all projected rainfall events. The S3 shows a moderate effectiveness with regard to reduce runoff peak from 10 to 18% on average. In contrast, the S1 show the less efficiency with an average reduction in the runoff peak of about 10%.

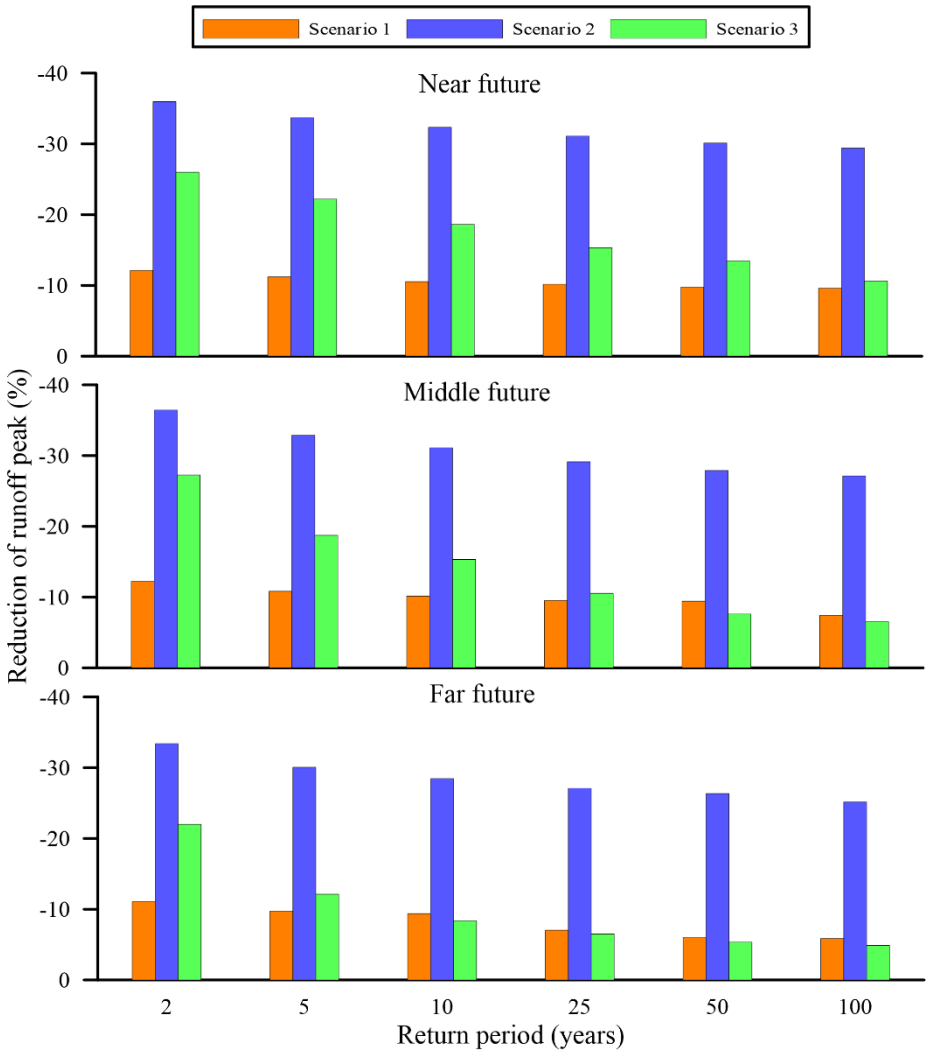

Figure 6 - Comparison of future runoff peak reduction according to the return period for individual LID practices. Scenario 1 (S1) – 50% PP, Scenario 2 (S2) – 50% RWH, and Scenario 3 (S3) – 50% IT. PP, RWH and IT is permeable pavement, rain water harvesting and infiltration trench, respectively.

The volume that flows into the RWH reservoirs and IT corresponds to the volume that precipitates over the percentage of the basin area treated by these LIDs (≃37% of the impervious area), which is larger than the area treated by the PP (≃14% of the impervious area). As consequence, the hydrological efficiency of the RWH reservoirs and trenches on reducing the runoff peak is greatest considering climate change.

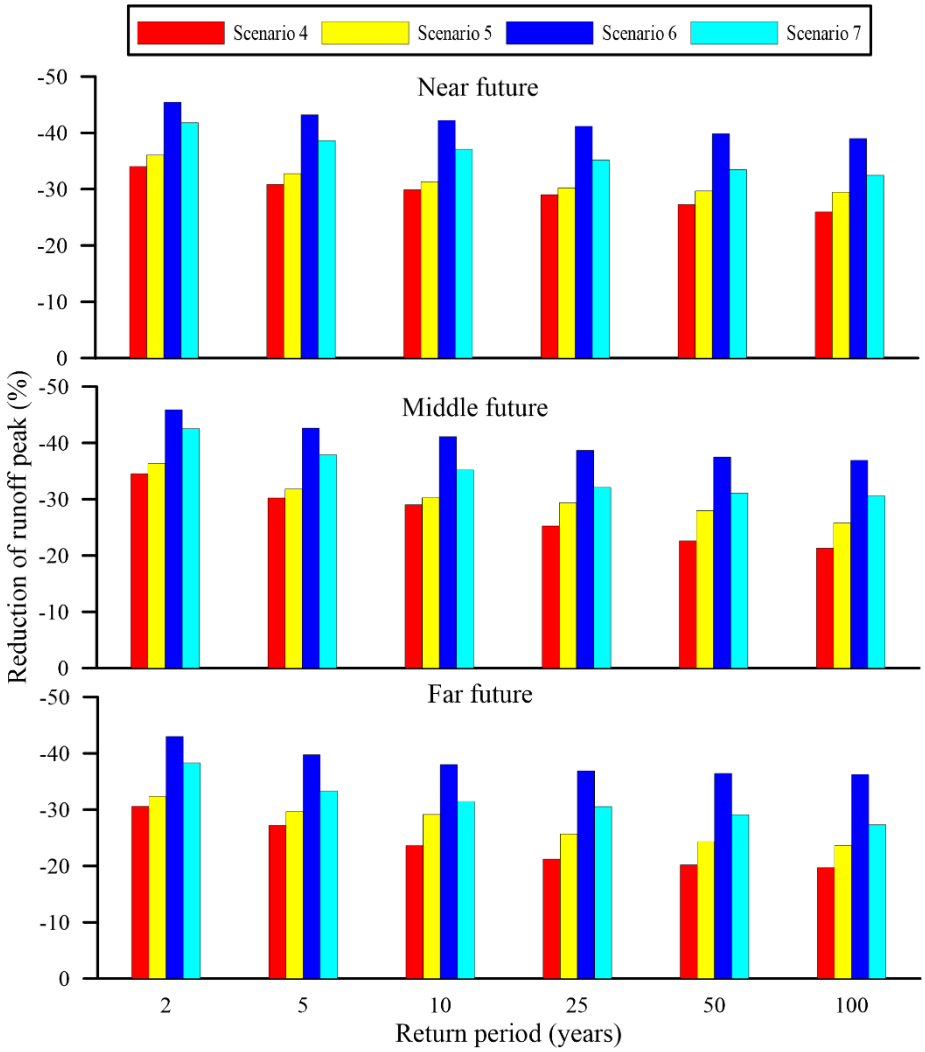

Figure 7 - Comparison of future runoff peak reduction according to the return period for LIDs combination. Scenario 4 (S4) – 25% PP + 25% RWH + 25% IT, Scenario 5 (S5) – 50% PP + 25% RWH + 25% IT, Scenario 6 (S6) – 50% PP + 50% RWH + 25% IT, and Scenario 7 (S7) – 50% PP + 25% RWH + 50% IT. PP, RWH and IT is permeable pavement, rain water harvesting and infiltration trench, respectively.

Figure 7 presents the reduction of runoff peak for scenarios of LIDs combination a under climate change (RCP 8.5). In general, all LIDs combination shows great reduction (>20%) in runoff peak. The most effective combined LID scenarios are those that combine higher percent of the basin treated by RWH. Thus, the S6 (50% PP + 50% RWH + 25% IT) presented the highest reduction in runoff peak, varying from 36 to 46%. It is important to note that for both individual and combined LID scenarios, the reduction in flow peak is higher for projected events with smaller rainfall intensity. For example, in Scenario 6 (S6) far future appears that, while the rainfall intensity varies from approximately 41 to 66 mm h^{-1} (Table 2), the reduction of runoff peak varies from 43% to 36% (Figure 7) from 2-year and 100-year period, respectively. Our results are in agreement with previous studies that observed more

effective reduction in runoff peak for low rainfall intensity (Damodaram et al., 2010; Behroozi et al., 2018).

3.4 Resilience analysis

The Resilience index is the ratio between the resilience of stormwater drainage system and the magnitude and duration of runoff., which was simulated by cross section of the stream channel, and is represented by the minimum, average and maximum values (Figure 8). To summarize the comparison between the current drainage system (i.e. without LID practices) and LID scenarios, we chose to evaluate only the best LIDs combination (i.e. S6; Figure 7) for the future rainfall events under climate change (RCP 8.5). Further, we assumed an acceptable level of resilience threshold of 0.8. This threshold represents the minimum acceptable flood protection level to be achieved.

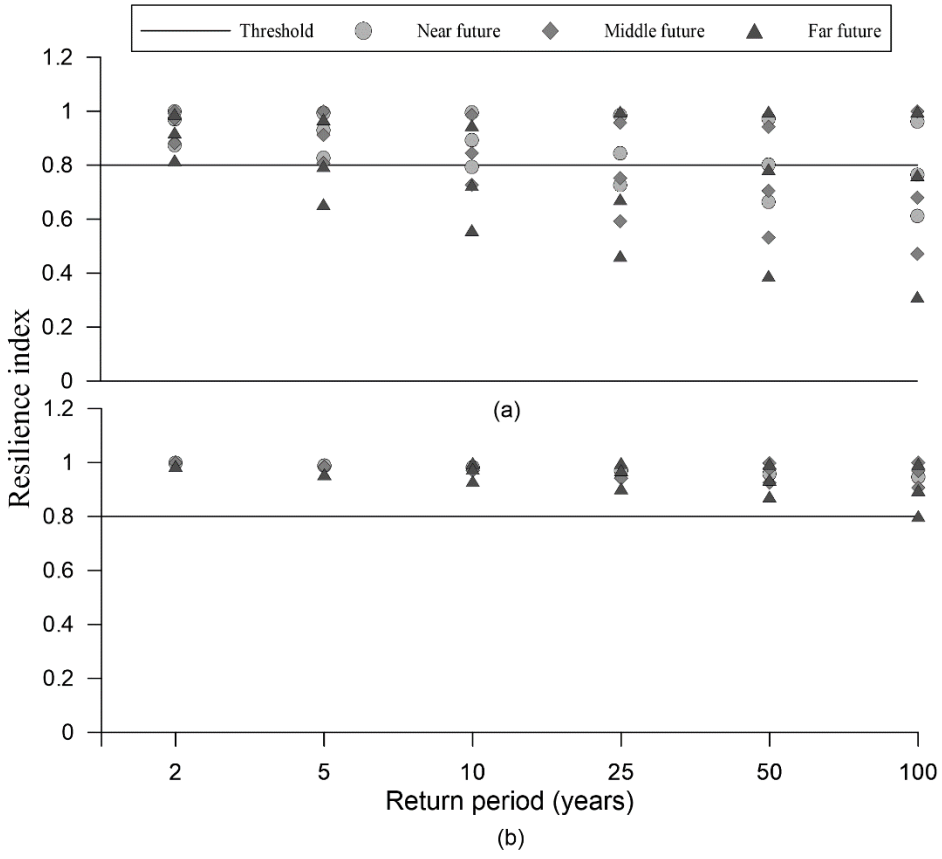

Figure 8 – The Resilience index under climate change conditions (RCP 8.5) for: (a) baseline (i.e. without LID practices) and (b) LIDs combination scenario (S6). The horizontal line is the minimum resilience level threshold of 0.80.

For the baseline scenario (Figure 8a), the values of R_h reveal large variations (from 0.31 to 0.99) according to the return period and a wide range from. When compared to the resilience threshold (0.8), the results indicate that the current drainage system crosses this threshold for all future rainfall events greater than 5 years of return period. This indicates that the current hydraulic capacity of the drainage system is insufficient and has low resilience to future extreme rainfall. Considering the LIDs combination (S6, Figure 8b), we found that the R_h ranges from 0.80 to 0.99. This is an important result and represent a significant improvement between 2 and 157% in the drainage system resilience.

4 Conclusions

In this study, we simulated future scenarios of urban stormwater runoff to evaluate the effect of LID practices in the resilience of stormwater drainage system under climate change. Hence, the resilience of the drainage system was quantified for several scenarios of LID practices and projected future rainfall under IPCC RCP 4.5 and RCP 8.5. To overcome the lack of LID modeling studies at catchment scale, we selected the Prosa Basin (32 km^2), Campo Grande city, in Brazil as study case. Further, we attempted to calibrate and validate the rainfall-runoff model using different rainfall events.

Our findings show an increase in runoff peak in the study area due to increased rainfall intensity until the end of the 21st century under both RCP 4.5 and RCP 8.5, while the impact of RCP 8.5 has potential to be more adverse than the RCP 4.5. Overall, runoff peak is projected (RCP 8.5) to increase on average by 24% over 2071–2095 period. The resilience index indicates that the current stormwater drainage system has low resilience to future rainfall events under climate change.

We demonstrate that the increased runoff peak can be mitigated satisfactory by using combined LID practices. In general, LID combinations showed reduction in runoff peak higher than 20%, and the best LID combination presented reduction up to 46%. As this represents a significant improvement in the resilience to flooding in the study area, LIDs can play a key role to increasing the city resilience.

Therefore, our study makes a major advance towards the comprehensive investigation of future urban flood under climate change by providing insights into urban flood management

at catchment scale. Our approach rises a calibrated modeling tool that could be used to enhance the adoption of LID practices.

5 Acknowledgements

This study was supported by grants from the Ministry of Science, Technology, Innovation and Communication – MCTIC and National Council for Scientific and Technological Development – CNPq (grants 441289/2017-7 and 306830/2017-5) and Coordenação de Aperfeiçoamento de Pessoal de Nível Superior - Brasil - CAPES (Finance Code 001 and Capes PrInt). The authors would like to acknowledge Computational Hydraulics International (CHI) for providing a university grant to use PCSWMM for the current project.

6 References

ABERA, L. E.; SURBECK, C. Q.; O'REILLY, A. M. Simulated Performance of In-Place Pervious Concrete under Varying Storms, Surface Areas, and Infiltration Rates. **Journal of Sustainable Water in the Built Environment,** v. 4, n. 2, p. 04018003, https://doi.org/10.1061/JSWBAY.0000852, 2018.

AHIABLAME, L. M.; ENGEL, B. A.; CHAUBEY, I. Effectiveness of low impact development practices in two urbanized watersheds: Retrofitting with rain barrel/cistern and porous pavement. **Journal of Environmental Management,** v. 119, p. 151-161, https://doi.org/10.1016/j.jenvman.2013.01.019, 2013.

AHMED, K.; SACHINDRA, D. A.; SHAHID, S.; DEMIREL, M. C.; CHUNG, E. S. Selection of multi-model ensemble of general circulation models for the simulation of precipitation and maximum and minimum temperature based on spatial assessment metrics. **Hydrol. Earth Syst. Sci.,** v. 23, n. 11, p. 4803-4824, https://doi.org/10.5194/hess-23-4803-2019, 2019.

ALVARES, C. A.; STAPE, J. L.; SENTELHAS, P. C.; DE MORAES GONÇALVES, J. L.; SPAROVEK, G. Köppen's climate classification map for Brazil. **Meteorologische Zeitschrift,** v. 22, n. 6, p. 711-728, http://dx.doi.org/10.1127/0941-2948/2013/0507, 2013.

AON. **Global Catastrophe Recap: March 2019**. AON Empower Results. 2019

BACK, Á. J.; OLIVEIRA, J. L. R.; HENN, A. Relações entre precipitações intensas de diferentes durações para desagregação da chuva diária em Santa Catarina. **Revista Brasileira**

de Engenharia Agrícola e Ambiental, v. 16, p. 391-398, http://dx.doi.org/10.1590/S1415-43662012000400009 2012.

BEHROOZI, A.; NIKSOKHAN, M. H.; NAZARIHA, M. Developing a simulation-optimisation model for quantitative and qualitative control of urban run-off using best management practices. **Journal of Flood Risk Management,** v. 11, n. S1, p. S340-S351, https://doi.org/10.1111/jfr3.12210, 2018.

BERTILSSON, L.; WIKLUND, K.; DE MOURA TEBALDI, I.; REZENDE, O. M.; VERÓL, A. P.; MIGUEZ, M. G. Urban flood resilience – A multi-criteria index to integrate flood resilience into urban planning. **Journal of Hydrology,** v. 573, p. 970-982, https://doi.org/10.1016/j.jhydrol.2018.06.052, 2019.

BIRGANI, Y. T.; YAZDANDOOST, F. Resilience in urban drainage risk management systems. **Proceedings of the Institution of Civil Engineers - Water Management,** v. 169, n. 1, p. 3-16, 10.1680/wama.14.00043, 2016.

BRAUD, I.; BREIL, P.; THOLLET, F.; LAGOUY, M.; BRANGER, F.; JACQUEMINET, C.; KERMADI, S.; MICHEL, K. Evidence of the impact of urbanization on the hydrological regime of a medium-sized periurban catchment in France. **Journal of Hydrology,** v. 485, p. 5-23, https://doi.org/10.1016/j.jhydrol.2012.04.049, 2013.

CHIN, D. A. **Water-resources engineering, 3rd Ed.** Upper Saddle River, NJ: Pearson, 2013. ISBN 9780273785910.

CHOW, V. T.; MAIDMENT, D. R.; MAYS, L. W. **Applied Hydrology, 2nd Ed**. New York: McGraw-Hill, 2013. ISBN 007174391X.

DAMODARAM, C.; GIACOMONI, M. H.; PRAKASH KHEDUN, C.; HOLMES, H.; RYAN, A.; SAOUR, W.; ZECHMAN, E. M. Simulation of Combined Best Management Practices and Low Impact Development for Sustainable Stormwater Management1. **JAWRA Journal of the American Water Resources Association,** v. 46, n. 5, p. 907-918, https://doi.org/10.1111/j.1752-1688.2010.00462.x, 2010.

DHAKAL, K.; KAKANI, V. G.; LINDE, E. Climate Change Impact on Wheat Production in the Southern Great Plains of the US Using Downscaled Climate Data. **Atmospheric and Climate Sciences,** v. 8, p. 143-162, https://doi.org/10.4236/acs.2018.82011, 2018.

DIETZ, M. E. Low Impact Development Practices: A Review of Current Research and Recommendations for Future Directions. **Water, Air, and Soil Pollution,** v. 186, n. 1, p. 351-363, https://doi.org/10.1007/s11270-007-9484-z, 2007.

DOTTORI, F.; SZEWCZYK, W.; CISCAR, J.-C.; ZHAO, F.; ALFIERI, L.; HIRABAYASHI, Y.; BIANCHI, A.; MONGELLI, I.; FRIELER, K.; BETTS, R. A.; FEYEN, L. Increased human and economic losses from river flooding with anthropogenic warming. **Nature Climate Change,** v. 8, n. 9, p. 781-786, https://doi.org/10.1038/s41558-018-0257-z, 2018.

GESUALDO, G. C.; OLIVEIRA, P. T. S.; RODRIGUES, D. B. B.; GUPTA, H. V. Assessing Water Security in the Sao Paulo Metropolitan Region Under Projected Climate Change.

Hydrol. Earth Syst. Sci. Discuss., v. 2019, p. 1-24, https://doi.org/10.5194/hess-23-4955-2019, 2019.

GHAZAVI, R.; MOAFI RABORI, A.; AHADNEJAD REVESHTY, M. Modelling and assessment of urban flood hazards based on rainfall intensity-duration-frequency curves reformation. **Nat. Hazards Earth Syst. Sci. Discuss.,** v. 2016, p. 1-19, https://doi.org/10.5194/nhess-2016-304, 2016.

GOLZ, S.; SCHINKE, R.; NAUMANN, T. Assessing the effects of flood resilience technologies on building scale. **Urban Water Journal,** v. 12, n. 1, p. 30-43, 10.1080/1573062X.2014.939090, 2015.

GONCALVES, M. L. R.; ZISCHG, J.; RAU, S.; SITZMANN, M.; RAUCH, W.; KLEIDORFER, M. Modeling the Effects of Introducing Low Impact Development in a Tropical City: A Case Study from Joinville, Brazil. **Sustainability,** v. 10, n. 3, p. 728, https://doi.org/10.3390/su10030728, 2018.

HAILEGEORGIS, T. T.; ALFREDSEN, K. Analyses of extreme precipitation and runoff events including uncertainties and reliability in design and management of urban water infrastructure. **Journal of Hydrology,** v. 544, p. 290-305, https://doi.org/10.1016/j.jhydrol.2016.11.037, 2017.

HAMMOND, M. J.; CHEN, A. S.; DJORDJEVIĆ, S.; BUTLER, D.; MARK, O. Urban flood impact assessment: A state-of-the-art review. **Urban Water Journal,** v. 12, n. 1, p. 14-29, https://doi.org/10.1080/1573062X.2013.857421, 2015.

HIRABAYASHI, Y.; MAHENDRAN, R.; KOIRALA, S.; KONOSHIMA, L.; YAMAZAKI, D.; WATANABE, S.; KIM, H.; KANAE, S. Global flood risk under climate change. **Nature Climate Change,** v. 3, n. 9, p. 816-821, https://doi.org/10.1038/nclimate1911, 2013.

HOLLING, C. S. Resilience and Stability of Ecological Systems. **Annual Review of Ecology and Systematics,** v. 4, n. 1, p. 1-23, 10.1146/annurev.es.04.110173.000245, 1973.

HUANG, J.; HE, J.; VALEO, C.; CHU, A. Temporal evolution modeling of hydraulic and water quality performance of permeable pavements. **Journal of Hydrology,** v. 533, p. 15-27, https://doi.org/10.1016/j.jhydrol.2015.11.042, 2016.

HUANG, Y.; LIU, Y.; LIU, Y.; KNIEVEL, J. C. Budget Analyses of a Record-Breaking Rainfall Event in the Coastal Metropolitan City of Guangzhou, China. **Journal of Geophysical Research: Atmospheres,** v. 124, n. 16, p. 9391-9406, https://doi.org/10.1029/2018JD030229, 2019.

JONES, P. G.; THORNTON, P. K. Generating downscaled weather data from a suite of climate models for agricultural modelling applications. **Agricultural Systems,** v. 114, p. 1-5, https://doi.org/10.1016/j.agsy.2012.08.002, 2013.

KHASTAGIR, A.; JAYASURIYA, L. N. N. Impacts of using rainwater tanks on stormwater harvesting and runoff quality. **Water Science and Technology,** v. 62, n. 2, p. 324-329, https://doi.org/10.2166/wst.2010.283, 2010.

KNUTTI, R.; FURRER, R.; TEBALDI, C.; CERMAK, J.; MEEHL, G. A. Challenges in Combining Projections from Multiple Climate Models. **Journal of Climate,** v. 23, n. 10, p. 2739-2758, https://doi.org/10.1175/2009JCLI3361.1, 2010.

LEHMANN, J.; COUMOU, D.; FRIELER, K. Increased record-breaking precipitation events under global warming. **Climatic Change,** v. 132, n. 4, p. 501-515, https://doi.org/10.1007/s10584-015-1434-y, 2015.

LIU, Y.; AHIABLAME, L. M.; BRALTS, V. F.; ENGEL, B. A. Enhancing a rainfall-runoff model to assess the impacts of BMPs and LID practices on storm runoff. **Journal of Environmental Management,** v. 147, p. 12-23, https://doi.org/10.1016/j.jenvman.2014.09.005, 2015.

MARENGO, J. A.; VALVERDE, M. C.; OBREGON, G. O. Observed and projected changes in rainfall extremes in the Metropolitan Area of São Paulo. **Climate Research,** v. 57, n. 1, p. 61-72, https://doi.org/10.3354/cr01160, 2013.

MIGUEZ, M. G.; VERÓL, A. P. A catchment scale Integrated Flood Resilience Index to support decision making in urban flood control design. **Environment and Planning B: Urban Analytics and City Science,** v. 44, n. 5, p. 925-946, 10.1177/0265813516655799, 2017.

MILLER, J. D.; HUTCHINS, M. The impacts of urbanisation and climate change on urban flooding and urban water quality: A review of the evidence concerning the United Kingdom. **Journal of Hydrology: Regional Studies,** v. 12, p. 345-362, https://doi.org/10.1016/j.ejrh.2017.06.006, 2017.

MILLER, J. D.; KIM, H.; KJELDSEN, T. R.; PACKMAN, J.; GREBBY, S.; DEARDEN, R. Assessing the impact of urbanization on storm runoff in a peri-urban catchment using historical change in impervious cover. **Journal of Hydrology,** v. 515, p. 59-70, https://doi.org/10.1016/j.jhydrol.2014.04.011, 2014.

MILLY, P. C. D.; BETANCOURT, J.; FALKENMARK, M.; HIRSCH, R. M.; KUNDZEWICZ, Z. W.; LETTENMAIER, D. P.; STOUFFER, R. J. Stationarity Is Dead: Whither Water Management? **Science,** v. 319, n. 5863, p. 573, https://doi.org/10.1126/science.1151915, 2008.

MISHRA, B. K.; RAFIEI EMAM, A.; MASAGO, Y.; KUMAR, P.; REGMI, R. K.; FUKUSHI, K. Assessment of future flood inundations under climate and land use change scenarios in the Ciliwung River Basin, Jakarta. **Journal of Flood Risk Management,** v. 11, n. S2, p. S1105-S1115, https://doi.org/10.1111/jfr3.12311, 2018.

MORIASI, D. N.; ARNOLD, J. G.; VAN LIEW, M. W.; BINGNER, R. L.; HARMEL, R. D.; VEITH, T. L. Model evaluation guidelines for systematic quantification of accuracy in watershed simulations. **Transactions of the ASABE**, http://dx.doi.org/10.13031/2013.23153, 2007.

MUGUME, S. N.; GOMEZ, D. E.; FU, G.; FARMANI, R.; BUTLER, D. A global analysis approach for investigating structural resilience in urban drainage systems. **Water Research,** v. 81, p. 15-26, https://doi.org/10.1016/j.watres.2015.05.030, 2015.

MUÑOZ, L. A.; OLIVERA, F.; GIGLIO, M.; BERKE, P. The impact of urbanization on the streamflows and the 100-year floodplain extent of the Sims Bayou in Houston, Texas. **International Journal of River Basin Management,** v. 16, n. 1, p. 61-69, https://doi.org/10.1080/15715124.2017.1372447, 2018.

NASH, J. E.; SUTCLIFFE, J. V. River flow forecasting through conceptual models part I — A discussion of principles. **Journal of Hydrology,** v. 10, n. 3, p. 282-290, https://doi.org/10.1016/0022-1694(70)90255-6, 1970.

OWOTOKI, P.; MANOJLOVIC, N.; MAYER-LINDENBERG, F.; PASCHE, E. A Data Mining Approach for Capacity Building of Stakeholders in Integrated Flood Management. Sixth International Conference on Data Mining (ICDM'06), 2006. 18-22 Dec. 2006. p.446-455.

PAGE, J. L.; WINSTON, R. J.; MAYES, D. B.; PERRIN, C.; HUNT, W. F. Retrofitting with innovative stormwater control measures: Hydrologic mitigation of impervious cover in the municipal right-of-way. **Journal of Hydrology,** v. 527, p. 923-932, https://doi.org/10.1016/j.jhydrol.2015.04.046, 2015.

PALLA, A.; GNECCO, I. Hydrologic modeling of Low Impact Development systems at the urban catchment scale. **Journal of Hydrology,** v. 528, p. 361-368, https://doi.org/10.1016/j.jhydrol.2015.06.050, 2015.

PDDU. **Plano Diretor de Drenagem Urbana de Campo Grande**. CONSÓRCIO-RES-PLANEJAMENTO-EM-DRENAGEM-URBANA. Campo Grande**:** 350 p. 2008.

PLANURB. **Carta Geotécnica de Campo Grande**. Prefeitura Municipal de Campo Grande. Campo Grande. 1991

PREGNOLATO, M.; FORD, A.; ROBSON, C.; GLENIS, V.; BARR, S.; DAWSON, R. Assessing urban strategies for reducing the impacts of extreme weather on infrastructure networks. **Royal Society Open Science,** v. 3, n. 5, p. 160023, doi:10.1098/rsos.160023, 2016.

QIN, H.-P.; LI, Z.-X.; FU, G. The effects of low impact development on urban flooding under different rainfall characteristics. **Journal of Environmental Management,** v. 129, p. 577-585, https://doi.org/10.1016/j.jenvman.2013.08.026, 2013.

QIU, Y.; ICHIBA, A.; PAZ, I. D. S. R.; CHEN, F.; VERSINI, P. A.; SCHERTZER, D.; TCHIGUIRINSKAIA, I. Evaluation of Low Impact Development and Nature-Based Solutions for stormwater management: a fully distributed modelling approach. **Hydrol. Earth Syst. Sci. Discuss.,** v. 2019, p. 1-27, https://doi.org/10.5194/hess-2019-347, 2019.

REZAEI, A. R.; ISMAIL, Z.; NIKSOKHAN, M. H.; DAYARIAN, M. A.; RAMLI, A. H.; SHIRAZI, S. M. A Quantity–Quality Model to Assess the Effects of Source Control Stormwater Management on Hydrology and Water Quality at the Catchment Scale. **Water,** v. 11, n. 7, p. 1415, https://doi.org/10.3390/w11071415, 2019.

ROSA, D. J.; CLAUSEN, J. C.; DIETZ, M. E. Calibration and Verification of SWMM for Low Impact Development. **JAWRA Journal of the American Water Resources Association,** v. 51, n. 3, p. 746-757, 10.1111/jawr.12272, 2015.

ROSSMAN, L. A. **Storm water management model user's manual, version 5.1**. National Risk Management Research Laboratory, Office of Research and Development. US Environmental Protection Agency, 2015.

SALMAN, S. A.; SHAHID, S.; ISMAIL, T.; AHMED, K.; WANG, X.-J. Selection of climate models for projection of spatiotemporal changes in temperature of Iraq with uncertainties. **Atmospheric Research,** v. 213, p. 509-522, https://doi.org/10.1016/j.atmosres.2018.07.008, 2018.

SAYERS, P.; YUANYUAN, L.; GALLOWAY, G.; PENNING-ROWSELL, E.; FUXIN, S.; KANG, W.; YIWEI, C.; QUESNE, T. L. **Flood Risk Management: A Strategic Approach**. Asian Development Bank, GIWP, UNESCO and WWF-UK, 2013. ISBN 978-92-3-001159-8.

SOBRINHO, T. A. **Relatório Técnico: Caracterização da infiltração da água e do escoamento superficial na área urbana de Campo Grande - MS**. Universidade Federal de Mato Grosso do Sul. Campo Grande, Mato Grosso do Sul. 2015

SOHN, W.; KIM, J. H.; LI, M. H.; BROWN, R. The influence of climate on the effectiveness of low impact development: A systematic review. **Journal of Environmental Management,** v. 236, p. 365-379, https://doi.org/10.1016/j.jenvman.2018.11.041, 2019.

SORENSEN, J.; EMILSSON, T. Evaluating Flood Risk Reduction by Urban Blue-Green Infrastructure Using Insurance Data. **Journal of Water Resources Planning and Management,** v. 145, n. 2, https://doi.org/10.1061/(ASCE)WR.1943-5452.0001037, 2019.

VAN VUUREN, D. P.; EDMONDS, J.; KAINUMA, M.; RIAHI, K.; THOMSON, A.; HIBBARD, K.; HURTT, G. C.; KRAM, T.; KREY, V.; LAMARQUE, J.-F.; MASUI, T.; MEINSHAUSEN, M.; NAKICENOVIC, N.; SMITH, S. J.; ROSE, S. K. The representative concentration pathways: an overview. **Climatic Change,** v. 109, n. 1, p. 5, https://doi.org/10.1007/s10584-011-0148-z, 2011.

VEMULA, S.; RAJU, K. S.; VEENA, S. S.; KUMAR, A. S. Urban floods in Hyderabad, India, under present and future rainfall scenarios: a case study. **Natural Hazards,** v. 95, n. 3, p. 637-655, https://doi.org/10.1007/s11069-018-3511-9, 2019.

WANG, M.; ZHANG, D. Q.; SU, J.; DONG, J. W.; TAN, S. K. Assessing hydrological effects and performance of low impact development practices based on future scenarios modeling. **Journal of Cleaner Production,** v. 179, p. 12-23, https://doi.org/10.1016/j.jclepro.2018.01.096, 2018.

WU, J.; YANG, R.; SONG, J. Effectiveness of low-impact development for urban inundation risk mitigation under different scenarios: a case study in Shenzhen, China. **Nat. Hazards Earth Syst. Sci.,** v. 18, n. 9, p. 2525-2536, https://doi.org/10.5194/nhess-18-2525-2018, 2018.

WU, J. Y.; THOMPSON, J. R.; KOLKA, R. K.; FRANZ, K. J.; STEWART, T. W. Using the Storm Water Management Model to predict urban headwater stream hydrological response to climate and land cover change. **Hydrol. Earth Syst. Sci.,** v. 17, n. 12, p. 4743-4758, 10.5194/hess-17-4743-2013, 2013.

XIONG, L.; YAN, L.; DU, T.; YAN, P.; LI, L.; XU, W. Impacts of Climate Change on Urban Extreme Rainfall and Drainage Infrastructure Performance: A Case Study in Wuhan City, China. **Irrigation and Drainage,** v. 68, n. 2, p. 152-164, https://doi.org/10.1002/ird.2316, 2019.

ZANANDREA, F.; SILVEIRA, A. L. L. D. Effects of LID Implementation on Hydrological Processes in an Urban Catchment under Consolidation in Brazil. **Journal of Environmental Engineering,** v. 144, n. 9, p. 04018072, https://doi.org/10.1061/(ASCE)EE.1943-7870.0001417, 2018.

ZHANG, W.; VILLARINI, G.; VECCHI, G. A.; SMITH, J. A. Urbanization exacerbated the rainfall and flooding caused by hurricane Harvey in Houston. **Nature,** v. 563, n. 7731, p. 384-388, https://doi.org/10.1038/s41586-018-0676-z, 2018.

ZHU, Z. H.; CHEN, Z. H.; CHEN, X. H.; YU, G. An assessment of the hydrologic effectiveness of low impact development (LID) practices for managing runoff with different objectives. **Journal of Environmental Management,** v. 231, p. 504-514, https://doi.org/10.1016/j.jenvman.2018.10.046, 2019.

CHAPTER 2

Towards an improved rainfall bias correction scheme using CDF Matching

Mattos, T. S., Oliveira, P. T. S., Ossuna, R., Oliveira, N. D., Roy, T., Lucas, M. C. Towards an improve on Rainfall Bias Correction Using CDF Matching. *Journal of Hydrometeorology*. In preparation. (Impact factor, 2019: 3.891; Qualis CAPES: A1)

Abstract

Accurate rainfall estimates are crucial for studies related to urban flooding. Weather data from radars is particularly useful for rainfall-runoff simulations since it provides high-resolution spatiotemporal estimates of rainfall. Because there are errors and uncertainties prevalent in the radar-based rainfall estimates, various statistical postprocessing techniques come into play, one of which is the bias correction. Several methods have been proposed for the bias correction of rainfall; however, these schemes are more commonly applied on the daily data. Finer timescale (e.g., sub-hourly) implementation is rare and is still challenging. Here, we propose a new bias correction approach based on cumulative distribution function (CDF) matching that focuses on correcting the biases in radar-based rainfall estimates at daily, hourly and sub-hourly levels. We considered in-situ rainfall measurements from on 34 rain gauges (at 1-minute timestep) as the ground truth. In total, 408 events were observed over the study period of two years (January_2016 to February_2018). The correction scheme resulted in an improvement of the Nash-Sutcliffe Efficiency (*NSE*) from 0.11 to 0.63 and Mean Absolute Error (*MAE*) from 11.66 mm to 6.97 mm for all rainfall events. Our findings are particularly useful in the case of rainfall-runoff modeling for urban flooding studies. Therefore, we highlight the effectiveness of our proposed bias correction scheme for improving radar-based rainfall estimates at fine timescales.

Keywords: Bias Correction, Radar, CDF Matching, Quantile Mapping, Urban Flooding

1 Introduction

There is an increasing trend of urbanization growth globally. For instance, 55% of the global population live in urban areas, which corresponds to an increase of 24% since 1950. Moreover, it is expected that 68% of global population will live in urban areas by 2050 (United Nations, 2018). The rapid increase in urban population density suggests a more vulnerable society to extreme weather events (Jahn, 2015), including heavy rainfall-driven flooding, which cause damage to human life, urban infrastructure, and environment (Luo et al., 2018). Rainfall-driven floods are among the most common type of natural disasters and have the greatest potential for damage compared to all other natural disasters worldwide (WMO, 2013).

One of the most valuable tools for flood mitigation planning is a hydrological (or rainfall-runoff) model, which can mathematically conceptualize the complex relations between the physical characteristics of a watershed and the input rainfall (Salvadore et al., 2015). The outputs from these models can be used to develop flood hazard maps and flood warning systems, which can potentially save lives and property. Flood warning systems facilitate evacuation in the riverfront buildings, lockdown of transportation infrastructures, and the application of emergency protocols in essential facilities services (WMO, 2011), such as hospitals and schools.

In an urban setting, hydrological models demand for high-resolution rainfall data (e.g., hour or sub-hour timescale) as input (Müller; Haberlandt, 2018), both spatially and temporally. This is particularly applicable in urban watersheds where the hydrology is characterized by fast surface runoff and short rainfall duration (Ficchì et al., 2016). In this context, there is a need to acquire rainfall data at high spatiotemporal resolutions, whereas coarse-resolution rainfall data can undermine model prediction and forecasting, thereby affecting the decision-making process on flood mitigation (McMillan et al., 2011; McKee; Binns, 2015). Radar rainfall estimates are suitable in this case, given the need for high-resolution input data in the rainfall-runoff models (Thorndahl et al., 2017).

A weather radar represents the spatial variability of rainfall more accurately than conventional rain gauges, and consequently, can improve rainfall-runoff modeling (Abon et al., 2016; Gurung, 2017). It is a remote sensing instrument that measures the reflectivity of precipitation to estimate the rainfall at the ground level. The uncertainty in the estimation arises from electronic miscalibration, signal attenuation, increase in sample volume due to beam broadening, non-uniform vertical profile of reflectivity, and the conversion of radar reflectivity

into rain rates (Z-R relationship) (Krajewski; Smith, 2002; Goudenhoofdt; Delobbe, 2009). Thus, radar-based rainfall estimates are still prone to large uncertainties due to random and systematic errors, which limit their hydrological applications (Berne; Krajewski, 2013)

The uncertainties in the radar-based rainfall estimates can be reduced by using polarimetric signals or increasing the density of radar network (Thorndahl et al., 2017). However, both solutions require significant financial investments, which, in many situations, are not feasible. Hence, the radar bias adjustment based on rain gauge network becomes relevant.

Several methods have been proposed for the bias correction of radar-based rainfall estimates using ground-based data, such as: mean field bias correction (Borga et al., 2002), Brandes spatial adjustment (Looper; Vieux, 2012), local bias correction with ordinary kriging (James et al., 1993), range-dependent bias correction (Michelson; Koistinen, 2000), Bayesian data combination (Todini, 2001), conditional merging (Sik Kim et al., 2008), and kriging with external drift (Schuurmans et al., 2007). For more details about these methods readers are referred to Wang et al. (2013) and McKee and Binns (2015). Although these methods have been successfully used in several applications, merging/adjustment methods need improvements at sub-hourly timescales to quantify flow in urban watersheds (McKee; Binns, 2015) covered by large impervious areas, and hence dominated by surface runoff (Thorndahl et al., 2014).

Here, the objective is to propose a new method for correcting biased radar rainfall against ground-based rain gauge data in daily, hourly, and sub-hourly timescale.

This article is organized as follows. First, we provided a description of the data sources used in the study area, which is followed by an explanation of our proposed method for bias correction. The statistical metrics used to evaluate the bias correction are then introduced. The results are discussed focusing on the advantages and limitations of the proposed method. Finally, we highlighted the major scientific contributions (implications and applications) of this paper.

2 Material and Methods

2.1 Study area and datasets

We used rainfall data from a dual-polarization S-band weather radar that is operated by The National Center for Monitoring and Early Warning of Natural Disasters (CEMADEN), an institution linked to the Ministry of Science and Technology. The radar is located in the Jaraguarí city (-20.278 S, -54.474 W), Mato Grosso do Sul State, at an elevation of 753 m above the mean sea level. The radar observations are commonly used for operational short-term precipitation forecasts and detection of severe thunder storms in Brazil.

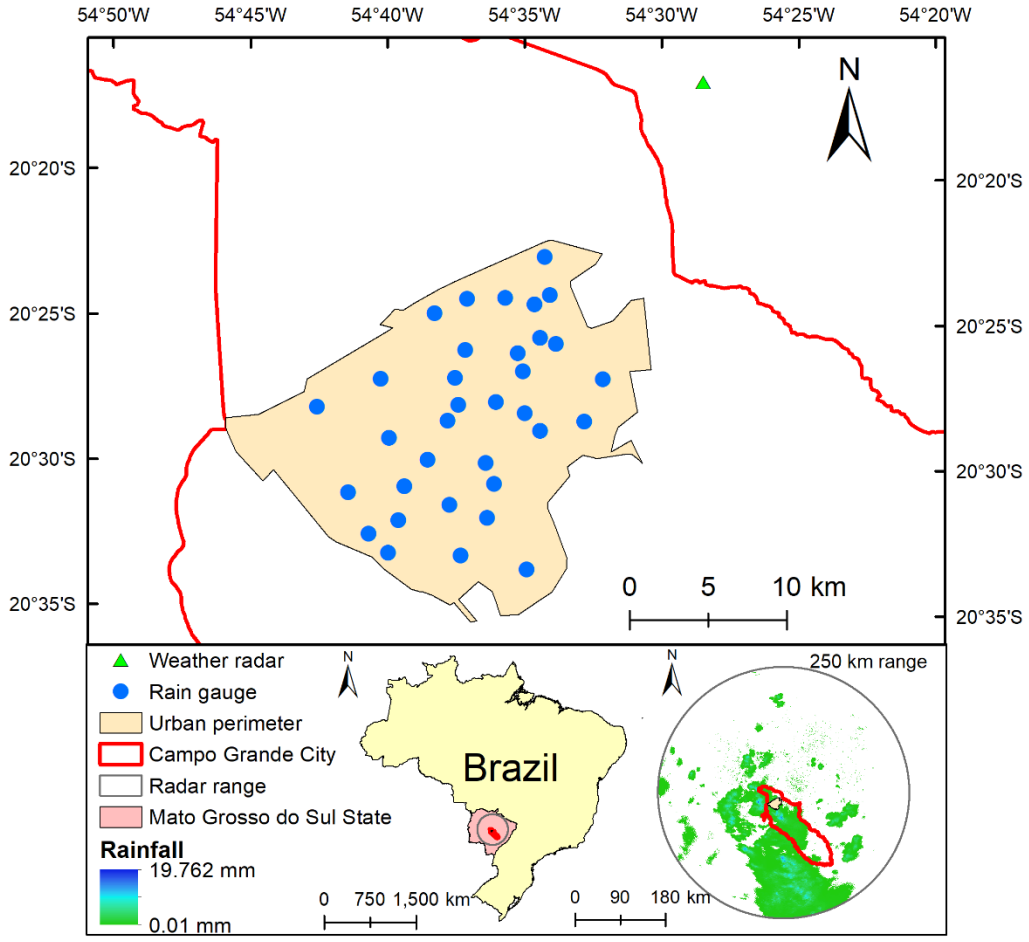

Figure 1 – Location of the study area within the 250 km range.

The radar data is sampled with a temporal resolution of 5 min and a 3 km altitude pseudo-CAPPI (Constant Altitude Plan Position Indicator) product is generated based on 12-elevation (from 0.5 to 20º) with reflectivity measurements up to 250 km. The resolution of the radar polar data is 250 m in range and 1-degree in azimuth angle. The beam width is approximately 1 degree. The spatial resolution of the pseudo-CAPPI product is 750 m × 750 m.

The rainfall rate is estimated by applying polarimetric variables according to the thresholds (Equations 1, 2, and 3), as proposed by Ryzhkov et al. (2005):

$$R = \frac{R(Z)}{0.4 + 5.0|Z_{dr} - 1|^{1.3}} \qquad \text{for R(Z)} < 6 \text{ mm/h} \qquad (1)$$

$$R = \frac{R(K_{dp})}{0.4 + 3.5|Z_{dr} - 1|^{1.7}} \qquad \text{for } 6 < \text{R(Z)} < 50 \text{ mm/h} \qquad (2)$$

$$R = R\left(K_{dp}\right) \qquad \text{for R(Z)} > 50 \text{ mm/h} \qquad (3)$$

where $R(Z)$ is the Marshall-Palmer relation for $Z=aRb$ with a = 200 and b = 1.6 (Marshall; Palmer, 1948), Z is reflectivity (dBZ), and Z_{dr} and K_{dp} are the differential reflectivity (dB) and phase (º / km), respectively.

The Marshall-Palmer relation was calculated by:

$$R(Z) = \frac{1}{a^{1/b}} Z^{1/b} \leftrightarrow Z = aR^b \qquad (4)$$

$$R\left(K_{dp}\right) = 44\left|K_{dp}\right|^{0.822}, \qquad \text{for } K_{dp} > 0 \qquad (5)$$

Additionally, we used rainfall data (2016–2018) from a monitoring network that comprises 34 tipping bucket rain gauges across the urban perimeter of Campo Grande city (Mato Grosso do Sul State) (Figure 1). This corresponds to a density of 1 gauge per 10 km². Each rain gauge has a volumetric resolution of 0.2 mm and rainfall records were acquired at 1-minute timescale.

2.2 Bias correction method

Cumulative Distribution Function (CDF) matching is a bias correction technique (Reichle; Koster, 2004) that has been widely applied in meteorological and hydrological applications. For instance, CDF matching has been used to develop reflectivity-rainfall relationships for

radar (or satellite) rainfall calibration (Atlas et al., 1990; Anagnostou et al., 1999), long-range hydrological forecasting (Wood et al., 2002), bias reduction in satellite retrieved soil moisture (Reichle; Koster, 2004; Brocca et al., 2011), and streamflow forecasts from satellite-based precipitation (Roy et al., 2017; Roy et al., 2020) for bias correction of climate data (Li et al., 2010; Switanek et al., 2017; Roy et al., 2018).

A CDF matching technique (also known as *quantile mapping*, *probability mapping* or *distribution mapping*) Gupta et al. (2019), is based on adjusting the CDF of the simulated values to agree (or match) with the CDF of the observed ones in a given reference period (Wang; Chen, 2014). This method focuses on eliminating the differences between all the statistical moments of simulated and observed values (Afshar et al., 2019). Figure 2 shows an illustrated scheme of the CDF matching method. It can be seen that the CDF of rainfall radar data has less variability than the CDF of rain gauge. The corrected rainfall estimate from radar is denoted by x', x is the biased rainfall estimate from rain gauge, and the arrows indicate the CDF matching procedure (Figure 2).

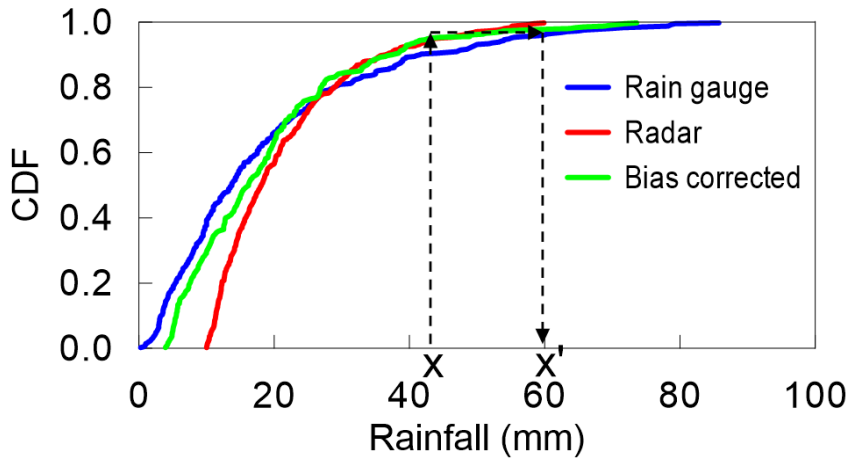

Figure 2 – Empirical CDF matching method applied to rainfall events from January of 2016 to February of 2018 in Campo Grande city, Brazil. The arrows illustrate how the radar data are corrected into the adjusted data set.

To eliminate the systematic bias, the two datasets need to be scaled in order to match each other. Thus, simulated and observed values must be ranked. Then, a polynomial equation can be used to fit the ranked simulated values and the corresponding differences between both datasets (Drusch et al., 2005). Figure 3 illustrates an example of the fitted polynomial equation.

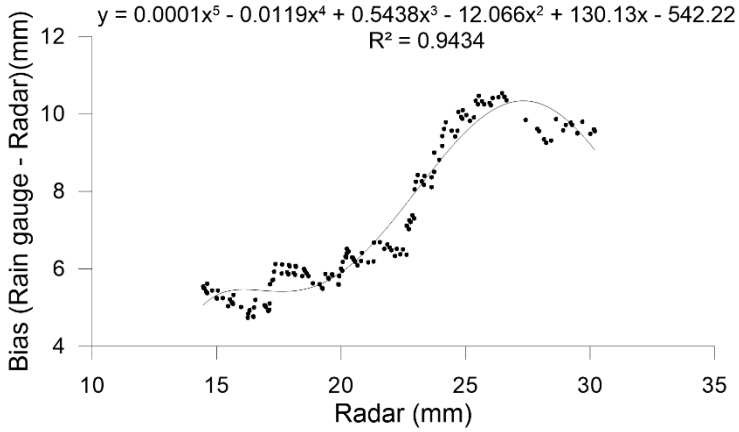

Figure 3 – Example of polynomial equation fitting of the differences between the ranked and radar values for a given reference period. R^2 is the coefficient of determination based on the fitted equation.

In general, CDF matching applied using polynomials will be dependent on the quality of the polynomial fit, and so perfect agreement might not exist (Drusch et al., 2005), especially while dealing with sub-daily rainfall events. This is because sub-daily rainfall presents greater variability between successive rainfall events throughout the day. Thus, an accurate CDF estimation would require a long time series (> 10 years).

Here, we developed a modified version of the conventional CDF matching method, referred to as CDF_{mod}, which is capable of bias correcting radar-based rainfall estimates using short data records (~ 2 years) at daily, hourly, and sub-hourly timescales. We used rainfall measurements from 34 tipping bucket rain gauges as the reference. The radar estimates and the rain gauge measurements were compared based on the point-pixel approach. The proposed CDF_{mod} scheme is outlined below:

1) We first identified the rainfall events from the radar and rain gauges. Following Oliveira et al. (2015), periods of rainfall were considered to be isolated events when they were separated by periods of precipitation between 0 (no rain) and 1.0 mm for at least 6 hours. We assumed that rainfall measurements from the rain gauges represent the ground truth;
2) The radar rainfall events were ranked and selected, according to the total rainfall by five intervals: 10-20 mm, 20-30 mm, 30-40 mm, 40-50 mm, and 50-60 mm;
3) We calculated the differences between the CDFs (i.e., radar and rain gauge) for each interval;
4) A 5^{th} order polynomial equation was fitted to the differences between the CDFs (i.e., radar and rain gauge) and radar rainfall for each interval (Figure3);

Radar rainfall bias was corrected using the relationship:

$$\boldsymbol{Rd_{cor} = Rd + f(Rd) \quad if\ bias > 0}$$
$$\boldsymbol{Rd_{cor} = Rd - f(Rd) \quad if\ bias < 0} \tag{6}$$

where Rd_{cor} is the radar rainfall after bias correction, *bias* = *G* – *Rd*; *G* is the rain gauge data; *Rd* is the radar data, and *f*(*Rd*) is the 5th order polynomial equation. We emphasize that the core of the CDF$_{mod}$ method is to improve the polynomial fit by grouping the rainfall events, and consequently reducing their intrinsic variability.

2.2.1 Performance evaluation

The performance was evaluated by comparing the adjusted rainfall radar estimates to the measurements from the rain gauges. Following Thorndahl et al. (2014), we used two performance metrics to evaluate the bias adjustment: the Nash-Sutcliffe-Efficiency (*NSE*) and Mean Absolute Error (*MAE*). The *NSE* is given by (Nash; Sutcliffe, 1970):

$$NSE = 1 - \frac{\sum_{i=1}^{N}\left(G_i - Rd_{cor_i}\right)^2}{\sum_{i=1}^{N}(G_i - \bar{G})^2} \tag{7}$$

where Rd_{cor_i} is *i*th rainfall value from the radar after bias correction, G_i is the *i*th rainfall value from rain gauge, $\bar{G}$ is the mean rainfall value from rain gauge. *NSE* ranges from -∞ to 1.0, is equal to 1.0 in case of perfect agreement. *NSE* = 0 means that the radar accuracy corresponding to the mean of the rain gauges estimates.

MAE was used to quantify the errors between radar and rain gauges estimates and is calculated by:

$$MAE = \frac{1}{N}\sum_{i=1}^{N}\left|G_i - Rd_{cor_i}\right| \tag{8}$$

3 Results and discussion

3.1 Comparison between uncorrected and corrected bias data

Figure 4 shows the rainfall event bias fluctuation from January of 2016 to February of 2018, where the bias is a difference between gauge and radar rainfall. Overall, the bias ranged from -50 mm to ~74 mm with an arithmetic mean of -2.44 mm. In addition, the radar overestimates and underestimates the rainfall in about 259 and 149 events, respectively.

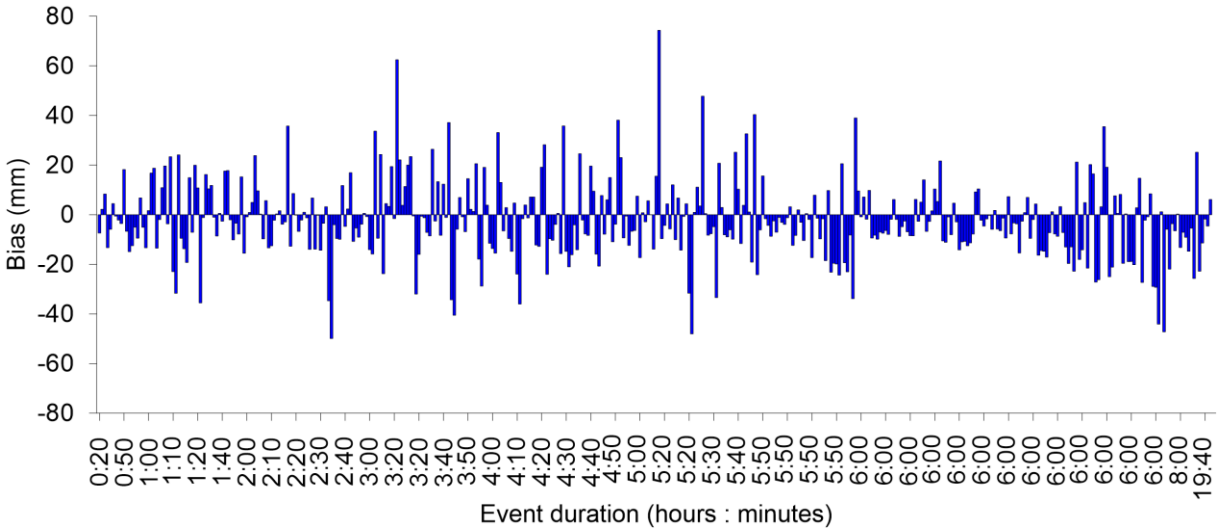

Figure 4 – Variability of bias between radar and rain gauges for rainfall events of different duration from January 2016 to February 2018. Each value corresponds to an independent rainfall event.

Thus, results evidence the presence of error between point rainfall measures (i.e., rain gauges) and areal radar estimates. This is in accordance with previous studies. For example, Bringi et al. (2011) compared point measurements from laser disdrometers with radar estimates. They found that the difference varied from 20 to 55 % for hourly rainfall accumulations larger 1 mm and 6 mm, respectively. In contrast, Nielsen et al. (2014) showed significantly lower errors comparing disdrometer to radar observations. According to Schleiss et al. (2019), only part of the bias (13-30%) can be explained by differences in measurement between gauges and radar.

Figure 5 shows the rainfall events obtained from the radar and rain gauge network. In total, 408 events were observed over the study period. As expected, the number of events decreases with the increase in rainfall height. In general, the frequency of events for the radar, considering an equivalent interval, was higher for the rain gauges, and consequently had a

smaller number of intervals. On the other hand, after correcting the bias or radar estimates (Figure 5c), we noted a remarkable change in the distribution of events that was similar to rain gauge (Figure 5a). Thus, the results demonstrate an improvement in the frequency distribution of rainfall events, mainly for the intervals of 0-10, 60-70 and 70-80 mm.

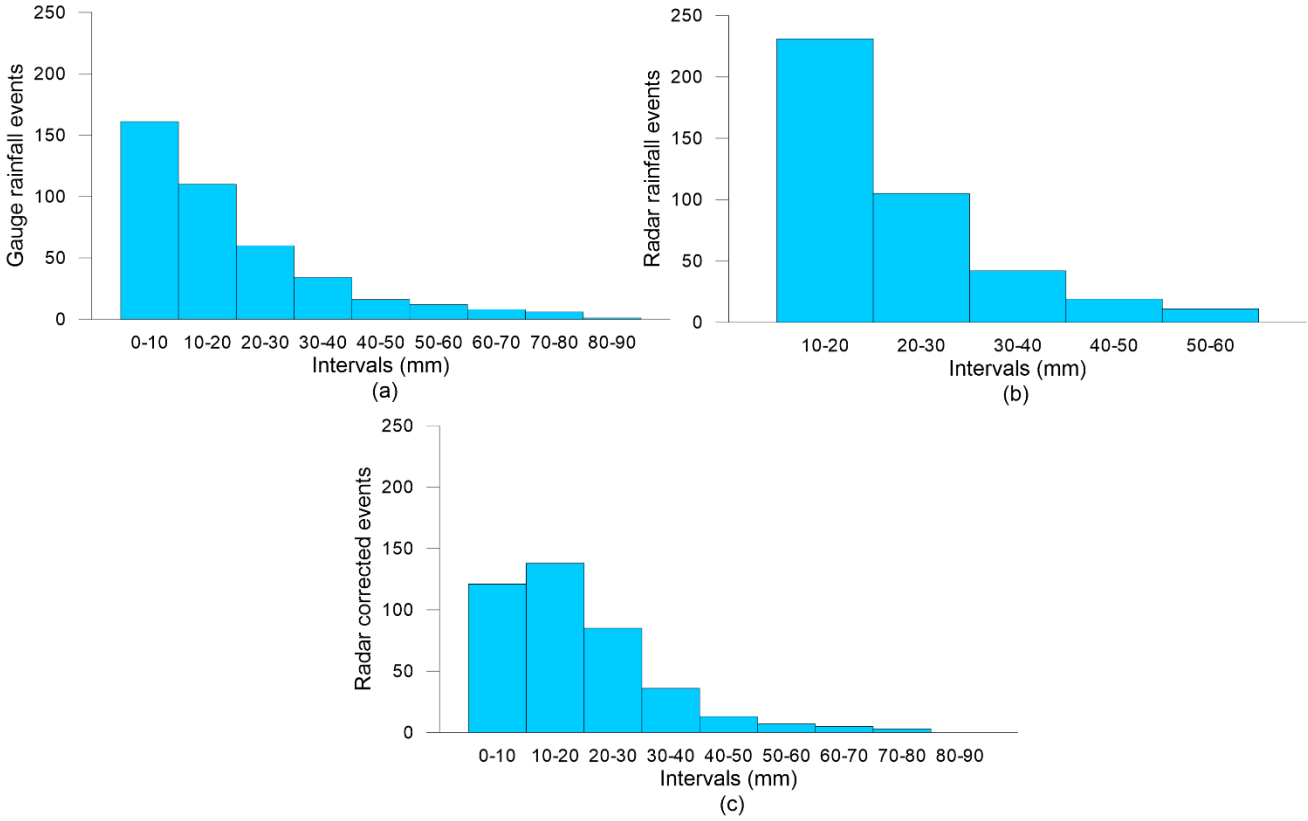

Figure 5 – Absolute frequency of rainfall events for each interval of duration (from January/2016 to February/2018) based on: (a) rain gauge data, and (b) radar data. (c) Absolute frequency of rainfall events estimated by the radar after bias correction.

Figure 6 shows the scatter plot between uncorrected and corrected bias in terms of rainfall event. We observed a poor linear correlation ($0.002 \leq r \leq 0.02$) between radar and rain gauge events for all rainfall intervals. The average value of coefficient of determination (R^2) was approximately 0.01. This indicates the low performance of the Jaraguarí weather radar in estimating rainfall events without any bias correction.

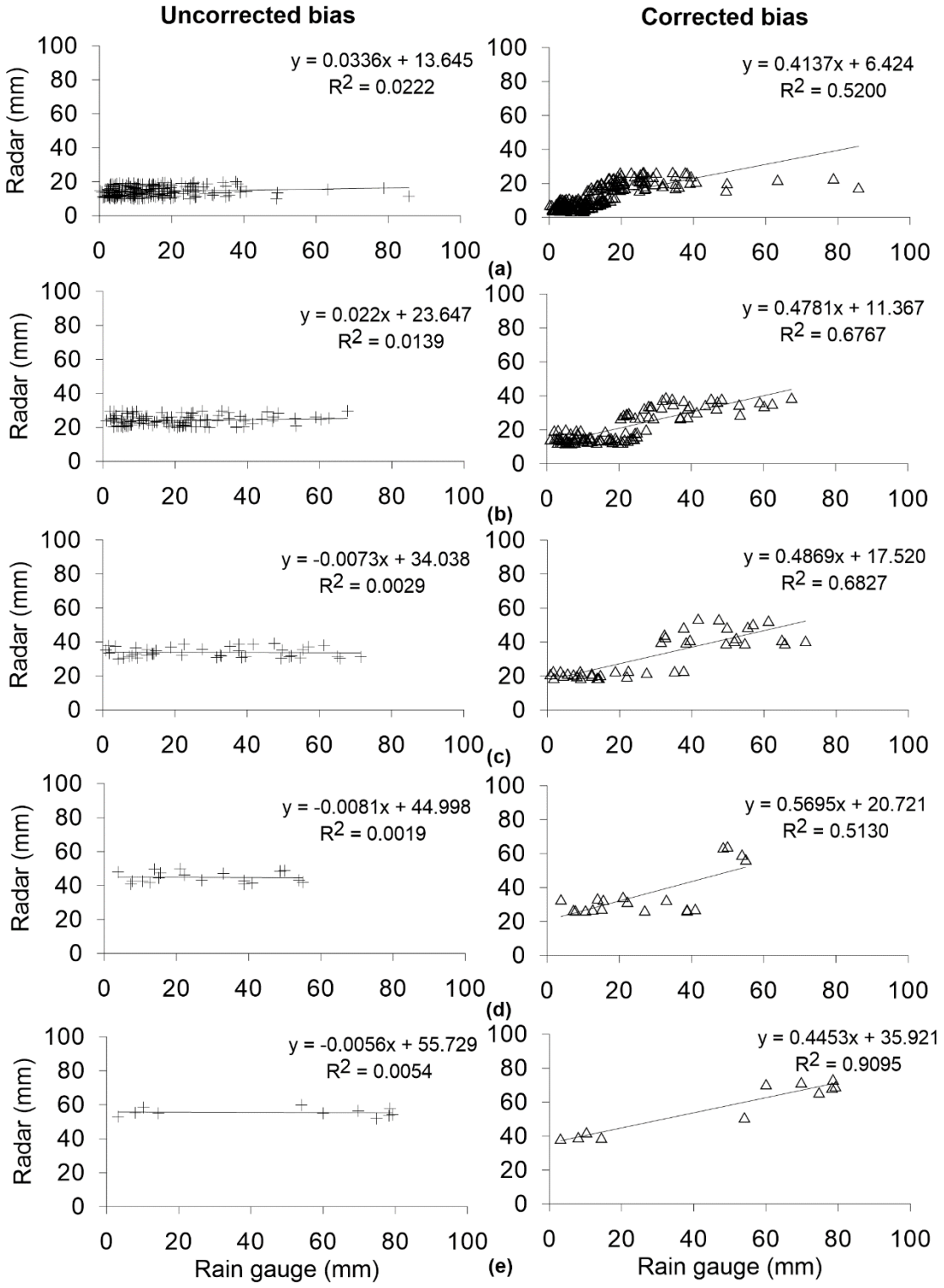

Figure 6 – Comparison between uncorrected and corrected radar rainfall events, according to the rainfall height intervals: (a) 10-20 mm, (b) 20-30 mm, (c) 30-40 mm, (d) 40-50 mm, (e) 50-60 mm.

Overall, there was a significant improvement in the R^2 ranging from 0.52 to 0.91 for the intervals 10-20 and 50-60 mm, respectively, with the average value of 0.66. This increasing in R^2 (from the 10-20 to 50-60 mm interval) can be explained by the less variability of the

rainfall events by intervals, which improves the polynomial fit and consequently the bias correction.

Figure 7 shows the performance of the CDF_{mod} method for adjusting rainfall radar estimated considering all rainfall events. We observed that there was a remarkable improvement after applying the bias correction scheme. The NSE increases from 0.11 to 0.63 and MAE decrease from 11.66 to 6.97 mm. As a result, the Figure 7c shows a CDF after bias corrected significantly improved, with the extreme values similar to those existing in the CDF of rain gauge data.

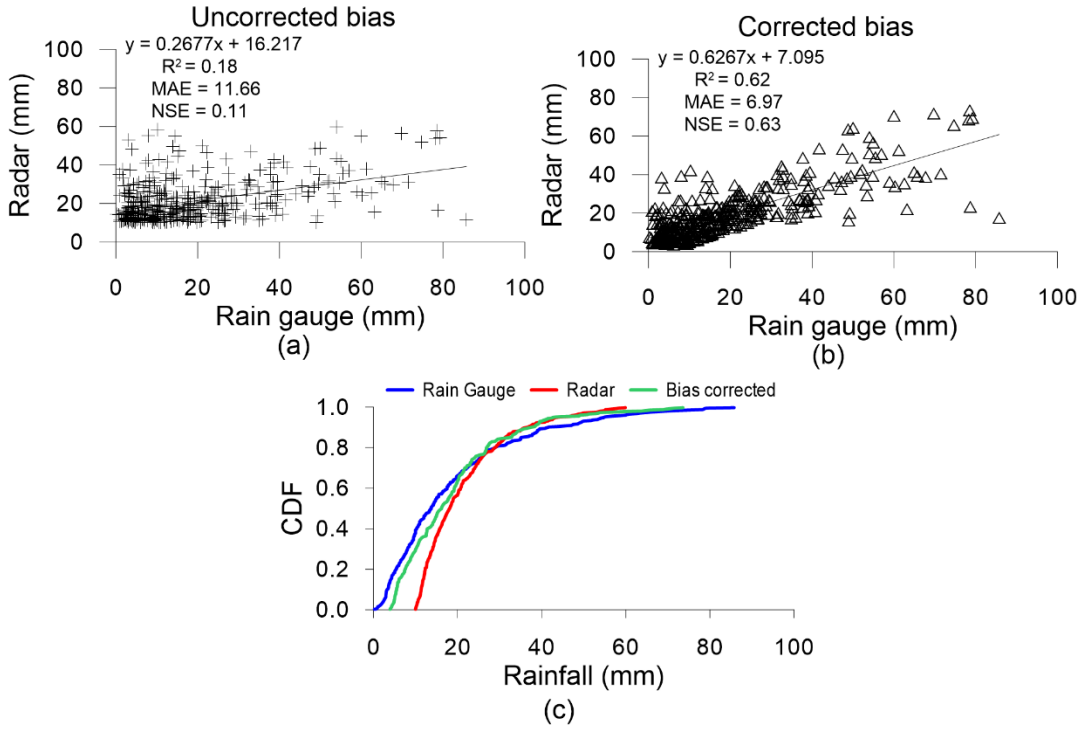

Figure 7 – Comparison between rainfall events based on radar and rain gauge, considering all rainfall events, for: (a) uncorrected bias, and (b) corrected bias. (c) Cumulative Density Function (CDF) of either rain gauge or (corrected) radar data.

From Figure 8, it can be seen the performance of bias adjustment in terms of rainfall duration: 0-1h, 1-3h, 3-6h, 6-9h, 9-24h. For all rainfall durations, we found that the radar data underestimated rainfall, and also presented a considerably low *NSE* values and high *MAE* values. This is in agreement with those reported in the literature (i.e., Thorndahl, Søren et al., 2014). Thus, the NSE values varied from – 0.01 to 0.53 and the MAE values varied from 8.38 to 14.53 mm for biased radar data. In contrast, after bias corrected, the events for all rainfall durations presented a great improvement in the *NSE* values ranging from 0.59 to 0.87 and *MAE*

values ranging from 4.53 to 7.73 mm. One should be note that the negative *NSE* value (6-9h event) was considerably improved, reaching a *NSE* value of 0.62.

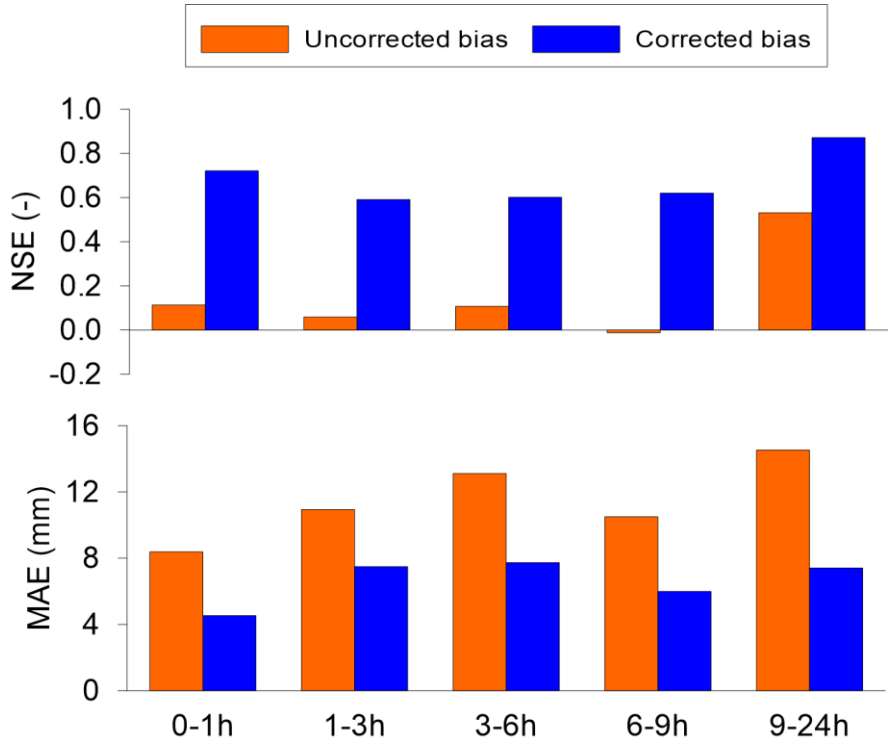

Figure 8 – Performance of bias adjustment on different rainfall events time scales.

3.2 Advantages and limitations

Our CDF_{mod} method has some advantages and limitations. The main advantage is that the method can be easy applied for rainfall events with daily, hourly, and sub-hourly duration. In addition, the choice for grouping the rainfall in intervals makes it possible to fit polynomial equations for bias correction at different periods of the year. This is possible because the method focuses on the use of rainfall height event instead of the period in which the event occurred.

Despite the advantages, the method presented here also has limitations, which can hinder its application. In general, the original CDF matching method (Reichle; Koster, 2004) might subject of overfitting in some cases (Lafon et al., 2013), which can give very precise results for a particular data set, but may not give similarly good results on new data, even over the same location. There is also the possibility of obtaining negative rainfall values for a few events, which is linked to an inappropriate fit of the polynomial equation. Furthermore,

although we have used only ~2 years of rainfall data, for some intervals a longer period may be necessary to fit a satisfactory polynomial equation.

4 Conclusions

We have developed a new modified version of the CDF matching approach (here called CDF_{mod}) to correct biased radar rainfall estimates on daily, hourly and sub-hourly basis. Our approach focusses on removing systematic biases by adopting intervals of rainfall height. To achieve this, rainfall data at 1-minute timestep from 34 tipping bucket were used as ground truth. We adjusted approximately 2-year high resolution (January_2016 to February_2018) radar rainfall dataset in the Campo Grande city, Mato Grosso do Sul State, Brazil.

We demonstrate the added value of the proposed bias correction scheme for radar-based rainfall estimates. The results showed that Nash-Sutcliffe Efficiency (*NSE*) index increased from 0.11 to 0.63 and Mean Absolute Error (*MAE*) decreased from 11.66 (biased data) to 6.97 mm (unbiased data) for all rainfall events (408 events).

The method is easy to apply, but the users must be careful about the potential overfitting issue of the polynomial equation. It can be applied for rainfall events with daily, hourly, and sub-hourly durations. Our findings are particularly useful in the case of rainfall-runoff models for urban flooding. Therefore, we highlight the opportunity of significant improvement on the radar rainfall estimates at sub-hour timescale.

5 Acknowledgements

The authors would like to thank the National Center for Monitoring and Early Warning of Natural Disasters (CEMADEN) for the use of radar dataset and the Campo Grande City Council for rain gauge data. This study was supported by grants from the Ministry of Science, Technology, Innovation and Communication – MCTIC and National Council for Scientific and Technological Development – CNPq (grants 441289/2017-7 and 306830/2017-5) and Coordination for the Improvement of Higher Education Personnel - CAPES (Finance Code 001 and Capes PrInt).

6 References

ABON, C. C.; KNEIS, D.; CRISOLOGO, I.; BRONSTERT, A.; DAVID, C. P. C.; HEISTERMANN, M. Evaluating the potential of radar-based rainfall estimates for streamflow and flood simulations in the Philippines. **Geomatics, Natural Hazards and Risk,** v. 7, n. 4, p. 1390-1405, https://doi.org/10.1080/19475705.2015.1058862, 2016.

AFSHAR, M. H.; YILMAZ, M. T.; CROW, W. T. Impact of Rescaling Approaches in Simple Fusion of Soil Moisture Products. **Water Resources Research,** v. 55, n. 9, p. 7804-7825, 10.1029/2019wr025111, 2019.

ANAGNOSTOU, E. N.; NEGRI, A. J.; ADLER, R. F. Statistical Adjustment of Satellite Microwave Monthly Rainfall Estimates over Amazonia. **Journal of Applied Meteorology,** v. 38, n. 11, p. 1590-1598, https://doi.org/10.1175/1520-0450(1999)038<1590:SAOSMM>2.0.CO;2, 1999.

ATLAS, D.; ROSENFELD, D.; WOLFF, D. B. Climatologically Tuned Reflectivity-Rain Rate Relations and Links to Area-Time Integrals. **Journal of Applied Meteorology,** v. 29, n. 11, p. 1120-1135, https://doi.org/10.1175/1520-0450(1990)029<1120:CTRRRR>2.0.CO;2, 1990.

BERNE, A.; KRAJEWSKI, W. F. Radar for hydrology: Unfulfilled promise or unrecognized potential? **Advances in Water Resources,** v. 51, p. 357-366, https://doi.org/10.1016/j.advwatres.2012.05.005, 2013.

BORGA, M.; TONELLI, F.; MOORE, R. J.; ANDRIEU, H. Long-term assessment of bias adjustment in radar rainfall estimation. **Water Resources Research,** v. 38, n. 11, p. 8-1-8-10, 10.1029/2001wr000555, 2002.

BRINGI, V. N.; RICO-RAMIREZ, M. A.; THURAI, M. Rainfall Estimation with an Operational Polarimetric C-Band Radar in the United Kingdom: Comparison with a Gauge Network and Error Analysis. **Journal of Hydrometeorology,** v. 12, n. 5, p. 935-954, https://doi.org/10.1175/jhm-d-10-05013.1, 2011.

BROCCA, L.; HASENAUER, S.; LACAVA, T.; MELONE, F.; MORAMARCO, T.; WAGNER, W.; DORIGO, W.; MATGEN, P.; MARTÍNEZ-FERNÁNDEZ, J.; LLORENS, P.; LATRON, J.; MARTIN, C.; BITTELLI, M. Soil moisture estimation through ASCAT and AMSR-E sensors: An intercomparison and validation study across Europe. **Remote Sensing of Environment,** v. 115, n. 12, p. 3390-3408, https://doi.org/10.1016/j.rse.2011.08.003, 2011.

DRUSCH, M.; WOOD, E. F.; GAO, H. Observation operators for the direct assimilation of TRMM microwave imager retrieved soil moisture. **Geophysical Research Letters,** v. 32, n. 15, https://doi.org/10.1029/2005GL023623, 2005.

FICCHÌ, A.; PERRIN, C.; ANDRÉASSIAN, V. Impact of temporal resolution of inputs on hydrological model performance: An analysis based on 2400 flood events. **Journal of Hydrology,** v. 538, p. 454-470, https://doi.org/10.1016/j.jhydrol.2016.04.016, 2016.

GOUDENHOOFDT, E.; DELOBBE, L. Evaluation of radar-gauge merging methods for quantitative precipitation estimates. **Hydrol. Earth Syst. Sci.,** v. 13, n. 2, p. 9, https://doi.org/10.5194/hess-13-195-2009, 2009.

GUPTA, R.; BHATTARAI, R.; MISHRA, A. Development of Climate Data Bias Corrector (CDBC) Tool and Its Application over the Agro-Ecological Zones of India. **Water,** v. 11, n. 5, p. 1102, https://doi.org/10.3390/w11051102, 2019.

GURUNG, P. Integration of gauge and radar rainfall to enable best simulation of hydrological parameters. **Hydrological Sciences Journal,** v. 62, n. 1, p. 114-123, https://doi.org/10.1080/02626667.2015.1117087, 2017.

JAHN, M. Economics of extreme weather events: Terminology and regional impact models. **Weather and Climate Extremes,** v. 10, p. 29-39, https://doi.org/10.1016/j.wace.2015.08.005, 2015.

JAMES, W. P.; ROBINSON, C. G.; BELL, J. F. Radar-Assisted Real-Time Flood Forecasting. **Journal of Water Resources Planning and Management,** v. 119, n. 1, p. 32-44, doi:10.1061/(ASCE)0733-9496(1993)119:1(32), 1993.

KRAJEWSKI, W. F.; SMITH, J. A. Radar hydrology: rainfall estimation. **Advances in Water Resources,** v. 25, n. 8–12, p. 1387-1394, http://dx.doi.org/10.1016/S0309-1708(02)00062-3, 2002.

LAFON, T.; DADSON, S.; BUYS, G.; PRUDHOMME, C. Bias correction of daily precipitation simulated by a regional climate model: a comparison of methods. **International Journal of Climatology,** v. 33, n. 6, p. 1367-1381, https://doi.org/10.1002/joc.3518, 2013.

LI, H.; SHEFFIELD, J.; WOOD, E. F. Bias correction of monthly precipitation and temperature fields from Intergovernmental Panel on Climate Change AR4 models using equidistant quantile matching. **Journal of Geophysical Research: Atmospheres,** v. 115, n. D10, https://doi.org/10.1029/2009JD012882, 2010.

LOOPER, J. P.; VIEUX, B. E. An assessment of distributed flash flood forecasting accuracy using radar and rain gauge input for a physics-based distributed hydrologic model. **Journal of Hydrology,** v. 412-413, p. 114-132, https://doi.org/10.1016/j.jhydrol.2011.05.046, 2012.

LUO, P.; MU, D.; XUE, H.; NGO-DUC, T.; DANG-DINH, K.; TAKARA, K.; NOVER, D.; SCHLADOW, G. Flood inundation assessment for the Hanoi Central Area, Vietnam under historical and extreme rainfall conditions. **Scientific Reports,** v. 8, n. 1, p. 12623, https://doi.org/10.1038/s41598-018-30024-5, 2018.

MARSHALL, J. S.; PALMER, W. M. K. THE DISTRIBUTION OF RAINDROPS WITH SIZE. **Journal of Meteorology,** v. 5, n. 4, p. 165-166, https://doi.org/10.1175/1520-0469(1948)005<0165:TDORWS>2.0.CO;2, 1948.

MCKEE, J. L.; BINNS, A. D. A review of gauge–radar merging methods for quantitative precipitation estimation in hydrology. **Canadian Water Resources Journal / Revue canadienne des ressources hydriques,** v. 41, n. 1-2, p. 186-203, https://doi.org/10.1080/07011784.2015.1064786, 2015.

MCMILLAN, H.; JACKSON, B.; CLARK, M.; KAVETSKI, D.; WOODS, R. Rainfall uncertainty in hydrological modelling: An evaluation of multiplicative error models. **Journal of Hydrology,** v. 400, n. 1, p. 83-94, https://doi.org/10.1016/j.jhydrol.2011.01.026, 2011.

MICHELSON, D. B.; KOISTINEN, J. Gauge-Radar network adjustment for the baltic sea experiment. **Physics and Chemistry of the Earth, Part B: Hydrology, Oceans and Atmosphere,** v. 25, n. 10, p. 915-920, https://doi.org/10.1016/S1464-1909(00)00125-8, 2000.

MÜLLER, H.; HABERLANDT, U. Temporal rainfall disaggregation using a multiplicative cascade model for spatial application in urban hydrology. **Journal of Hydrology,** v. 556, p. 847-864, https://doi.org/10.1016/j.jhydrol.2016.01.031, 2018.

NASH, J. E.; SUTCLIFFE, J. V. River flow forecasting through conceptual models part I — A discussion of principles. **Journal of Hydrology,** v. 10, n. 3, p. 282-290, https://doi.org/10.1016/0022-1694(70)90255-6, 1970.

NIELSEN, J. E.; THORNDAHL, S.; RASMUSSEN, M. R. A numerical method to generate high temporal resolution precipitation time series by combining weather radar measurements with a nowcast model. **Atmospheric Research,** v. 138, p. 1–12, https://doi.org/10.1016/j.atmosres.2013.10.015, 2014.

OLIVEIRA, P. T. S.; WENDLAND, E.; NEARING, M. A.; SCOTT, R. L.; ROSOLEM, R.; DA ROCHA, H. R. The water balance components of undisturbed tropical woodlands in the Brazilian cerrado. **Hydrol. Earth Syst. Sci.,** v. 19, n. 6, p. 2899-2910, 10.5194/hess-19-2899-2015, 2015.

REICHLE, R. H.; KOSTER, R. D. Bias reduction in short records of satellite soil moisture. **Geophysical Research Letters,** v. 31, n. 19, https://doi.org/10.1029/2004GL020938, 2004.

ROY, T.; SERRAT-CAPDEVILA, A.; GUPTA, H.; VALDES, J. A platform for probabilistic Multimodel and Multiproduct Streamflow Forecasting. **Water Resources Research,** v. 53, n. 1, p. 376-399, https://doi.org/10.1002/2016WR019752, 2017.

ROY, T.; VALDÉS, J. B.; LYON, B.; DEMARIA, E. M. C.; SERRAT-CAPDEVILA, A.; GUPTA, H. V.; VALDÉS-PINEDA, R.; DURCIK, M. Assessing hydrological impacts of short-term climate change in the Mara River basin of East Africa. **Journal of Hydrology,** v. 566, p. 818-829, https://doi.org/10.1016/j.jhydrol.2018.08.051, 2018.

ROY, T.; VALDÉS, J. B.; SERRAT-CAPDEVILA, A.; DURCIK, M.; DEMARIA, E. M. C.; VALDÉS-PINEDA, R.; GUPTA, H. V. Detailed overview of the multimodel multiproduct streamflow forecasting platform. **Journal of Applied Water Engineering and Research,** v. 8, n. 4, p. 277-289, 10.1080/23249676.2020.1799442, 2020.

RYZHKOV, A. V.; GIANGRANDE, S. E.; SCHUUR, T. J. Rainfall Estimation with a Polarimetric Prototype of WSR-88D. **Journal of Applied Meteorology,** v. 44, n. 4, p. 502-515, https://doi.org/10.1175/JAM2213.1, 2005.

SALVADORE, E.; BRONDERS, J.; BATELAAN, O. Hydrological modelling of urbanized catchments: A review and future directions. **Journal of Hydrology,** v. 529, p. 62-81, https://doi.org/10.1016/j.jhydrol.2015.06.028, 2015.

SCHLEISS, M.; OLSSON, J.; BERG, P.; NIEMI, T.; KOKKONEN, T.; THORNDAHL, S.; NIELSEN, R.; NIELSEN, J. E.; BOZHINOVA, D.; PULKKINEN, S. The accuracy of weather radar in heavy rain: a comparative study for Denmark, the Netherlands, Finland and Sweden. **Hydrol. Earth Syst. Sci. Discuss.,** v. 2019, p. 1-42, https://doi.org/10.5194/hess-2019-427, 2019.

SCHUURMANS, J. M.; BIERKENS, M. F. P.; PEBESMA, E. J.; UIJLENHOET, R. Automatic Prediction of High-Resolution Daily Rainfall Fields for Multiple Extents: The Potential of Operational Radar. **Journal of Hydrometeorology,** v. 8, n. 6, p. 1204-1224, 10.1175/2007jhm792.1, 2007.

SIK KIM, B.; KYUNG KIM, B.; SOO KIM, H. Flood simulation using the gauge-adjusted radar rainfall and physics-based distributed hydrologic model. **Hydrological Processes,** v. 22, n. 22, p. 4400-4414, doi:10.1002/hyp.7043, 2008.

SWITANEK, M. B.; TROCH, P. A.; CASTRO, C. L.; LEUPRECHT, A.; CHANG, H. I.; MUKHERJEE, R.; DEMARIA, E. M. C. Scaled distribution mapping: a bias correction method that preserves raw climate model projected changes. **Hydrol. Earth Syst. Sci.,** v. 21, n. 6, p. 2649-2666, https://doi.org/10.5194/hess-21-2649-2017, 2017.

THORNDAHL, S.; EINFALT, T.; WILLEMS, P.; NIELSEN, J. E.; TEN VELDHUIS, M. C.; ARNBJERG-NIELSEN, K.; RASMUSSEN, M. R.; MOLNAR, P. Weather radar rainfall data in urban hydrology. **Hydrol. Earth Syst. Sci.,** v. 21, n. 3, p. 1359-1380, https://doi.org/10.5194/hess-21-1359-2017, 2017.

THORNDAHL, S.; NIELSEN, J. E.; RASMUSSEN, M. R. Bias adjustment and advection interpolation of long-term high resolution radar rainfall series. **Journal of Hydrology,** v. 508, p. 214-226, https://doi.org/10.1016/j.jhydrol.2013.10.056, 2014.

TODINI, E. A Bayesian technique for conditioning radar precipitation estimates to rain-gauge measurements. **Hydrol. Earth Syst. Sci.,** v. 5, n. 2, p. 187-199, 10.5194/hess-5-187-2001, 2001.

UNITED NATIONS. **World Urbanization Prospects: The 2018 Revision**. United Nations, Department of Economic and Social Affairs, Population Department. 2018

WANG, L.-P.; OCHOA-RODRÍGUEZ, S.; SIMÕES, N. E.; ONOF, C.; MAKSIMOVIĆ, Č. Radar–raingauge data combination techniques: a revision and analysis of their suitability for urban hydrology. **Water Science and Technology,** v. 68, n. 4, p. 737-747, https://doi.org/10.2166/wst.2013.300, 2013.

WANG, L.; CHEN, W. Equiratio cumulative distribution function matching as an improvement to the equidistant approach in bias correction of precipitation. **Atmospheric Science Letters,** v. 15, n. 1, p. 1-6, doi:10.1002/asl2.454, 2014.

WMO. **Manual on Flood Forecasting and Warning**. World Meteorological Organization, 2011. ISBN 9789263110725.

_____. **Flood Forecasting and Early Warning**. World Meteorological Organization, 2013.

WOOD, A. W.; MAURER, E. P.; KUMAR, A.; LETTENMAIER, D. P. Long-range experimental hydrologic forecasting for the eastern United States. **Journal of Geophysical Research: Atmospheres,** v. 107, n. D20, p. ACL 6-1-ACL 6-15, https://doi.org/10.1029/2001JD000659, 2002.

CHAPTER 3

Towards reducing flood disasters in the Prosa basin (Brazil) by the development of early alert mobile application

Mattos, T. S., Oliveira, P. T. S., Bruno, L. S., Crivellaro, L. L., Roy, T., Carvalho, G. A., Pereira, R. B., Lucas, M. C. Towards Reducing Flood Disasters in the Prosa Basin (Brazil) by the Development of Early Alert Mobile Application. *Environmental Modelling & Software*. In preparation. (Impact factor, 2019: 4.807; Qualis CAPES: A1)

Abstract

Climate change threats, increasing urbanization, and a poor stormwater drainage network increase the risk of flood disaster if no effective risk management is done. To prevent the death of people and/or property damage due to floods, it is important to warn people in advance as possible. The Brazil often experiences floods that cause traumatic conditions in built environment followed by huge economic impact. Here, a Decision Support System coupled with a mobile application is used to develop a flood alert system across the Prosa basin (Brazil) to send early flood warning messages to population. Hydrologic Engineering Center's Hydrologic Modeling System (HEC-HMS) and River Analysis System (HEC-RAS) was used as the core of flood alert system because they provide forecasting of flood inundation areas and water level in the main river channel. The quantitative precipitation forecast (QPF) of Weather Research and Forecasting (WRF) was used here. The application based on Progressive Web Application was used to support the visualization of flood status and to deliver early warning messages for mobile devices. The flood hazard maps developed here is an essential information to decision making by the public authorities as well as to population for reducing flood disasters in the study area. Therefore, the widespread adoption of this mobile technology supported by scientific study has great potential for saving financial costs and reducing loss of lives.

Keywords: flood alert, flood prediction, runoff, stormwater

1 Introduction

Flooding in urban areas due to extreme stormwater in short time has caused material, economic, environmental and human losses in several places worldwide. It is the most devastating, widespread and frequent natural disaster present in human society (Teng et al., 2017; Nkwunonwo et al., 2020). According to WMO (2013), floods are among the most common natural disaster and have the greatest potential for damage of all natural disasters globally. For example, in the Brazil, some metropolises have experienced unprecedented heavy rainfall events, leading to deadly floods. The city of Sao Paulo (~12.3 million people) received about 114 mm of rainfall on 10 February 2020. It was the second-highest volume in 24 hours (on February) in the last 77 years of weather records. The city of Belo Horizonte (~2.5 million people) received the largest 24-hour rainfall (171.8 mm) in 110 years of rainfall records on January 2020.

Typically, urban flooding occurs when intense rainfall generates rapid runoff volumes from paved and built-up areas, exceeding the capacity of stormwater drainage systems. This condition can be exacerbated during flash floods (Norbiato et al., 2008), in which water level burden the crest of drainage network in shot time (minutes to a few hours) since the begin of rainfall event (Georgakakos, 1992). Further, debris in the drainage network due to lack of maintenance can aggravates urban flooding. Additionally, climate change threats, increasing urbanization, and poor drainage network, increases the risk of flooding if no risk management is performed (Henonin et al., 2013; Muñoz et al., 2018).

Since floods represent a significant role in the number of natural disasters globally (Freer et al., 2011), a great effort has been made to understand, assess and predict flood events and their negative impacts. Thus, computational models have been developed to address this purpose, for example in early alert system. The development and application of flood models usually comprises three steps during simulation: the conversion of rainfall to runoff (flood hydrograph), the propagation of flood wave across the river channel, and mapping of flood areas (Dimitriadis et al., 2016). Models are widely used to map flooding and flood exposure in urban areas (Ramirez et al., 2016), assessing the damage caused by extreme rainfall events (Silvestro et al., 2016), quantification of flood economic risk (Garrote et al., 2016), assessing the impact of urbanization (Campana; Tucci, 2001; Miller; Hess, 2017) and climate change on urban flood volumes (Zhou et al., 2018), real time early flood forecasting (Nester et al., 2016; Neri et al., 2020).

Early alert system is a fundamental part of the whole flood risk management because can enhance people preparedness against floods disasters (Plate, 2002; Neri et al., 2020). Establishing a flood warning system at risk requires the combination of data collection, forecasting computational models, warning and human resources (WMO, 2013). The major technological infrastructure required for the flood alert system is a data collection from gauging, an operating system and hardware (workstations), software (needed to process, analyze, and display observation data), an application program to dissemination of flood warning, and maintenance and backup program (to ensure the data availability over time) (UCAR, 2010). In general, the flood alert application programs have the following tasks (Azam et al., 2017): real time processing and storing of collected data, display streamflow forecasting and predicted water level information, checking the predicted water level for exceedance of threshold value, and determination of parameters using observed data.

Flood alert systems can operate with Decision Support Systems (DSS) that has been developed by using models of flood management. For example, Todini (1999) developed an integrated tool for planning and management that allows location of areas at risk and estimation of expected damages to forecast floods and inundation. Koussis et al. (2003) proposed an operational system for forecasting flood risk using an integrated hydro-meteorological model. Ahmad and Simonovic (2006) created a DSS by integrating the database (topographic, hydrologic, and land use data), model base, and graphical tools to assist decision makers during different phases of food management. Qi and Altinakar (2011) presented a Geographical Information System (GIS)-based DSS for flood management using a framework based on a two-dimensional (2D) flood analysis model. Mure-Ravaud et al. (2016) developed an operational real-time flood forecasting system using data assimilation to provide hourly flood alerts.

In a flood alert system, the warning lead time is critical because longer the lead time, earlier the people will be aware about flood. Hence, increasing this time improves the potential to limit possible loss of property and/or human lives. The developed Numerical Weather Prediction (NWP) models in the past decades is a good form to provide a longer lead time Quantitative Precipitation Forecast (QPF) (WMO, 2011; Li et al., 2017). There are many weather prediction models into operational use, such as the European Centre Medium-Range Weather Forecasts (ECMWF) Ensemble Prediction System (EPS) (Molteni et al., 1996; Ye et al., 2014), the numerical forecast model of the China Meteorological Agency (Xue; Liu, 2007), the NWP model of the Japan Meteorological Agency (Yamaguchi et al., 2009), and the Weather Research and Forecasting (WRF) model (Maussion et al., 2011; Chu et al., 2018).

In Brazil, the Center for Natural Disaster Monitoring and Alert (CEMADEN), led by the Ministry of Science and Technology (MCT), aims at developing, testing and implementing

monitoring and forecast systems for natural disasters. However, as it is a recently created center, operational flood forecast systems have not been developed yet (Fan et al., 2016).

Most of the operational flood forecast systems in Brazil are led by the Geological Survey of Brazil (CPRM). It operates forecast systems in vulnerable areas at some rivers, such as Doce (MG), Caí (RS), Taquari (RS), Parnaíba (Piauí), Muriaé (RJ e MG); Negro (AM), Acre (AC), and Branco (RR). The forecasts are available at CPRM website (http://www.cprm.gov.br) in a system called *Sistema de Alerta Contra Enchentes* (Fan et al., 2016). Despite this, alert systems is a challenge in Brazil because early flood forecasting is still deficient (Casagrande et al., 2017), despite the fact that floods are a recurring phenomenon in urban areas. For instance, the city of Campo Grande (~906,000 people), Mato Grosso do Sul State (Brazil), has been subject to flooding despite having get started a hydrometeorological monitoring system since 2014 and many structural measures against floods (e.g. dams and detention basins) have been implemented. The Prosa basin, located northwest of the municipality's urban region, is among the most affected by floods. The development of a flood alert mobile application would be minimizing negative impacts due flooding. Thus, the main objective of this study is to develop a flood alert system in the Prosa basin, and disseminate its warning messages by means of an application for mobile devices.

2 Material and methods

2.1 Study Area

The Prosa Basin (PB) has an area of ≃32 km², and it is located in the municipality of Campo Grande, Mato Grosso do Sul State, Brazil (Figure 1). This basin is mainly flat, with slope steepness of ranging from 3.8 to 8.0%. The main rivers in the basin are Prosa, Sóter, Desbarrancado, Joaquim Portugues, Revellion and Vendas River (PDDU, 2008).

The annual mean rainfall (between 1992 and 2016) considering the hydrological year, from October to September, is 1,417 ± 203 mm. The monthly minimum and maximum rainfall events occur in winter (34 mm in July) and summer (217 mm in January), respectively. The daily mean air temperature is 24.2 ± 5.2 °C. According to the Köppen climate type, the climate in the PB is Aw type, tropical with dry winter and rainy summer (Alvares et al., 2013).

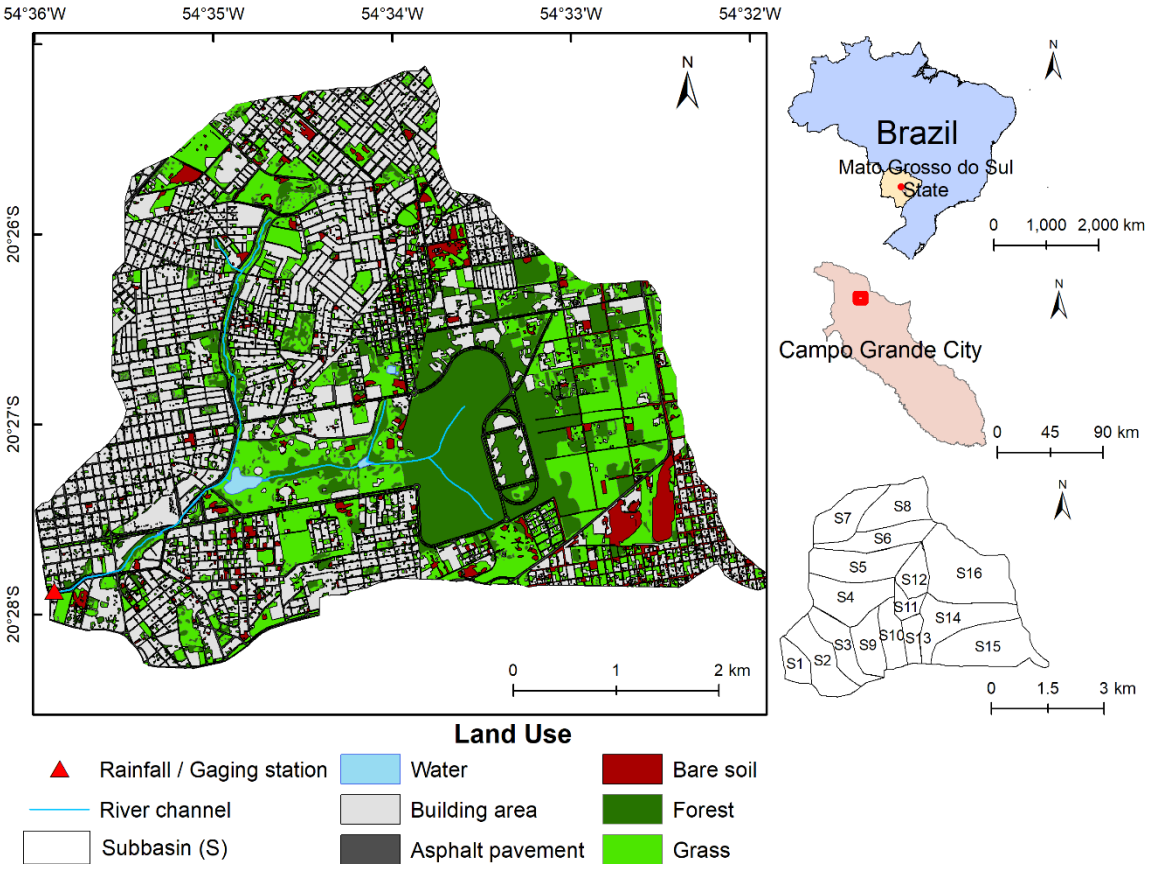

Figure 1 – Location and land cover of study area over the 2016 year.

The PB is characterized by large fraction of impervious surface, mostly commercial and residential areas. The land use types in the region can be classified into five categories: grass (24%), forests (19%), bare soil (6%), asphalt pavement (10%), building area (i.e. residential and commercial areas, 41%). The predominant soil type in the basin area has sandy clay loam texture, and stable infiltration rate changes approximately from 10 $mm.h^{-1}$ to 50 $mm.h^{-1}$ (Planurb, 1991; Sobrinho, 2015).

This basin has recurrence of flood events and the flow regime is influenced by dams, bridges, holding basins, power dissipation structures and channels with different wear layer. Historical records of stormwater drainage and flood damage indicate that the region has experienced an increase in flood frequency and magnitude due to urbanization (PDDU, 2008).

3 Decision support framework components

For develop the flood alert system, we used a Decision Support Framework (Figure 2) for flood management by an integrated computational modelling approach. *Ad hoc*, (1) QPF data acquisition fed by online network data transfer is utilized; (2) The streamflow is forecasted by a semi-distributed hydrological model; and (3) routed by a 1D-2D unsteady river flow to producing flood maps; and (4) the flood alert is sent to an application developed for mobile devices.

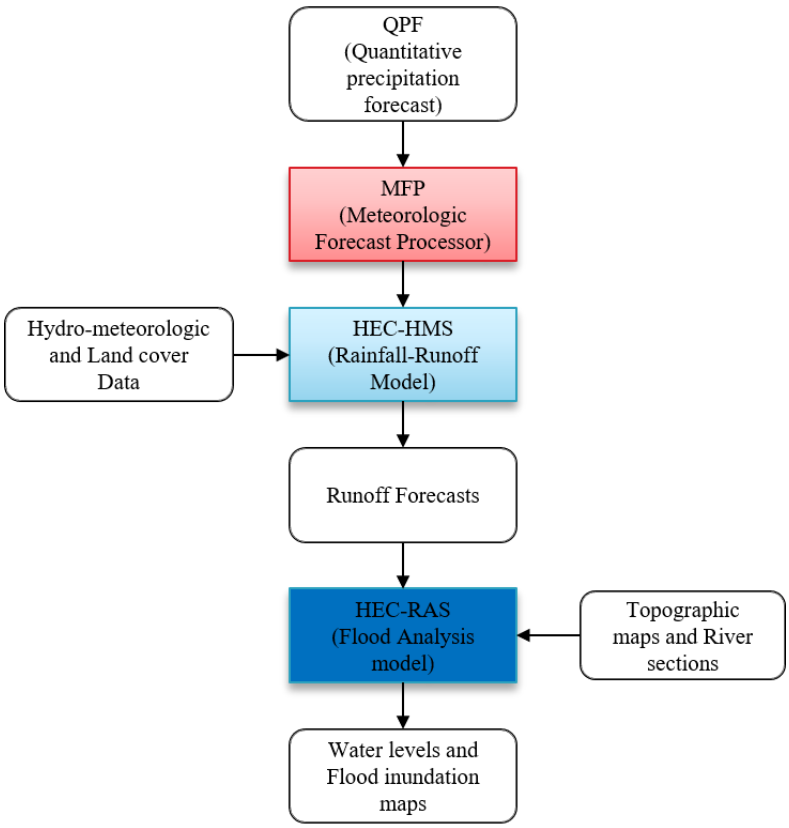

Figure 2 – Flowchart of the Decision Support System (DSS).

As shown in Figure 2, we used programs developed by the Hydrologic Engineering Center (HEC) of U.S. Army Corps of Engineers (USACE), which has been developing computer software for hydrological engineering and water resource management procedures since 1964 (available at http://www.hec.usace.army.mil/). Here, HEC programs was selected because they are peer reviewed, user friendly and free of change in the public domain. For the application of rainfall-runoff and river analysis, HEC-HMS (Hydrological Modeling System) and HEC-RAS (River Analysis System) programs were selected, respectively. The MFP was used to combine observed precipitation data and future precipitation (QPF) into a single precipitation dataset that is used by HEC-HMS. Moreover, the HEC-RTS (Real-Time Simulation) program was used to communicate between the data and programs. The framework

uses the HEC-Data Storage System (HEC-DSS) database file format to send data between models.

HEC-RTS is a public version of CWMS (The U.S. Army Corps of Engineers Corps Water Management System), which provides support for operational decision making by forecast simulation modeling using HEC models, such as rainfall-runoff modeling with HEC-HMS based on gaged or radar-based precipitation, and QPF or other future precipitation scenarios; The river hydraulics program HEC-RAS computes river stages and water surface profiles for these scenarios and an inundation boundary and depth map of water in the flood plain can be calculated (Charley, 2010).

3.1 HEC-HMS hydrological model

The HEC-HMS is a conceptual hydrological model designed to simulate the rainfall-runoff process of dendritic watershed systems, and can be applied to analyze urban flooding, flood frequency, flood loss reduction, and flood warning system planning (USACE-HEC, 2015). Several studies have used HEC-HMS as a part of DSS to flood forecasting events. Reichel et al. (2009) proposed a framework to assess real-time flood forecast integrating radar rainfall data, GIS, HEC-HMS, and a short-term precipitation nowcasting system. Fakhruddin (2015) presented a flood forecasting model by assimilating the satellite and hydrological gauge rainfall data into HEC-HMS. Şensoy et al. (2018) developed a DSS for real-time flood management using integrated models (i.e. HEC-HMS and HEC-RAS).

The HEC-HMS contains four main components (USACE-HEC, 2016): a) An analytical model to calculate overland flow (runoff) as well as flow routing (flood wave propagation), b) a graphical user interface illustrating hydrologic system components, c) a system for storing and managing data, and d) a means for displaying and reporting model outputs. The model includes all necessary hydrological components of runoff such as loss, transform, baseflow, and channel routing.

In this study, the PB was discretized into 16 subcatchments (Figure 1) and the HEC-HMS event simulation approach was adopted. The model components include computing runoff depth (Soil Conservation Service Curve number (CN) method), overland flow and interflow transformation (the Clark's unit hydrograph), baseflow (via Recession method) and channel routing scheme (Muskingum-Cunge method). The datasets used in catchment

delineation, land cover classification, transformation method, were obtained from remote sensing, whereas baseflow, routing and loss method parameters were derived from both, observed data and remote sensing data, and literature (USDA-NRCS, 1986).

3.2 HEC RAS hydraulic model

The downstream river channel capacity may be exceeded during a flood event, and the information on downstream water levels and flood inundation areas are fundamental for the flood alert system. Many studies have used the HEC-RAS to flood forecasting modeling (Mashriqui et al., 2014; Merkuryeva et al., 2015; Adams et al., 2018; Şensoy et al., 2018), and it is shown that accuracy comparable to more sophisticated hydraulic models can be achieved (Hicks; Peacock, 2005). Here, the HEC-RAS model was utilized in the DSS to compute stages and potential flooding from the forecasted flood hydrographs.

HEC-RAS is an integrated system of software, designed for interactive use in a multi-tasking, multi-user network environment. The system is comprised of a graphical user interface (GUI), separate hydraulic analysis components, data storage and management capabilities, graphics and reporting facilities. The HEC-RAS system contains four one-dimensional river analysis components, and the current version of HEC-RAS supports: Steady and Unsteady flow water surface profile calculations, combined 1D and 2D hydrodynamics, spatial mapping of many computed parameters (Depth, water surface elevation, velocity, etc), water temperature analysis, water quality analyses and solves the 1D and 2D full Saint-Venant equations for an unsteady open channel flow (Brunner, 2016). Here, HEC-RAS simulations was performed by combining 1D and 2D within a single unsteady flow model, that is, 1D modeling in the river channel and 2D modeling on floodplain surrounding the main river channel.

3.3 Flood model calibration and validation

The models HEC-HMS and HEC-RAS was calibrated and validated using rainfall and discharge measured data between April 2015 and November 2017 at the rainfall-gauging station (Figure 1). The permeable area information was used according to the land cover study over the 2016 year. The HEC-HMS was calibrated using the Time of Concentration (*Tc*) of Prosa

basin, Storage Coefficient (*R*), and Curve Number (*CN*), whereas HEC-RAS was calibrated by means of the Manning`s roughness coefficient (*n*).

The initial values of parameters needed for the calibration are required to start an optimization process and were calculated mostly by using the mathematical methods available from hydrologic text books. The time of concentration was calculated by using Technical Report 55 (TR-55) method, which is computed by accumulating runoff travel times for consecutive components of the drainage conveyance system (sheet flow, shallow concentrated flow, and open channel flow) (USDA-NRCS, 1986). The initial values of the Storage Coefficient were estimate by Nash Model (Yoo et al., 2014), and the Curve Number was estimated as a function of land use, soil type, and watershed antecedent moisture according to TR-55 (USDA-NRCS, 1986). The initial value of the Manning`s roughness coefficient was selected by field campaigns, photographs, and literature values (Brunner, 2016).

The flood model was calibrated using two rainfall events and validated against six other events. The calibrated hydrological and hydraulic parameters are presented in Table 1 and Table 2, respectively. To evaluate the performance of model calibration and validation, the Coefficient of determination (R^2), the RMSE - Observations Standard Deviation Ratio (RSR), Nash–Sutcliffe Efficiency (NSE) index, and the Kling-Gupta efficiency (KGE) was used against measured discharge data in the PB outlet.

Table 1. Calibrated parameters of the HEC-HMS hydrological model.

Method	Clark unit hydrograph		Loss model
Sub-basin	Time of concentration (h)	Storage coefficient (h)	Curve number[1] (CN)
S1	0.09	0.10	81
S2	0.08	0.10	71
S3	0.09	0.10	70
S4	0.22	0.10	62
S5	0.20	0.10	72
S6	0.72	0.11	47
S7	0.69	0.09	58
S8	0.67	0.09	51
S9	0.31	2.26	81
S10	0.31	2.29	82
S11	0.72	2.35	80
S12	0.95	2.34	77
S13	0.29	2.33	74
S14	1.01	1.66	69
S15	1.34	1.74	67
S16	0.89	1.84	72

[1]CN for average runoff condition.

Table 2. Calibrated parameters of the HEC-RAS hydraulic model.

River	left overbank	main channel	right overbank
Desbarrancado	0.1	0.06	0.1
Joaquim	0.1	0.06	0.1
Pindare	0.015 - 0.06	0.015 - 0.20	0.015 - 0.06
Prosa[1]	0.015 - 0.10	0.015 - 0.20	0.015 - 0.10
Reveillon	0.040 - 0.08	0.020 - 0.04	0.030 - 0.08
Soter	0.015 - 0.09	0.015 - 0.10	0.015 - 0.06

[1]The main river channel.

3.4 WRF model

The quantitative precipitation forecast (QPF) of Weather Research and Forecasting (WRF) is provide by Weather Forecasting and Climate Research (CPTEC) in Brazil. The QPF is available at with five lead times, 24, 36, 48, 60 and 72h, temporal resolution of 1h and grid spatial resolution of 5 km x 5 km. The effort to develop WRF has begun in the latter 1990's as a collaborative partnership of the National Center for Atmospheric Research (NCAR) with several institutions in the United States of America (Powers et al., 2017). Since August 1 2018, the data are available at the CPTEC website (http://ftp.cptec.inpe.br/modelos/tempo/WRF/ams_05km/).

Several studies have evaluated WRF QPFs. Kumar et al. (2008) used the WRF model to study heavy rainfall in 2005, and showed that the WRF model could reproduce the rainfall event and its dynamical and thermodynamical characteristics. Givati et al. (2012) verified that the daily precipitation amount estimated by WRF showed good agreement against the measurements rain gauges. Jabbari et al. (2018) evaluated the forecasted precipitation and the observed precipitation, and concluded that the WRF model underestimated precipitation at the point and catchment scale; it performed better at the catchment scale. Rogelis and Werner (2018) assessed the potential of numerical weather prediction models for flood early warning, and verified that post-processed WRF precipitation adds value to the flood early warning system, although it showed little added value when compared to climatology.

3.5 Developing of the flood alert application

The flood alert mobile application was developed to provide information for flood potential risk, so that early effective practices could be taken. The application was developed with Progressive Web Application (PWA) standards, a web application that can be executed by the most varied hardware and devices, it also can be installed as a mobile application (Biørn-Hansen et al., 2017). The PWA was developed with the frameworks VueJS and Vuetify in javascript language, and is hosted by Google Firebase platform hosting services.

For the data storage it was chosen a non-relational database that is hosted also by Google Firebase platform and given its practical API to maintenance. Moreover, the "real time database" was chosen for storage and sync attributes to obtain updated data in real time (Chatterjee et al., 2018). Google Maps API was used to display the city map and markers on pre-established places, and the information about the channels, such as water stage, channel design illustration and threshold water level are displayed through graphs created using Google Charts API.

4 Results and Discussion

4.1 Calibration and validation of model

The calibrated model parameters (Table 1; Table 2) were used to generate hydrographs for Prosa Basin using the DSS (Figure 2). The assessment of the model performance is summarized in Table 3, according to rainfall events. In general, model simulation was satisfactory ($R^2 > 0.50$, $RSR \leq 0.70$, and $NSE > 0.50$) (Moriasi et al., 2007). In addition, the performance can be classified based on the value of KGE (Thiemig et al., 2013): good ($KGE \geq 0.75$); intermediate ($0.75 > KGE \geq 0.5$); poor ($0.5 > KGE > 0$); very poor ($KGE \leq 0$). Figure 3 shows the flood hydrographs performance results of two calibration and validation events.

Table 3 - Performance index for calibration and validation events.

Events Date (month/day/year)	NSE (-)	KGE (-)	R^2 (-)	RSR (-)
04/17/2015	0.63	0.12	0.87	0.61
05/27/2015 *	0.91	0.55	0.94	0.30
11/09/2015 *	0.88	0.50	0.92	0.35
12/25/2015	0.84	0.68	0.87	0.41
01/06/2016	0.83	0.59	0.85	0.42
01/08/2016	0.94	0.70	0.96	0.25
02/15/2016	0.85	0.82	0.86	0.38
05/23/2017	0.90	0.74	0.94	0.32
Mean	0.85	0.59	0.90	0.38
Standard deviation	0.10	0.22	0.04	0.11

* calibration events.

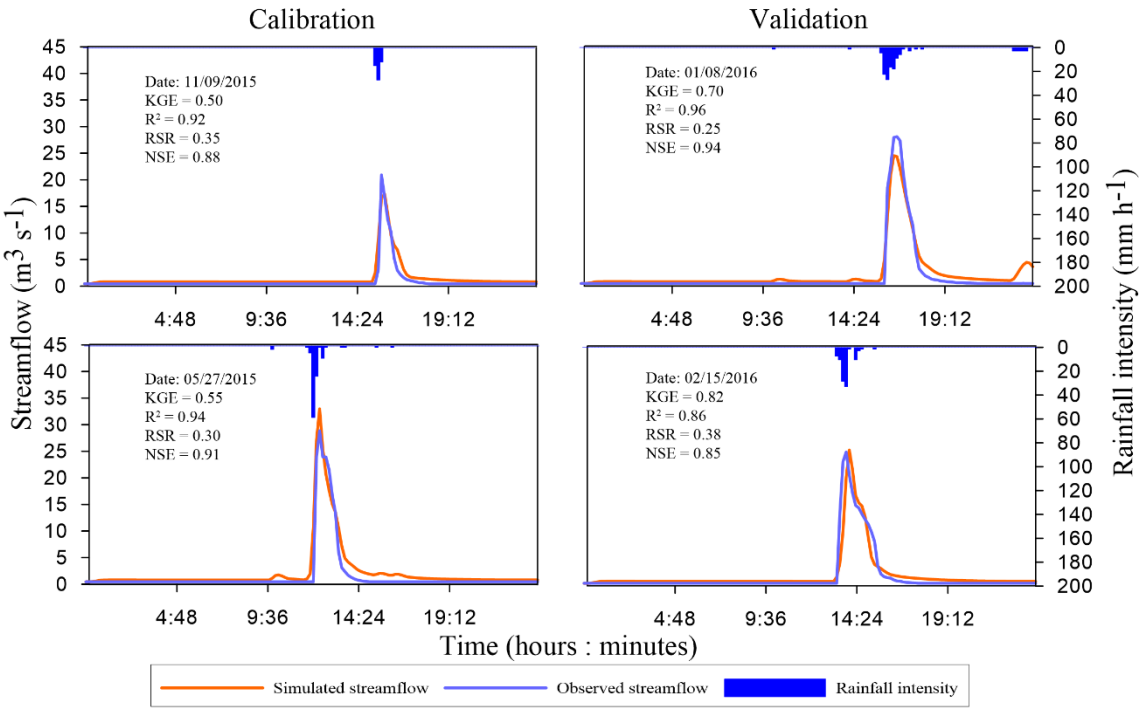

Figure 3 - The flood hydrographs for two calibration and validation events. The discharge and rainfall were measured in the Prosa basin outlet.

The results suggest that flood model has good performance for both calibration and validation periods. The mean RSR value of 0.38 and mean R^2 and NSE values both exceeding 0.80 indicates that the model is able to simulate the rainfall-runoff process in the Prosa basin. Considering the aim of this study, the mean value of the KGE higher than 0.5 is suitable and reveal the model accuracy in predicting the streamflow rate.

4.2 Flood alert application structure

After the model calibration and validation, the DSS output (water level and flood inundation maps) was used as input data into flood alert application to send warning to end users. Thus, it was created a python application to extract the flood inundation area and the water stage in pre-established cross sections of the main river channel. The specific river sections were chosen based on historical records of places with dangerous flood occurrences. Flow chart for the designing of flood alert application is shown in Figure 4.

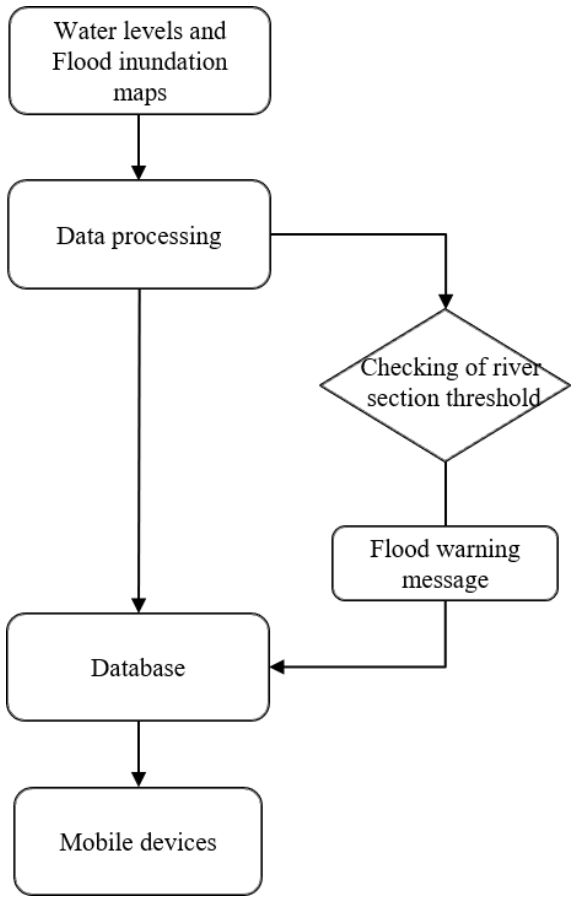

Figure 4 – Flowchart of the flood alert application.

The water stage and flood inundation map data generated by the models are processed before of sent to the database. The python application processes the data formatting them, respectively, as a GEOJSON and JSON following its patterns (Figure 5). In these files there are coordinates of the polygon vertices and the water stage, with its occurrence. The formatted data are sent to the database through the ‘pyrebase’ library that facilitates communications.

In the meantime, it is checked if the water stage surpasses the threshold of any pre-established section of the river. Threshold value is the maximum water level of each river section, after reaching it the communities living in prosa basin are vulnerable to flood hazard. If the condition occurs, a flood alert is generated and send to the users. The alert message is sent to users mobile devices through the Google Firebase's tool called 'Cloud Messaging' capable of sending 'push notifications' (Li et al., 2013).

The application collects data from the database and displays the flood surface and water level on the city map. If an alert was generated, it would be displayed as a notification even with the application closed.

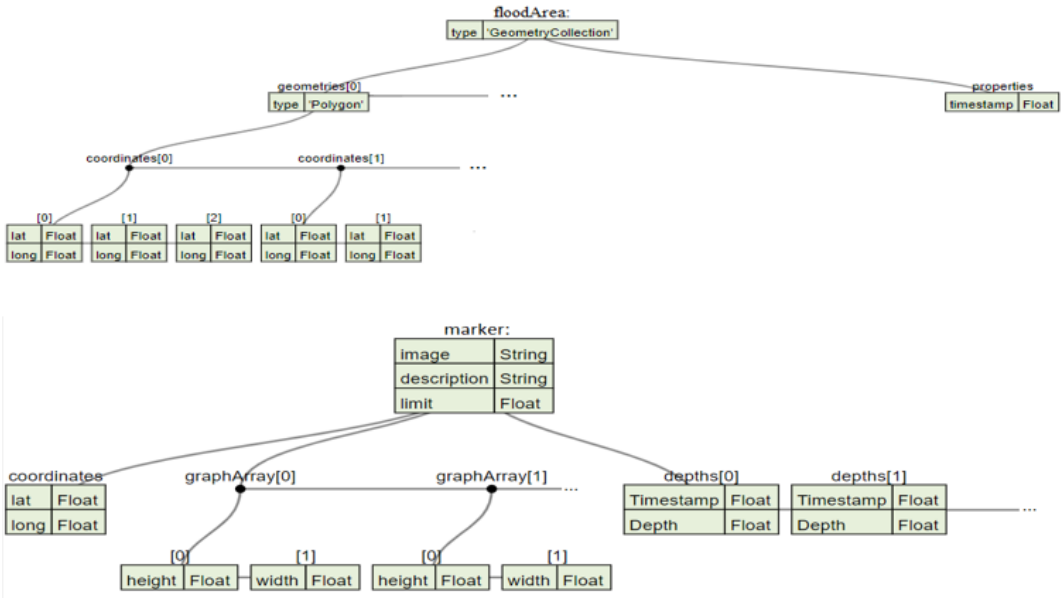

Figure 5 – Data structure for sending and storing it in the database.

4.2.1 Interface and features of application

To introduce the application`s interface and features, it was simulated the event of 18 November 2020 using WRF data (Figure 6). Here, it was used QPF with 48h lead time. Overall, the flow simulated ranged from 0.41 to ~21 $m^3 s^{-1}$ for an event rainfall estimated of 25.8 mm. Unfortunately, due to the lack of observed data, we cannot assess the WRF rainfall and the Flow simulated. Nevertheless, we will use the data from this simulation to present the interface and the characteristics of the application.

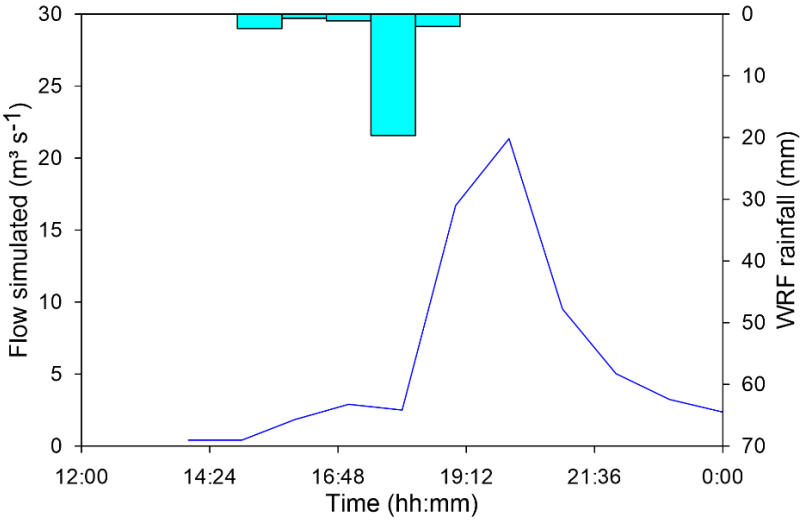

Figure 6 – Flow simulated using WRF rainfall data of the 18 November 2020.

After the water stage and flood inundation map data are processed and sent to the database, the Progressive Web Application (PWA) searches for the information and shows them to the user. The Figure 7a presents the home screen of the application which includes its main functions:

- A map with the flood surface area highlighted in blue and colored markers represent the predicted state of the water level at that point. The green color means that the area is safe, the yellow color means it is in a warning state and the red color means it is a dangerous area. For the event of 18 November 2020 all markers were green, indicating that the predicted level is less than the threshold of the selected time (20:00).
- On the top left corner of the screen, there is a date picker box. The initial selected date is the next available date forecasted.
- On the top right corner of the screen, there is a floating button that expands and shows options like “information about the application” and “report bugs”.

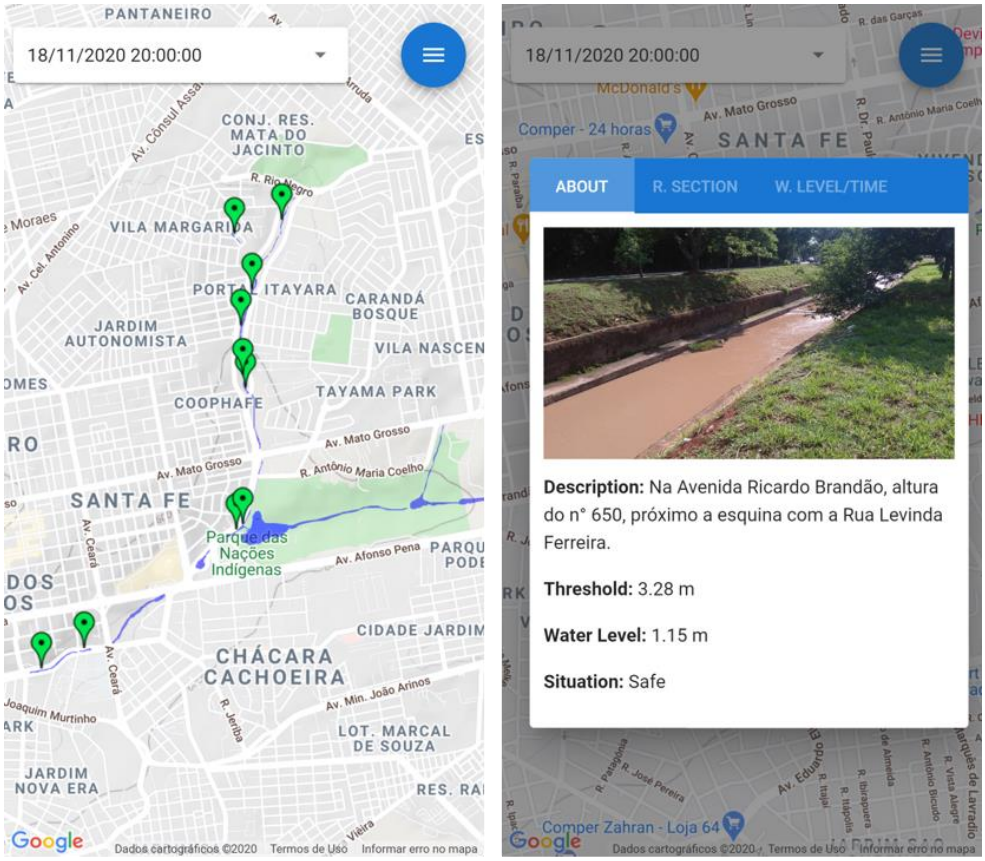

a) b)

Figure 7 – Flood risk are locations map in Prosa basin.

When the user clicks on the markers, they show information about the selected river section. As shown in Figure 7b, the first tab shows an image of the area, its description, the water level and the state of the river on the date. Furthermore, there are two other tabs with more information about the chosen section.

The second tab (Figure 8a), presents an illustration of the river cross section, in black, and the forecasted water level, in blue, where the horizontal axis represents its width and the vertical axis represents its depth in meters. In this option there is a slider picker on the bottom side of the screen in which the user can select the hour to be presented in the illustration, it changes the water level and the state of the river section accordingly to the chosen hour.

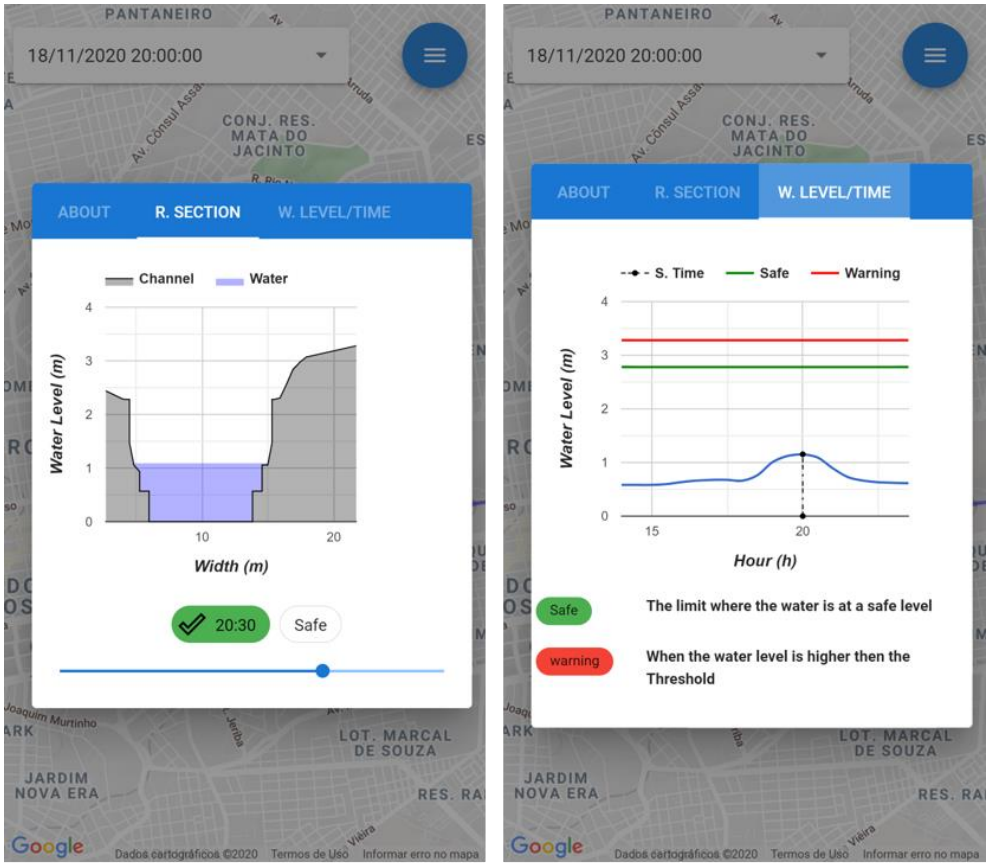

a) b)

Figure 8 – Forecasted water level situation graph.

The third tab (Figure 8b), it is possible to observe the forecasted water level according to the time of simulation. The water level is on the vertical axis and the time on the horizontal axis. There is a black dot that marks the hour and water level on the previously selected date in the homepage.

5 Conclusions

Flood alert systems are vital as risk management tool to mitigate flood disasters. This study focuses on the development of a flood alert application to send warning message via mobile devices to population. The Prosa Basin (32 km²), in Campo Grande city (Brazil) was selected as a case study.

Here, the core of flood alert system is the hydrological (HEC-HMS) and hydraulic model (HEC-RAS). As an important aspect, the hydrological-hydraulic model was calibrated and validated using different rainfall events.

A flood alert software with Progressive Web Application (PWA) was developed for a variety of hardware and mobile devices. For the data storage it was chosen a non-relational database that is hosted by Google Firebase platform, which can provide updated data in real time. Further, Google Maps API was used to display the city map, markers on pre-established places, and information about the channels, such as water stage and channel design illustration are displayed through graphs created using Google Charts API. This flood alert application has potential to facilitate the widespread of the warning messages quickly among population. Ultimately, this software has potential to be used in other catchments.

This flood alert system will be useful to policy-makers, as well as to local residents, for reducing flood risk in the study area. In future, flood alert application expected to incorporate new forecast data, particularly quantitative precipitation estimation (QPE) of weather radar.

6 Acknowledgments

This study was supported by grants from the Ministry of Science, Technology, Innovation and Communication – MCTIC and National Council for Scientific and Technological Development – CNPq (grants 441289/2017-7 and 306830/2017-5) and Coordenação de Aperfeiçoamento de Pessoal de Nível Superior - Brasil – CAPES (Finance Code 001 and Capes PrInt).

7 references

ADAMS, T. E.; CHEN, S.; DYMOND, R. Results from Operational Hydrologic Forecasts Using the NOAA/NWS OHRFC Ohio River Community HEC-RAS Model. **Journal of Hydrologic Engineering,** v. 23, n. 7, p. 04018028, doi:10.1061/(ASCE)HE.1943-5584.0001663, 2018.

AHMAD, S.; SIMONOVIC, S. P. An Intelligent Decision Support System for Management of Floods. **Water Resources Management,** v. 20, n. 3, p. 391-410, 10.1007/s11269-006-0326-3, 2006.

ALVARES, C. A.; STAPE, J. L.; SENTELHAS, P. C.; DE MORAES GONÇALVES, J. L.; SPAROVEK, G. Köppen's climate classification map for Brazil. **Meteorologische Zeitschrift,** v. 22, n. 6, p. 711-728, http://dx.doi.org/10.1127/0941-2948/2013/0507, 2013.

AZAM, M.; KIM, H. S.; MAENG, S. J. Development of flood alert application in Mushim stream watershed Korea. **International Journal of Disaster Risk Reduction,** v. 21, p. 11-26, https://doi.org/10.1016/j.ijdrr.2016.11.008, 2017.

BIØRN-HANSEN, A.; MAJCHRZAK, T.; GRØNLI, T. **Progressive Web Apps: The Possible Web-native Unifier for Mobile Development**. 13th International Conference on Web Information Systems and Technologies SciTePress. 1**:** 344-351 p. 2017.

BRUNNER, G. W. **HEC-RAS - River Analysis System. User's Manual**. Davis, CA: US Army Corps of Engineers - HEC: Hydrologic Engineering Center 2016.

CAMPANA, N. A.; TUCCI, C. E. M. Predicting floods from urban development scenarios: case study of the Dilúvio Basin, Porto Alegre, Brazil. **Urban Water,** v. 3, n. 1, p. 113-124, https://doi.org/10.1016/S1462-0758(01)00004-8, 2001.

CASAGRANDE, L.; TOMASELLA, J.; DOS SANTOS ALVALÁ, R. C.; BOTTINO, M. J.; DE OLIVEIRA CARAM, R. Early flood warning in the Itajaí-Açu River basin using numerical weather forecasting and hydrological modeling. **Natural Hazards,** v. 88, n. 2, p. 741-757, 10.1007/s11069-017-2889-0, 2017.

CHARLEY, W. J. **HEC-RTS (Real-Time Simulation) Version 2 for real time flood forecasting and water control**. 2nd Joint Federal Interagency Conference. Las Vegas, NV 2010.

CHATTERJEE, N.; CHAKRABORTY, S.; DECOSTA, A.; NATH, A. Real-time Communication Application Based on Android Using Google Firebase. **International Journal of Advance Research in Computer Science and Management Studies,** v. 6, n. 4, 2018.

CHU, Q.; XU, Z.; CHEN, Y.; HAN, D. Evaluation of the ability of the Weather Research and Forecasting model to reproduce a sub-daily extreme rainfall event in Beijing, China using different domain configurations and spin-up times. **Hydrol. Earth Syst. Sci.,** v. 22, n. 6, p. 3391-3407, 10.5194/hess-22-3391-2018, 2018.

DIMITRIADIS, P.; TEGOS, A.; OIKONOMOU, A.; PAGANA, V.; KOUKOUVINOS, A.; MAMASSIS, N.; KOUTSOYIANNIS, D.; EFSTRATIADIS, A. Comparative evaluation of 1D and quasi-2D hydraulic models based on benchmark and real-world applications for uncertainty assessment in flood mapping. **Journal of Hydrology,** v. 534, p. 478-492, https://doi.org/10.1016/j.jhydrol.2016.01.020, 2016.

FAKHRUDDIN, S. H. M. Development of Flood Forecasting System for the Wangchhu River Basin in Bhutan. **Journal of Geography and Geology,** v. 7, n. 2, 10.5539/jgg.v7n2P70, 2015.

FAN, F. M.; PAIVA, R. C. D.; COLLISCHONN, W. Chapter 2 - Hydrological Forecasting Practices in Brazil. In: ADAMS, T. E. e PAGANO, T. C. (Ed.). **Flood Forecasting**. Boston: Academic Press, 2016. p.41-66. ISBN 978-0-12-801884-2.

FREER, J.; BEVEN, K. J.; NEAL, J.; SCHUMANN, G.; HALL, J.; BATES, P. Flood risk and uncertainty. In: (Ed.). **Risk and Uncertainty Assessment for Natural Hazards**: Cambridge University Press, 2011. p.190-233.

GARROTE, J.; ALVARENGA, F. M.; DÍEZ-HERRERO, A. Quantification of flash flood economic risk using ultra-detailed stage–damage functions and 2-D hydraulic models. **Journal of Hydrology,** v. 541, Part A, p. 611-625, http://dx.doi.org/10.1016/j.jhydrol.2016.02.006, 2016.

GEORGAKAKOS, K. P. Advances in forecasting flash floods. In Proceedings of the CCNAA-AIT Joint Seminar on Prediction and Damage Mitigation of Meteorologically Induced Natural Disasters, 1992. National Taiwan University, Taipei, Taiwan. 21–24 May 1992. p.280–293.

GIVATI, A.; LYNN, B.; LIU, Y.; RIMMER, A. Using the WRF Model in an Operational Streamflow Forecast System for the Jordan River. **Journal of Applied Meteorology and Climatology,** v. 51, n. 2, p. 285-299, 10.1175/jamc-d-11-082.1, 2012.

HENONIN, J.; RUSSO, B.; MARK, O.; GOURBESVILLE, P. Real-time urban flood forecasting and modelling - a state of the art. **Journal of Hydroinformatics,** v. 15, n. 3, p. 717-736, 10.2166/hydro.2013.132, 2013.

HICKS, F. E.; PEACOCK, T. Suitability of HEC-RAS for Flood Forecasting. **Canadian Water Resources Journal / Revue canadienne des ressources hydriques,** v. 30, n. 2, p. 159-174, 10.4296/cwrj3002159, 2005.

JABBARI, A.; SO, J. M.; BAE, D. H. Accuracy assessment of real-time flood forecasting of coupled hydrological and mesoscale meteorological models. **Nat. Hazards Earth Syst. Sci. Discuss.,** v. 2018, p. 1-36, 10.5194/nhess-2017-447, 2018.

KOUSSIS, A. D.; LAGOUVARDOS, K.; MAZI, K.; KOTRONI, V.; SITZMANN, D.; LANG, J.; ZAISS, H.; BUZZI, A.; MALGUZZI, P. Flood Forecasts for Urban Basin with Integrated Hydro‐Meteorological Model. **Journal of Hydrologic Engineering,** v. 8, n. 1, p. 1-11, doi:10.1061/(ASCE)1084-0699(2003)8:1(1), 2003.

KUMAR, A.; DUDHIA, J.; ROTUNNO, R.; NIYOGI, D.; MOHANTY, U. C. Analysis of the 26 July 2005 heavy rain event over Mumbai, India using the Weather Research and Forecasting (WRF) model. **Quarterly Journal of the Royal Meteorological Society,** v. 134, n. 636, p. 1897-1910, 10.1002/qj.325, 2008.

LI, J.; CHEN, Y.; WANG, H.; QIN, J.; LI, J.; CHIAO, S. Extending flood forecasting lead time in a large watershed by coupling WRF QPF with a distributed hydrological model. **Hydrol. Earth Syst. Sci.,** v. 21, n. 2, p. 15, https://doi.org/10.5194/hess-21-1279-2017, 2017.

LI, P.; CHEN, Y.; LI, T.; WANG, R.; SUN, J. Implementation of Cloud Messaging System Based on GCM Service. 2013 International Conference on Computational and Information Sciences, 2013. 21-23 June 2013. p.1509-1512.

MASHRIQUI, H. S.; HALGREN, J. S.; REED, S. M. 1D River Hydraulic Model for Operational Flood Forecasting in the Tidal Potomac: Evaluation for Freshwater, Tidal, and Wind-Driven Events. **Journal of Hydraulic Engineering,** v. 140, n. 5, p. 04014005, doi:10.1061/(ASCE)HY.1943-7900.0000862, 2014.

MAUSSION, F.; SCHERER, D.; FINKELNBURG, R.; RICHTERS, J.; YANG, W.; YAO, T. WRF simulation of a precipitation event over the Tibetan Plateau, China – an assessment using remote sensing and ground observations. **Hydrol. Earth Syst. Sci.,** v. 15, n. 6, p. 1795-1817, https://doi.org/10.5194/hess-15-1795-2011, 2011.

MERKURYEVA, G.; MERKURYEV, Y.; SOKOLOV, B. V.; POTRYASAEV, S.; ZELENTSOV, V. A.; LEKTAUERS, A. Advanced river flood monitoring, modelling and forecasting. **Journal of Computational Science,** v. 10, p. 77-85, https://doi.org/10.1016/j.jocs.2014.10.004, 2015.

MILLER, J. D.; HESS, T. Urbanisation impacts on storm runoff along a rural-urban gradient. **Journal of Hydrology,** v. 552, p. 474-489, https://doi.org/10.1016/j.jhydrol.2017.06.025, 2017.

MOLTENI, F.; BUIZZA, R.; PALMER, T. N.; PETROLIAGIS, T. The ECMWF Ensemble Prediction System: Methodology and validation. **Quarterly Journal of the Royal Meteorological Society,** v. 122, n. 529, p. 73-119, https://doi.org/10.1002/qj.49712252905, 1996.

MORIASI, D. N.; ARNOLD, J. G.; VAN LIEW, M. W.; BINGNER, R. L.; HARMEL, R. D.; VEITH, T. L. Model evaluation guidelines for systematic quantification of accuracy in watershed simulations. **Transactions of the ASABE**, http://dx.doi.org/10.13031/2013.23153, 2007.

MUÑOZ, L. A.; OLIVERA, F.; GIGLIO, M.; BERKE, P. The impact of urbanization on the streamflows and the 100-year floodplain extent of the Sims Bayou in Houston, Texas. **International Journal of River Basin Management,** v. 16, n. 1, p. 61-69, https://doi.org/10.1080/15715124.2017.1372447, 2018.

MURE-RAVAUD, M.; BINET, G.; BRACQ, M.; PERARNAUD, J.-J.; FRADIN, A.; LITRICO, X. A web based tool for operational real-time flood forecasting using data assimilation to update hydraulic states. **Environmental Modelling & Software,** v. 84, p. 35-49, https://doi.org/10.1016/j.envsoft.2016.06.002, 2016.

NERI, A.; VILLARINI, G.; NAPOLITANO, F. Intraseasonal predictability of the duration of flooding above National Weather Service flood warning levels across the U.S. Midwest. **Hydrological Processes,** v. 34, n. 23, p. 4505-4511, 10.1002/hyp.13902, 2020.

NESTER, T.; KOMMA, J.; BLÖSCHL, G. Real time flood forecasting in the Upper Danube basin. **Journal of Hydrology and Hydromechanics,** v. 64, n. 4, p. 404-414, https://doi.org/10.1515/johh-2016-0033, 2016.

NKWUNONWO, U. C.; WHITWORTH, M.; BAILY, B. A review of the current status of flood modelling for urban flood risk management in the developing countries. **Scientific African,** v. 7, p. e00269, https://doi.org/10.1016/j.sciaf.2020.e00269, 2020.

NORBIATO, D.; BORGA, M.; DEGLI ESPOSTI, S.; GAUME, E.; ANQUETIN, S. Flash flood warning based on rainfall thresholds and soil moisture conditions: An assessment for gauged and ungauged basins. **Journal of Hydrology,** v. 362, n. 3, p. 274-290, https://doi.org/10.1016/j.jhydrol.2008.08.023, 2008.

PDDU. **Plano Diretor de Drenagem Urbana de Campo Grande**. CONSÓRCIO-RES-PLANEJAMENTO-EM-DRENAGEM-URBANA. Campo Grande**:** 350 p. 2008.

PLANURB. **Carta Geotécnica de Campo Grande**. Prefeitura Municipal de Campo Grande. Campo Grande. 1991

PLATE, E. J. Flood risk and flood management. **Journal of Hydrology,** v. 267, n. 1, p. 2-11, https://doi.org/10.1016/S0022-1694(02)00135-X, 2002.

POWERS, J. G.; KLEMP, J. B.; SKAMAROCK, W. C.; DAVIS, C. A.; DUDHIA, J.; GILL, D. O.; COEN, J. L.; GOCHIS, D. J.; AHMADOV, R.; PECKHAM, S. E.; GRELL, G. A.; MICHALAKES, J.; TRAHAN, S.; BENJAMIN, S. G.; ALEXANDER, C. R.; DIMEGO, G. J.; WANG, W.; SCHWARTZ, C. S.; ROMINE, G. S.; LIU, Z.; SNYDER, C.; CHEN, F.; BARLAGE, M. J.; YU, W.; DUDA, M. G. The Weather Research and Forecasting Model: Overview, System Efforts, and Future Directions. **Bulletin of the American Meteorological Society,** v. 98, n. 8, p. 1717-1737, 10.1175/bams-d-15-00308.1, 2017.

QI, H.; ALTINAKAR, M. S. A GIS-based decision support system for integrated flood management under uncertainty with two dimensional numerical simulations. **Environmental Modelling & Software,** v. 26, n. 6, p. 817-821, https://doi.org/10.1016/j.envsoft.2010.11.006, 2011.

RAMIREZ, J. A.; RAJASEKAR, U.; PATEL, D. P.; COULTHARD, T. J.; KEILER, M. Flood modeling can make a difference: Disaster risk-reduction and resilience-building in urban areas. **Hydrol. Earth Syst. Sci. Discuss.,** v. 2016, p. 1-21, https://doi.org/10.5194/hess-2016-544, 2016.

REICHEL, F.; VERWORN, H.-R.; KRÄMER, S.; CLUCKIE, I.; RICO-RAMIREZ, M. A. Radar-based flood forecasting for river catchments. **Proceedings of the Institution of Civil Engineers - Water Management,** v. 162, n. 2, p. 159-168, 10.1680/wama.2009.162.2.159, 2009.

ROGELIS, M. C.; WERNER, M. Streamflow forecasts from WRF precipitation for flood early warning in mountain tropical areas. **Hydrol. Earth Syst. Sci.,** v. 22, n. 1, p. 853-870, 10.5194/hess-22-853-2018, 2018.

ŞENSOY, A.; UYSAL, G.; ŞORMAN, A. A. Developing a decision support framework for real-time flood management using integrated models. **Journal of Flood Risk Management,** v. 11, n. S2, p. S866-S883, 10.1111/jfr3.12280, 2018.

SILVESTRO, F.; REBORA, N.; GIANNONI, F.; CAVALLO, A.; FERRARIS, L. The flash flood of the Bisagno Creek on 9th October 2014: An "unfortunate" combination of spatial and temporal scales. **Journal of Hydrology,** v. 541, Part A, p. 50-62, http://dx.doi.org/10.1016/j.jhydrol.2015.08.004, 2016.

SOBRINHO, T. A. **Relatório Técnico: Caracterização da infiltração da água e do escoamento superficial na área urbana de Campo Grande - MS**. Universidade Federal de Mato Grosso do Sul. Campo Grande, Mato Grosso do Sul. 2015

TENG, J.; JAKEMAN, A. J.; VAZE, J.; CROKE, B. F. W.; DUTTA, D.; KIM, S. Flood inundation modelling: A review of methods, recent advances and uncertainty analysis. **Environmental Modelling & Software,** v. 90, p. 201-216, https://doi.org/10.1016/j.envsoft.2017.01.006, 2017.

THIEMIG, V.; ROJAS, R.; ZAMBRANO-BIGIARINI, M.; DE ROO, A. Hydrological evaluation of satellite-based rainfall estimates over the Volta and Baro-Akobo Basin. **Journal of Hydrology,** v. 499, p. 324-338, https://doi.org/10.1016/j.jhydrol.2013.07.012, 2013.

TODINI, E. An operational decision support system for flood risk mapping, forecasting and management. **Urban Water,** v. 1, n. 2, p. 131-143, https://doi.org/10.1016/S1462-0758(00)00010-8, 1999.

UCAR. **Flash flood early warning system reference guide**. The University Corporation for Atmospheric Research, 2010. ISBN 978-0-615-37421-5.

USACE-HEC. **Hydrologic Modeling System (HEC-HMS) Applications Guide: Version 4.2.1**. Davis, CA: Institute for Water Resources, Hydrologic Engineering Center, 2015.

_____. **Hydrologic Modeling System HEC-HMS, user's manual, version 4.2**. Davis, CA: US Army Corps of Engineers, Hydrologic Engineering Center, 2016.

USDA-NRCS. **Urban Hydrology for Small Watersheds. Technical Release No. 55 (TR-55)**. Washington DC. 1986

WMO. **Manual on Flood Forecasting and Warning**. World Meteorological Organization, 2011. ISBN 9789263110725.

_____. **Flood Forecasting and Early Warning**. World Meteorological Organization, 2013.

XUE, J.; LIU, Y. Numerical weather prediction in China in the new century—Progress, problems and prospects. **Advances in Atmospheric Sciences,** v. 24, n. 6, p. 1099-1108, https://doi.org/10.1007/s00376-007-1099-1, 2007.

YAMAGUCHI, M.; SAKAI, R.; KYODA, M.; KOMORI, T.; KADOWAKI, T. Typhoon Ensemble Prediction System Developed at the Japan Meteorological Agency. **Monthly Weather Review,** v. 137, n. 8, p. 2592-2604, https://doi.org/10.1175/2009MWR2697.1, 2009.

YE, J.; HE, Y.; PAPPENBERGER, F.; CLOKE, H. L.; MANFUL, D. Y.; LI, Z. Evaluation of ECMWF medium-range ensemble forecasts of precipitation for river basins. **Quarterly**

Journal of the Royal Meteorological Society, v. 140, n. 682, p. 1615-1628, https://doi.org/10.1002/qj.2243, 2014.

YOO, C.; LEE, J.; PARK, C.; JUN, C. Method for Estimating Concentration Time and Storage Coefficient of the Clark Model Using Rainfall-Runoff Measurements. **Journal of Hydrologic Engineering,** v. 19, n. 3, p. 626-634, doi:10.1061/(ASCE)HE.1943-5584.0000828, 2014.

ZHOU, Q.; LENG, G.; HUANG, M. Impacts of future climate change on urban flood volumes in Hohhot in northern China: benefits of climate change mitigation and adaptations. **Hydrol. Earth Syst. Sci.,** v. 22, n. 1, p. 11, https://doi.org/10.5194/hess-22-305-2018, 2018.

GENERAL CONCLUSION

The potential impacts of climate change on current urban drainage systems have received increasing attention during recent decades because of the devastating impacts of urban flooding on the economy. In this study, we try to evaluate and develop techniques to improving the urban flood resilience. The Prosa Basin (32 km²), in Campo Grande city (Brazil), was selected as a case study because historical records of rainfall and flood damage indicate that the region has experienced an increase in flood frequency and magnitude due to urbanization. Thus, in the **first chapter**, we evaluated how LID practices affect the resilience of stormwater drainage system under climate change scenarios. Our findings show an increase in runoff peak in the study area due to increased rainfall intensity until the end of the 21st century under both RCP 4.5 and RCP 8.5, while the impact of RCP 8.5 has potential to be more adverse than the RCP 4.5. Overall, runoff peak is projected (RCP 8.5) to increase on average by 24% over 2071–2095 period.

The resilience index used to quantitatively assess the degree of resilience to floods indicated that the current stormwater drainage system has low resilience to future rainfall events under climate change. In addition, we demonstrate that the increased runoff peak can be mitigated satisfactory by using combined LID practices. In general, LID combinations showed reduction in runoff peak higher than 20%, and the best LID combination presented reduction up to 46%. As this represents a significant improvement in the resilience to flooding in the study area, we conclude that LIDs can play a key role to increasing the city resilience.

Despite the promising results, it is important to emphasize that these results depend directly on the considerations adopted in this work. In addition, new research opportunities have been identified during the development of this work, such as: a) evaluate future scenarios for sustainable measures based on changes in land use legislation; b) assess the impact of increased soil impermeability to verify if there will be a significant increase in peak runoff.

In the **second chapter**, we propose a new method for correcting biased radar rainfall against ground-based rain gauge data in daily, hourly, and sub-hourly timescale. We demonstrate the added value of the proposed bias correction scheme for radar-based rainfall estimates. The results showed that Nash-Sutcliffe Efficiency (*NSE*) index increased from 0.11 to 0.63 and Mean Absolute Error (*MAE*) decreased from 11.66 (biased data) to 6.97 mm (unbiased data) for all rainfall events (408 events). In addition, we noted that the method is easy to apply, but the users must be careful about the potential overfitting issue of the polynomial equation. It can be applied for rainfall events with daily, hourly, and sub-hourly durations. Our

findings are particularly useful in the case of rainfall-runoff models for urban flooding. Therefore, we highlight the opportunity of significant improvement on the radar rainfall estimates at sub-hour timescale. Despite the good results, it is important to note that the method still needs to be validated from its application at a different period from the used in its development.

In the **third chapter**, a Decision Support System coupled with a mobile application is used to develop a flood alert system to send early flood warning messages to population. The core of flood alert system is the hydrological (HEC-HMS) and hydraulic model (HEC-RAS). As an important aspect, the hydrological-hydraulic model was calibrated and validated using different rainfall events.

A flood alert software with Progressive Web Application (PWA) was developed for a variety of hardware and mobile devices. For the data storage it was chosen a non-relational database that is hosted by Google Firebase platform, which can provide updated data in real time. Further, Google Maps API was used to display the city map, markers on pre-established places, and information about the channels, such as water stage and channel design illustration are displayed through graphs created using Google Charts API. This flood alert application has potential to facilitate the widespread of the warning messages quickly among population. Ultimately, this software has potential to be used in other catchments. In future, flood alert application expected to incorporate new forecast data, particularly quantitative precipitation estimation (QPE) of weather radar.

The chapters presented in this doctoral thesis were already under review in peer reviewed journals or are in preparation. The process of elaboration of these chapters provided great advances in the methodological delineation and discussion aspects, mainly with the valuable contributions and cooperation of co-authors, journals reviewers and editors.

APPENDIX

Chapter 1

Table S1. Parameters of the rainfall-runoff model to the baseline scenario

Parameter	Unit	Subcatchment															
		S1	**S2**	**S3**	**S4**	**S5**	**S6**	**S7**	**S8**	**S9**	**S10**	**S11**	**S12**	**S13**	**S14**	**S15**	**S16**
Area	ha	68.16	173.72	130.77	201.32	206.63	139.58	153.77	170.21	115.91	97.59	46.88	83.80	56.95	210.50	272.06	354.07
Width	m	1794.51	5128.66	8425.42	6853.58	9193.58	1261.31	1669.13	1539.47	2654.34	2308.39	507.19	848.72	2734.82	2467.46	3872.39	6067.65
Slope	%	10.37	7.65	7.01	6.87	5.07	5.35	2.67	4.92	7.18	7.14	7.59	4.45	7.02	5.32	3.50	4.05
Flow Length	m	379.83	338.73	155.21	293.75	224.76	1106.59	921.24	1105.65	436.67	422.74	924.34	987.38	208.25	853.09	702.56	583.54
Impervious areas	%	49.83	52.56	54.65	49.81	53.11	48.63	46.35	46.39	29.68	33.23	22.83	33.44	35.13	7.42	19.75	21.09
Manning`s n for impervious areas	-	0.015	0.015	0.015	0.015	0.015	0.015	0.015	0.015	0.03	0.03	0.03	0.03	0.03	0.03	0.03	0.03
Manning`s n for pervious areas	-	0.364	0.362	0.34	0.373	0.358	0.345	0.351	0.357	0.393	0.418	0.502	0.432	0.444	0.636	0.41	0.5
Depression storage of impervious	mm	2.5	2.5	2.5	1.25	1.25	1.25	1.25	1.25	1.25	1.25	1.25	1.25	1.25	1.25	1.25	1.25
Depression storage of pervious	mm	3.433	3.378	3.125	3.525	3.319	3.305	3.384	3.467	4.16	4.239	5.083	4.344	4.418	6.54	4.184	5.128
Curve Number	-	87	87	87	87	87	73	71	73	71	71	68	68	65	59	60	58
Time of Concentration (SCS Method)	min	9.30	9.89	5.53	9.43	8.86	47.29	61.97	49.30	20.56	20.09	39.46	54.37	13.62	56.11	57.57	48.74

Table S2 - Performance index and RPD values for the calibration and validation events

Events Date (dd/mm/yyyy)	NSE (-)	R^2 (-)	RSR (-)	RPD Peak (%)
4/17/2015	0.67	0.92	0.58	9.41
5/27/2015	0.92	0.92	0.28	-1.61
12/25/2015	0.85	0.89	0.38	-28
1/8/2016	0.94	0.96	0.24	-5.35
2/15/2016	0.75	0.77	0.50	-13.47
3/2/2016	0.74	0.77	0.51	2.61
Mean	0.81	0.87	0.42	-6.07
Standard deviation	0.11	0.08	0.14	13.20

Chapter 2

Rainfall observed, uncorrected and corrected radar data:

Event	Station	duration	Rainfall	Uncorr. Bias	Correc. Bias
1/1/2016 10:00	MB_SEG1	0 days 06:00:00	35.00	13.32	20.03
1/1/2016 10:10	MB_PRO1	0 days 06:00:00	23.25	12.90	19.56
1/1/2016 10:20	MB_PRO2	0 days 06:00:00	25.25	17.96	25.47
1/1/2016 16:10	MB_PRO1	0 days 05:30:00	18.75	15.25	22.07
1/2/2016 18:10	MB_SEG1	0 days 03:00:00	7.25	16.32	9.32
1/2/2016 18:30	MB_PRO2	0 days 02:30:00	11.00	12.27	5.73
1/5/2016 10:20	MB_SEG1	0 days 01:40:00	35.00	17.42	24.76
1/5/2016 11:30	MB_GAM1	0 days 01:30:00	28.75	16.94	24.12
1/6/2016 5:40	MB_SEG1	0 days 06:00:00	17.50	10.39	16.53
1/8/2016 10:50	MB_GAM1	0 days 06:00:00	11.50	14.41	7.64
1/8/2016 15:10	MB_SEG1	0 days 02:20:00	24.25	24.44	14.81
1/8/2016 15:20	MB_PRO2	0 days 01:00:00	19.50	12.72	19.35
1/8/2016 15:50	MB_COQ2	0 days 03:00:00	65.00	31.34	41.42
1/8/2016 16:00	MB_PRO1	0 days 02:00:00	14.75	15.64	8.78
1/8/2016 16:50	MB_GAM1	0 days 07:20:00	7.75	11.40	5.10
1/8/2016 22:40	MB_PRO1	0 days 06:00:00	10.00	16.43	9.41
1/9/2016 0:10	MB_GAM1	0 days 06:00:00	9.50	10.38	4.25
1/9/2016 0:30	MB_PRO2	0 days 05:30:00	16.75	16.29	23.28
1/9/2016 4:00	MB_SEG1	0 days 02:00:00	32.75	31.85	43.28
1/9/2016 4:40	MB_PRO1	0 days 01:40:00	22.00	32.15	19.95
1/10/2016 7:20	MB_PRO2	0 days 06:00:00	10.00	12.74	6.11
1/10/2016 7:40	MB_COQ2	0 days 06:00:00	9.50	12.17	5.66
1/10/2016 12:50	MB_SEG1	0 days 05:50:00	19.75	21.20	12.66
1/10/2016 13:10	MB_PRO1	0 days 05:20:00	17.00	17.70	10.26
1/10/2016 13:20	MB_GAM1	0 days 06:00:00	17.25	12.19	18.70

1/10/2016 13:20	MB_PRO2	0 days 19:40:00	15.50	17.26	9.97
1/10/2016 13:40	MB_COQ2	0 days 06:00:00	18.25	12.94	19.61
1/11/2016 8:40	MB_SEG1	0 days 05:20:00	26.75	14.70	21.49
1/11/2016 9:00	MB_GAM1	0 days 05:20:00	23.75	17.02	24.23
1/11/2016 9:00	MB_PRO1	0 days 05:10:00	25.75	20.15	27.43
1/13/2016 5:50	MB_COQ2	0 days 07:30:00	4.25	10.75	4.59
1/13/2016 11:50	MB_SEG1	0 days 04:10:00	29.00	24.31	33.85
1/13/2016 12:20	MB_GAM1	0 days 04:10:00	14.25	11.41	17.72
1/13/2016 12:30	MB_PRO2	0 days 03:40:00	13.25	14.40	7.62
1/13/2016 12:30	MB_PRO1	0 days 03:50:00	15.50	16.37	9.37
1/14/2016 12:20	MB_PRO1	0 days 04:40:00	31.75	24.01	33.35
1/14/2016 12:30	MB_PRO2	0 days 04:40:00	10.00	12.15	5.64
1/14/2016 12:30	MB_GAM1	0 days 05:50:00	13.75	14.97	8.17
1/27/2016 0:00	MB_PRO1	0 days 05:20:00	17.50	13.13	19.82
1/27/2016 0:00	MB_PRO2	0 days 05:50:00	19.00	17.05	24.26
2/2/2016 13:30	MB_PRO1	0 days 02:30:00	11.00	10.02	16.20
2/5/2016 14:00	MB_GAM1	0 days 01:00:00	39.00	20.23	27.68
2/6/2016 15:50	MB_PRO2	0 days 06:00:00	8.75	10.59	4.45
2/6/2016 16:00	MB_GAM1	0 days 00:50:00	16.25	11.78	18.19
2/15/2016 13:00	MB_COQ2	0 days 02:10:00	48.75	48.47	63.74
2/15/2016 13:10	MB_SEG1	0 days 01:40:00	10.00	12.64	6.03
2/15/2016 13:10	MB_PRO2	0 days 01:20:00	19.00	26.09	15.43
2/15/2016 13:10	MB_PRO1	0 days 02:10:00	16.25	28.81	19.11
2/21/2016 12:50	MB_SEG1	0 days 05:00:00	26.00	18.53	26.16
2/21/2016 12:50	MB_ANHA7	0 days 04:50:00	8.06	19.02	11.44
2/21/2016 12:50	MB_PRO1	0 days 05:10:00	22.50	22.57	13.80
2/21/2016 14:00	MB_COQ2	0 days 03:20:00	15.50	11.04	17.25
2/22/2016 14:00	MB_SEG1	0 days 05:40:00	22.75	18.93	26.53
2/22/2016 14:00	MB_ANHA7	0 days 03:00:00	7.63	23.51	14.44
2/26/2016 11:00	MB_PRO1	0 days 05:50:00	8.50	16.85	9.70
2/28/2016 23:30	MB_PRO1	0 days 06:00:00	49.75	35.02	48.93
2/28/2016 23:30	MB_ANHA7	0 days 06:00:00	9.13	36.44	22.88
2/28/2016 23:30	MB_SEG1	0 days 06:00:00	35.25	37.48	22.98
2/28/2016 23:40	MB_COQ2	0 days 06:00:00	37.75	34.96	48.91
2/28/2016 23:40	MB_PRO2	0 days 06:00:00	50.00	48.83	64.49
2/28/2016 23:50	MB_GAM1	0 days 06:00:00	47.50	39.07	53.55
2/29/2016 0:10	MB_LAJ7	0 days 06:00:00	54.00	59.88	51.24
2/29/2016 5:30	MB_ANHA7	0 days 08:00:00	4.06	17.28	9.99
2/29/2016 5:40	MB_PRO2	0 days 08:00:00	16.50	16.28	23.26
2/29/2016 5:50	MB_GAM1	0 days 02:20:00	12.00	10.38	16.51
2/29/2016 13:10	MB_GAM1	0 days 03:20:00	28.25	24.45	34.08
2/29/2016 13:20	MB_COQ2	0 days 01:50:00	9.25	12.67	6.05
2/29/2016 13:40	MB_LAJ7	0 days 02:30:00	10.75	25.10	15.00
3/2/2016 1:50	MB_ANHA7	0 days 05:20:00	15.56	47.21	33.01
3/2/2016 2:00	MB_SEG1	0 days 04:30:00	38.75	42.82	26.72
3/2/2016 2:10	MB_GAM1	0 days 11:30:00	79.25	54.04	69.55
3/2/2016 2:50	MB_COQ2	0 days 04:00:00	55.00	41.99	56.79
3/7/2016 13:20	MB_PRO1	0 days 01:20:00	39.50	24.58	34.32

3/7/2016 13:30	MB_ANHA7	0 days 01:00:00	2.81	12.29	5.74
3/7/2016 13:40	MB_SEG1	0 days 00:50:00	12.00	12.59	5.98
3/14/2016 15:20	MB_PRO1	0 days 03:20:00	39.25	17.13	24.37
3/14/2016 15:20	MB_COQ2	0 days 01:10:00	29.75	18.87	26.48
3/14/2016 15:20	MB_SEG1	0 days 01:20:00	55.50	35.54	49.15
3/14/2016 15:30	MB_ANHA7	0 days 01:20:00	3.50	13.02	6.34
3/18/2016 23:50	MB_COQ2	0 days 02:10:00	20.00	14.33	21.10
3/24/2016 12:40	MB_SEG1	0 days 05:50:00	28.25	20.39	28.15
3/24/2016 12:50	MB_COQ2	0 days 04:30:00	13.25	12.73	19.37
3/24/2016 12:50	MB_PRO1	0 days 05:50:00	20.50	20.05	27.07
3/24/2016 12:50	MB_ANHA7	0 days 06:00:00	6.63	28.19	18.01
3/24/2016 13:10	MB_SEG6	0 days 06:00:00	17.75	16.01	22.93
3/24/2016 13:20	MB_GAM1	0 days 06:00:00	19.00	14.36	21.13
3/24/2016 13:40	MB_LAJ7	0 days 06:00:00	16.25	18.87	11.26
3/24/2016 18:50	MB_ANHA7	0 days 06:00:00	9.56	30.72	21.69
3/24/2016 18:50	MB_PRO1	0 days 06:00:00	38.50	30.88	40.09
3/24/2016 18:50	MB_COQ2	0 days 06:00:00	39.50	31.33	41.40
3/24/2016 18:50	MB_SEG1	0 days 06:00:00	37.75	38.62	23.35
3/24/2016 19:00	MB_PRO2	0 days 06:00:00	32.50	32.21	44.55
3/24/2016 19:10	MB_SEG6	0 days 06:00:00	33.00	29.79	39.22
3/24/2016 19:20	MB_GAM1	0 days 06:00:00	45.50	29.01	38.59
3/24/2016 19:40	MB_LAJ7	0 days 06:00:00	32.00	27.12	37.86
3/29/2016 14:10	MB_ANHA7	0 days 01:50:00	8.19	23.75	14.56
3/30/2016 19:40	MB_GAM1	0 days 04:40:00	29.50	20.03	27.01
4/2/2016 16:00	MB_PRO1	0 days 00:50:00	10.00	22.49	13.73
4/2/2016 22:20	MB_SEG1	0 days 00:40:00	12.50	10.29	16.43
4/2/2016 22:20	MB_SEG6	0 days 00:50:00	11.00	13.19	6.49
4/5/2016 15:30	MB_SEG6	0 days 00:50:00	4.50	10.42	4.29
4/7/2016 19:30	MB_COQ2	0 days 02:40:00	20.00	17.69	25.13
4/7/2016 19:40	MB_SEG6	0 days 01:30:00	29.25	13.06	19.74
4/7/2016 20:00	MB_SEG1	0 days 01:00:00	8.50	13.62	6.88
4/8/2016 15:00	MB_ANHA7	0 days 01:00:00	7.81	21.30	12.73
4/8/2016 15:10	MB_PRO1	0 days 01:00:00	18.00	16.34	23.34
4/15/2016 4:30	MB_COQ2	0 days 03:30:00	9.00	10.24	4.10
4/25/2016 15:00	MB_PRO1	0 days 05:50:00	9.50	11.12	4.89
4/25/2016 15:20	MB_GAM1	0 days 06:00:00	11.00	15.61	8.75
4/25/2016 16:10	MB_COQ2	0 days 06:00:00	20.50	10.69	16.84
4/25/2016 16:10	MB_LAJ7	0 days 06:00:00	9.25	11.81	5.39
4/25/2016 20:50	MB_SEG1	0 days 05:50:00	21.50	23.16	14.24
4/25/2016 21:00	MB_ANHA7	0 days 06:00:00	4.13	14.87	8.08
4/25/2016 21:00	MB_PRO2	0 days 05:40:00	22.00	20.93	29.31
4/25/2016 21:20	MB_GAM1	0 days 06:00:00	17.75	11.63	18.00
4/25/2016 22:10	MB_LAJ7	0 days 05:30:00	25.75	14.65	21.43
4/26/2016 9:00	MB_SEG6	0 days 05:50:00	7.00	11.35	5.06
5/9/2016 11:40	MB_ANHA7	0 days 10:00:00	3.63	18.40	10.79
5/9/2016 13:10	MB_PRO2	0 days 05:00:00	12.00	18.41	10.79
5/9/2016 17:50	MB_GAM1	0 days 06:00:00	31.50	30.97	40.29
5/9/2016 19:40	MB_PRO2	0 days 03:50:00	11.25	18.10	10.54

5/9/2016 20:40	MB_SEG1	0 days 05:10:00	14.75	17.62	10.21
5/9/2016 20:40	MB_PRO1	0 days 02:50:00	11.25	22.01	13.31
5/9/2016 21:40	MB_ANHA7	0 days 04:30:00	5.06	20.77	12.53
5/10/2016 0:40	MB_GAM1	0 days 06:00:00	15.00	22.77	13.96
5/10/2016 1:40	MB_SEG6	0 days 05:50:00	11.00	14.14	7.37
5/10/2016 1:50	MB_LAJ7	0 days 06:00:00	13.25	15.48	8.64
5/10/2016 2:10	MB_COQ2	0 days 06:00:00	15.50	15.83	8.94
5/10/2016 4:20	MB_PRO2	0 days 05:50:00	13.00	14.13	7.37
5/10/2016 4:40	MB_SEG1	0 days 05:30:00	14.50	13.57	20.31
5/10/2016 4:40	MB_PRO1	0 days 05:30:00	13.75	18.59	10.96
5/10/2016 4:40	MB_ANHA7	0 days 05:50:00	5.06	23.59	14.49
5/10/2016 6:40	MB_GAM1	0 days 06:00:00	27.00	23.73	32.91
5/10/2016 10:30	MB_PRO2	0 days 05:50:00	10.25	14.19	7.42
5/10/2016 10:50	MB_PRO1	0 days 06:00:00	15.00	18.31	10.71
5/10/2016 11:00	MB_ANHA7	0 days 06:00:00	2.94	13.50	6.77
5/10/2016 11:10	MB_SEG1	0 days 06:00:00	17.50	19.46	12.12
5/10/2016 13:50	MB_LAJ7	0 days 06:00:00	25.75	15.33	22.16
5/10/2016 14:10	MB_SEG6	0 days 06:00:00	13.25	14.15	7.38
5/10/2016 16:40	MB_PRO2	0 days 06:00:00	48.50	28.31	38.40
5/10/2016 16:50	MB_PRO1	0 days 06:00:00	49.50	30.33	39.45
5/10/2016 17:00	MB_ANHA7	0 days 06:00:00	12.25	31.89	20.36
5/10/2016 17:10	MB_SEG1	0 days 06:00:00	47.25	26.05	36.69
5/10/2016 19:50	MB_LAJ7	0 days 05:40:00	53.50	20.89	29.24
5/10/2016 20:20	MB_COQ2	0 days 05:30:00	78.50	57.74	73.58
5/10/2016 22:40	MB_PRO2	0 days 04:20:00	16.50	12.58	19.18
5/10/2016 22:50	MB_PRO1	0 days 04:20:00	20.50	13.36	20.07
5/10/2016 23:10	MB_ANHA7	0 days 03:50:00	4.69	10.56	4.42
5/10/2016 23:10	MB_SEG1	0 days 03:50:00	22.75	21.44	30.05
5/26/2016 23:30	MB_ANHA7	0 days 08:50:00	5.19	12.28	5.74
5/28/2016 19:40	MB_SEG1	0 days 05:50:00	12.50	22.28	13.55
5/28/2016 19:50	MB_GAM1	0 days 06:00:00	24.50	15.31	22.13
5/28/2016 19:50	MB_LAJ7	0 days 06:00:00	13.75	21.02	12.58
5/28/2016 19:50	MB_ANHA7	0 days 06:00:00	5.25	24.92	14.94
5/28/2016 20:00	MB_PRO1	0 days 06:00:00	17.00	24.18	14.73
5/28/2016 20:20	MB_COQ2	0 days 06:00:00	19.75	18.92	26.52
5/29/2016 1:40	MB_SEG1	0 days 02:20:00	9.75	12.66	6.04
5/29/2016 1:40	MB_SEG6	0 days 01:50:00	10.75	18.58	10.95
5/29/2016 1:50	MB_LAJ7	0 days 02:10:00	11.75	11.51	17.84
5/29/2016 1:50	MB_GAM1	0 days 03:20:00	15.00	11.64	18.01
5/29/2016 1:50	MB_ANHA7	0 days 02:10:00	2.50	12.27	5.74
6/2/2016 14:20	MB_SEG6	0 days 06:00:00	18.25	12.10	18.60
6/6/2016 1:00	MB_ANHA7	0 days 05:20:00	2.44	12.09	5.59
10/5/2016 6:10	MB_COQ3	0 days 05:50:00	52.25	31.67	42.63
10/5/2016 7:30	MB_SEG6	0 days 04:40:00	34.75	28.73	38.49
10/5/2016 7:40	MB_SEG3A	0 days 04:40:00	38.25	18.67	26.29
10/5/2016 10:00	MB_PRO1	0 days 02:20:00	25.25	16.70	23.80
10/5/2016 10:00	MB_ANHA7	0 days 02:10:00	5.56	18.94	11.35
10/5/2016 10:00	MB_PRO2	0 days 02:30:00	21.00	21.22	12.68

10/5/2016 10:00	MB_LAJ7	0 days 03:00:00	20.50	21.29	12.72
10/5/2016 10:00	MB_SEG1	0 days 02:20:00	27.50	29.68	20.28
10/5/2016 10:00	MB_PRO4	0 days 02:30:00	7.88	42.59	26.81
10/5/2016 10:10	MB_COQ2	0 days 02:30:00	41.75	38.53	53.84
10/14/2016 8:10	MB_SEG3A	0 days 06:00:00	19.75	10.17	16.32
10/14/2016 8:30	MB_PRO4	0 days 06:00:00	3.56	11.52	5.18
10/20/2016 15:40	MB_PRO1	0 days 04:50:00	24.50	28.35	18.29
10/23/2016 14:00	MB_SEG6	0 days 02:20:00	8.50	12.32	5.77
10/26/2016 16:00	MB_PRO1	0 days 03:20:00	38.00	26.63	37.41
10/26/2016 16:00	MB_SEG6	0 days 03:20:00	41.00	41.50	27.42
10/26/2016 16:50	MB_LAG1	0 days 03:40:00	26.25	13.92	20.67
10/31/2016 13:30	MB_SEG6	0 days 01:30:00	14.75	23.35	14.35
10/31/2016 13:50	MB_SEG3A	0 days 02:10:00	21.00	11.34	17.63
11/2/2016 10:20	MB_LAG1	0 days 06:00:00	26.25	12.19	18.71
11/25/2016 12:00	MB_LAG1	0 days 05:40:00	39.00	13.81	20.56
11/25/2016 14:30	MB_PRO1	0 days 02:30:00	26.25	19.52	26.80
11/25/2016 14:40	MB_PRO4	0 days 02:40:00	10.31	15.06	8.26
11/30/2016 13:30	MB_ANHA1	0 days 05:20:00	85.75	11.44	17.76
11/30/2016 14:10	MB_ANHA4	0 days 04:20:00	22.25	46.33	31.89
11/30/2016 14:20	MB_PRO1	0 days 03:10:00	54.75	30.46	39.46
11/30/2016 15:40	MB_LAJ2	0 days 05:40:00	71.50	31.15	40.80
11/30/2016 15:50	MB_GAM1	0 days 06:00:00	65.75	30.25	39.52
12/8/2016 11:30	MB_SEG3A	0 days 04:50:00	67.75	29.63	39.02
12/8/2016 11:50	MB_SEG1	0 days 04:50:00	74.75	51.71	65.77
12/8/2016 12:00	MB_SEG6	0 days 03:30:00	69.75	56.45	71.76
12/8/2016 12:50	MB_LAJ2	0 days 04:00:00	31.25	12.15	18.65
12/8/2016 12:50	MB_BAL1	0 days 03:20:00	11.00	12.60	5.99
12/8/2016 12:50	MB_BAND1A	0 days 04:00:00	59.00	25.88	36.46
12/8/2016 12:50	MB_BAL2	0 days 03:50:00	51.75	31.17	40.88
12/8/2016 13:00	MB_ANHA7	0 days 03:50:00	18.88	36.78	23.02
12/8/2016 13:00	MB_ANHA8	0 days 03:50:00	21.06	49.87	34.62
12/8/2016 13:30	MB_LAG4	0 days 04:20:00	12.00	13.32	6.60
12/8/2016 13:30	MB_LAG2	0 days 04:00:00	7.69	21.32	12.74
12/8/2016 13:30	MB_LAJ9	0 days 03:20:00	57.00	36.97	50.90
12/8/2016 13:40	MB_PRO4	0 days 03:40:00	14.44	54.99	39.29
12/8/2016 14:00	MB_COQ2	0 days 03:20:00	78.75	16.32	23.32
12/8/2016 14:00	MB_LAJ7	0 days 03:20:00	61.25	37.84	52.77
12/9/2016 10:10	MB_PRO4	0 days 04:10:00	4.75	11.29	5.01
12/21/2016 10:20	MB_PRO1	0 days 05:40:00	25.00	14.70	21.48
12/23/2016 10:10	MB_PRO1	0 days 04:30:00	33.00	47.12	32.94
12/23/2016 12:20	MB_BAND1A	0 days 03:30:00	9.50	10.13	3.97
12/30/2016 13:00	MB_PRO1	0 days 03:50:00	34.25	19.72	26.78
12/30/2016 14:00	MB_SEG1	0 days 03:50:00	17.50	10.58	16.72
12/30/2016 14:00	MB_LAJ9	0 days 03:40:00	62.50	25.36	35.64
12/30/2016 14:20	MB_BAL2	0 days 03:30:00	40.75	14.35	21.12
12/31/2016 13:40	MB_ANHA4	0 days 02:30:00	4.75	18.76	11.14
1/4/2017 13:10	MB_PRO1	0 days 05:50:00	26.50	10.86	17.04
1/18/2017 17:00	MB_PRO1	0 days 01:20:00	54.00	43.20	59.68

1/18/2017 17:20	MB_PRO3	0 days 02:40:00	6.06	10.09	3.92
1/18/2017 17:40	MB_ANHA3	0 days 01:40:00	10.63	10.09	16.26
1/19/2017 14:50	MB_PRO1	0 days 05:50:00	27.50	35.73	22.19
1/19/2017 15:40	MB_IMB3	0 days 05:30:00	63.25	15.48	22.32
1/20/2017 16:00	MB_ANHA3	0 days 03:40:00	3.44	11.75	5.35
1/20/2017 16:00	MB_ANHA4	0 days 02:30:00	6.81	20.70	12.53
1/20/2017 21:50	MB_SEG6	0 days 04:10:00	5.50	20.29	12.72
1/20/2017 22:00	MB_SEG6A	0 days 02:20:00	21.75	28.52	18.60
1/20/2017 22:20	MB_SEG3A	0 days 02:30:00	25.00	28.46	18.50
1/25/2017 9:30	MB_BAL2	0 days 06:00:00	3.94	11.38	5.08
1/25/2017 10:30	MB_PRO1	0 days 05:40:00	13.50	10.60	16.75
1/25/2017 11:10	MB_IMB3	0 days 05:20:00	28.75	24.36	33.93
1/25/2017 11:20	MB_ANHA3	0 days 10:20:00	6.50	11.96	5.50
1/25/2017 11:20	MB_ANHA4	0 days 05:40:00	6.50	18.16	10.59
1/25/2017 11:30	MB_SEG3	0 days 06:00:00	49.00	10.01	16.19
1/25/2017 11:30	MB_LAJ3	0 days 05:20:00	26.75	11.20	17.45
1/29/2017 16:30	MB_LAJ3	0 days 02:20:00	49.25	13.52	20.25
2/1/2017 9:20	MB_PRO1	0 days 01:10:00	19.25	22.95	14.10
2/6/2017 13:30	MB_SEG6A	0 days 01:10:00	41.50	21.87	30.56
2/7/2017 13:30	MB_PRO1	0 days 01:50:00	39.00	23.75	32.93
2/8/2017 13:10	MB_LAJ3	0 days 01:20:00	36.00	11.87	18.31
2/14/2017 10:00	MB_PRO1	0 days 05:20:00	8.50	12.86	6.20
2/24/2017 13:30	MB_LAJ9	0 days 05:50:00	35.00	25.23	35.43
2/24/2017 15:10	MB_BAL2	0 days 04:10:00	6.50	16.14	9.19
2/24/2017 15:40	MB_ANHA3	0 days 03:30:00	5.69	14.27	7.50
2/24/2017 16:00	MB_ANHA1	0 days 06:00:00	8.25	26.33	15.59
2/26/2017 15:00	MB_LAJ7	0 days 00:50:00	9.75	13.32	6.61
2/26/2017 15:00	MB_PRO6	0 days 01:10:00	1.75	33.46	19.17
2/26/2017 15:10	MB_PRO4	0 days 01:20:00	13.94	49.49	33.67
2/26/2017 15:20	MB_PRO1	0 days 00:50:00	9.00	15.70	8.83
2/26/2017 15:30	MB_SEG3	0 days 01:00:00	37.00	20.23	27.68
3/1/2017 14:50	MB_ANHA1	0 days 00:40:00	2.38	15.65	8.78
3/3/2017 21:10	MB_LAJ2	0 days 03:50:00	23.00	20.80	29.07
3/5/2017 13:30	MB_BAL2	0 days 05:40:00	3.69	13.59	6.85
3/5/2017 14:20	MB_IMB3	0 days 04:50:00	25.00	10.04	16.22
3/5/2017 14:30	MB_LAJ3	0 days 04:20:00	44.00	24.83	34.74
3/5/2017 14:40	MB_LAJ2	0 days 04:30:00	22.50	38.65	23.40
3/5/2017 15:10	MB_PRO1	0 days 04:20:00	9.50	11.12	4.88
3/10/2017 14:10	MB_LAJ9	0 days 04:30:00	60.25	24.46	34.10
3/10/2017 14:10	MB_LAJ3	0 days 04:20:00	53.25	25.06	35.14
3/10/2017 14:20	MB_ANHA3	0 days 04:30:00	11.81	26.62	15.84
3/10/2017 14:20	MB_BAL2	0 days 04:30:00	8.13	29.17	19.68
3/10/2017 14:30	MB_LAJ2	0 days 03:00:00	21.25	20.69	28.86
3/10/2017 14:30	MB_LAJ7	0 days 04:30:00	78.25	53.68	68.86
3/10/2017 14:40	MB_PRO1	0 days 04:20:00	20.75	13.62	20.36
3/10/2017 14:50	MB_SEG3A	0 days 03:20:00	31.50	12.09	18.59
3/10/2017 15:00	MB_LAG2	0 days 05:00:00	9.81	16.50	9.46
3/10/2017 15:10	MB_SEG3	0 days 02:40:00	37.00	20.07	27.16

3/10/2017 15:30	MB_ANHA1	0 days 04:00:00	6.44	17.95	10.44
3/12/2017 16:10	MB_BAL2	0 days 04:40:00	6.19	14.56	7.78
3/12/2017 16:20	MB_ANHA3	0 days 01:00:00	6.00	11.04	4.82
3/13/2017 18:40	MB_ANHA3	0 days 04:40:00	4.81	12.58	5.98
3/13/2017 18:40	MB_PRO1	0 days 05:00:00	14.25	14.81	8.02
3/13/2017 18:50	MB_BAL2	0 days 05:00:00	3.69	16.05	9.12
3/13/2017 19:00	MB_LAJ2	0 days 04:40:00	17.75	25.64	15.19
3/13/2017 19:10	MB_SEG3	0 days 05:10:00	13.50	12.70	19.33
3/13/2017 19:10	MB_ANHA1	0 days 04:40:00	6.00	21.92	13.22
3/13/2017 20:30	MB_LAJ3	0 days 02:50:00	17.50	22.87	14.04
3/13/2017 20:40	MB_PRO6	0 days 03:10:00	1.81	11.31	5.03
3/13/2017 20:40	MB_LAJ9	0 days 03:00:00	13.50	17.35	10.03
3/14/2017 13:10	MB_ANHA3	0 days 03:00:00	7.25	21.33	12.75
3/14/2017 13:30	MB_ANHA1	0 days 03:10:00	9.19	33.00	19.15
3/14/2017 13:40	MB_LAG2	0 days 04:00:00	10.00	25.53	15.15
3/16/2017 16:00	MB_LAJ2	0 days 06:00:00	9.75	11.63	5.26
3/16/2017 19:30	MB_LAJ3	0 days 03:20:00	27.00	43.02	26.70
3/16/2017 19:40	MB_ANHA3	0 days 07:10:00	3.25	25.19	15.03
3/16/2017 19:40	MB_BAL2	0 days 03:20:00	10.63	42.62	26.80
3/16/2017 20:10	MB_PRO1	0 days 02:40:00	26.50	14.74	21.52
3/16/2017 20:30	MB_LAG2	0 days 04:30:00	7.75	11.68	5.30
3/16/2017 20:30	MB_LAJ9	0 days 02:10:00	38.75	40.95	27.13
3/18/2017 14:10	MB_PRO1	0 days 01:40:00	37.75	19.97	26.66
3/18/2017 14:20	MB_LAJ9	0 days 00:50:00	31.75	13.53	20.27
3/19/2017 12:20	MB_LAJ9	0 days 04:00:00	16.50	12.65	19.27
3/19/2017 12:30	MB_PRO4	0 days 04:10:00	8.13	32.06	20.08
3/19/2017 14:00	MB_PRO1	0 days 01:30:00	18.25	19.25	11.78
3/19/2017 14:20	MB_COQ3	0 days 02:10:00	35.00	11.20	17.45
3/19/2017 14:20	MB_PRO6	0 days 02:30:00	3.13	53.05	38.67
3/22/2017 5:40	MB_PRO6	0 days 01:00:00	0.69	14.04	7.28
3/23/2017 15:50	MB_LAJ2	0 days 00:40:00	19.75	11.40	17.71
3/23/2017 16:20	MB_COQ1	0 days 00:20:00	3.00	10.42	4.29
3/24/2017 12:00	MB_LAJ3	0 days 01:30:00	10.00	11.18	4.93
3/24/2017 12:20	MB_LAJ9	0 days 01:40:00	25.00	27.08	16.32
3/24/2017 12:20	MB_PRO1	0 days 02:00:00	60.00	55.05	70.73
3/24/2017 12:30	MB_LAJ2	0 days 01:30:00	27.25	16.80	23.94
3/24/2017 12:30	MB_BAL2	0 days 01:20:00	3.81	23.07	14.18
3/24/2017 12:50	MB_IMB3	0 days 01:10:00	47.00	23.64	32.77
3/25/2017 15:20	MB_PRO6	0 days 04:30:00	1.00	10.66	4.51
3/26/2017 12:20	MB_LAJ3	0 days 05:50:00	19.75	16.55	23.60
3/26/2017 13:00	MB_LAJ2	0 days 06:00:00	26.00	19.02	26.59
3/26/2017 13:30	MB_COQ3	0 days 06:00:00	22.25	21.04	29.49
3/26/2017 13:40	MB_PRO1	0 days 06:00:00	24.50	20.17	27.49
3/26/2017 13:40	MB_LAJ9	0 days 05:50:00	18.25	20.17	12.85
3/26/2017 13:40	MB_BAL2	0 days 06:00:00	4.31	20.65	12.53
3/26/2017 13:50	MB_PRO6	0 days 05:50:00	2.94	20.24	12.77
3/26/2017 14:10	MB_PRO4	0 days 06:00:00	5.06	11.98	5.51
4/5/2017 9:00	MB_ANHA4	0 days 06:00:00	0.25	14.46	7.68

4/5/2017 10:50	MB_BAL2	0 days 04:20:00	2.63	14.87	8.08
4/5/2017 11:50	MB_LAJ2	0 days 03:30:00	23.25	25.84	15.29
4/8/2017 13:00	MB_PRO6	0 days 01:10:00	1.00	23.93	14.64
4/8/2017 13:00	MB_PRO1	0 days 01:00:00	23.75	25.75	15.24
4/8/2017 13:10	MB_BAL2	0 days 00:50:00	2.94	17.84	10.36
4/26/2017 9:10	MB_SEG3	0 days 03:30:00	3.94	11.11	4.88
5/15/2017 12:50	MB_ANHA5	0 days 04:30:00	0.94	11.25	4.98
6/8/2017 22:10	MB_SEG6	0 days 05:20:00	5.38	15.43	8.60
8/17/2017 1:10	MB_PRO5	0 days 05:00:00	2.19	11.54	5.19
9/29/2017 5:00	MB_SEG6	0 days 06:00:00	2.50	15.02	8.22
9/29/2017 6:50	MB_SEG3A	0 days 06:00:00	1.38	10.82	4.65
9/29/2017 8:00	MB_PRO6	0 days 06:00:00	3.50	12.03	5.55
9/29/2017 8:10	MB_PRO1	0 days 06:00:00	2.69	10.95	4.76
9/29/2017 8:20	MB_SEG9	0 days 06:00:00	2.94	11.72	5.32
9/29/2017 8:30	MB_COQ3	0 days 05:40:00	3.06	12.01	5.54
9/29/2017 8:40	MB_SEG3	0 days 06:00:00	2.88	14.02	7.26
9/29/2017 8:50	MB_PRO4	0 days 06:00:00	3.56	12.03	5.55
9/29/2017 11:00	MB_SEG6	0 days 02:40:00	2.31	11.95	5.49
10/1/2017 15:50	MB_IMB5	0 days 05:50:00	4.19	10.31	4.18
10/1/2017 20:50	MB_ANHA5	0 days 11:20:00	4.38	30.10	20.44
10/1/2017 22:20	MB_SEG6	0 days 05:50:00	8.44	28.02	17.73
10/2/2017 0:20	MB_LAJ3	0 days 05:40:00	6.06	12.17	5.66
10/2/2017 1:30	MB_PRO6	0 days 05:50:00	4.31	16.69	9.59
10/2/2017 1:30	MB_PRO1	0 days 05:50:00	7.44	17.88	10.38
10/2/2017 1:50	MB_SEG9	0 days 06:00:00	9.56	19.11	11.58
10/2/2017 2:10	MB_PRO4	0 days 06:00:00	10.00	15.90	9.00
10/2/2017 2:10	MB_SEG3	0 days 05:30:00	8.75	17.03	9.82
10/2/2017 2:10	MB_COQ3	0 days 05:30:00	10.69	18.33	10.73
10/2/2017 4:30	MB_SEG6	0 days 06:00:00	3.81	20.94	12.55
10/22/2017 4:30	MB_ANHA5	0 days 03:40:00	0.88	35.21	21.42
10/22/2017 5:30	MB_IMB5	0 days 04:10:00	1.63	37.66	22.94
10/22/2017 5:40	MB_SEG6	0 days 06:00:00	7.94	55.16	39.51
10/22/2017 7:00	MB_LAJ3	0 days 06:00:00	12.63	41.56	27.41
10/22/2017 7:40	MB_SEG3A	0 days 06:00:00	3.88	48.00	33.25
10/22/2017 8:10	MB_BAL2	0 days 06:00:00	12.00	24.98	14.96
10/22/2017 8:50	MB_PRO6	0 days 06:00:00	5.69	30.71	21.69
10/22/2017 9:00	MB_PRO1	0 days 06:00:00	11.19	24.21	14.74
10/22/2017 9:10	MB_SEG9	0 days 06:00:00	8.00	17.40	10.07
10/22/2017 9:40	MB_COQ3	0 days 06:00:00	6.88	11.73	5.33
10/22/2017 9:40	MB_LAJ2	0 days 06:00:00	10.38	16.17	9.21
10/22/2017 9:40	MB_SEG3	0 days 06:00:00	10.50	18.28	10.68
10/22/2017 9:40	MB_PRO4	0 days 06:00:00	6.38	20.86	12.54
10/27/2017 20:50	MB_SEG6	0 days 02:40:00	3.94	13.86	7.11
10/30/2017 15:50	MB_SEG6	0 days 05:20:00	8.00	13.75	7.01
11/4/2017 14:00	MB_SEG6	0 days 05:50:00	7.06	14.13	7.37
11/4/2017 15:10	MB_IMB5	0 days 05:20:00	3.00	17.28	9.99
11/4/2017 17:20	MB_PRO6	0 days 05:50:00	3.00	11.70	5.31
11/4/2017 17:50	MB_SEG9	0 days 06:00:00	12.25	26.46	15.70

11/4/2017 18:10	MB_SEG3	0 days 05:50:00	9.38	29.28	19.83
11/4/2017 18:10	MB_PRO4	0 days 05:40:00	7.25	31.44	21.09
11/4/2017 18:10	MB_COQ3	0 days 05:30:00	7.38	40.80	26.85
11/4/2017 22:10	MB_SEG3A	0 days 06:00:00	3.13	29.36	19.95
11/4/2017 23:20	MB_SEG6	0 days 04:40:00	2.94	23.66	14.52
11/6/2017 16:30	MB_BAL2	0 days 06:00:00	7.44	15.25	8.43
11/6/2017 17:00	MB_LAJ3	0 days 06:00:00	14.69	34.88	20.88
11/6/2017 19:30	MB_SEG3A	0 days 06:00:00	5.50	12.23	5.70
11/6/2017 20:00	MB_LAJ2	0 days 06:00:00	15.56	16.95	9.77
11/16/2017 15:00	MB_SEG6	0 days 06:00:00	6.13	20.88	12.54
11/16/2017 17:10	MB_SEG3A	0 days 06:00:00	3.19	18.62	11.00
11/18/2017 14:00	MB_SEG3A	0 days 06:00:00	2.06	29.25	19.79
11/18/2017 15:20	MB_LAJ2	0 days 06:00:00	2.75	25.53	15.15
11/18/2017 16:30	MB_LAJ3	0 days 06:00:00	13.88	15.61	8.75
11/18/2017 17:10	MB_BAL2	0 days 06:00:00	14.25	22.99	14.12
11/21/2017 13:50	MB_SEG3A	0 days 13:20:00	2.13	24.91	14.94
11/21/2017 23:10	MB_SEG6	0 days 05:00:00	5.56	22.89	14.05
11/25/2017 23:00	MB_SEG3A	0 days 06:00:00	1.31	11.16	4.92
11/26/2017 11:10	MB_SEG3A	0 days 06:30:00	17.81	22.42	13.67
11/26/2017 14:40	MB_SEG6	0 days 04:20:00	3.06	15.87	8.98
11/26/2017 15:10	MB_SEG3	0 days 06:00:00	9.75	11.66	5.28
11/30/2017 12:00	MB_SEG6	0 days 05:20:00	10.25	58.32	42.31
11/30/2017 12:40	MB_LAJ3	0 days 05:10:00	10.13	24.04	14.68
12/20/2017 18:00	MB_SEG3A	0 days 06:20:00	20.81	14.69	21.48
1/2/2018 15:50	MB_SEG9	0 days 09:10:00	4.44	13.54	6.80
1/7/2018 13:50	MB_SEG6	0 days 05:40:00	3.06	11.17	4.92
1/26/2018 17:40	MB_SEG6	0 days 01:20:00	4.38	18.10	10.55
2/8/2018 0:00	MB_SEG6	0 days 02:20:00	1.94	14.66	7.88
2/13/2018 14:10	MB_SEG6	0 days 05:40:00	7.00	26.11	15.44
2/18/2018 14:30	MB_SEG6	0 days 19:10:00	3.06	14.50	7.72
2/19/2018 21:30	MB_IMB5	0 days 06:00:00	6.25	14.32	7.55
2/20/2018 3:50	MB_IMB5	0 days 05:50:00	3.56	37.44	22.99
2/20/2018 6:30	MB_LAJ2	0 days 06:00:00	15.13	44.41	27.95
2/20/2018 6:50	MB_PRO3	0 days 06:00:00	14.25	33.13	19.12
2/20/2018 7:10	MB_PRO6	0 days 05:50:00	5.31	29.69	20.29
2/20/2018 7:10	MB_PRO1	0 days 05:50:00	13.75	33.12	19.12
2/20/2018 7:20	MB_BAL2	0 days 05:50:00	12.31	35.35	21.65
2/20/2018 7:30	MB_COQ3	0 days 06:00:00	14.44	12.90	19.56
2/20/2018 7:40	MB_SEG9	0 days 06:00:00	14.00	32.94	19.17
2/20/2018 8:00	MB_SEG3	0 days 05:50:00	14.50	17.58	10.18
2/20/2018 8:10	MB_PRO4	0 days 05:50:00	9.63	12.18	5.66
2/20/2018 9:20	MB_SEG6	0 days 05:50:00	3.56	26.78	15.99
2/20/2018 12:50	MB_PRO3	0 days 06:00:00	4.31	11.32	5.04
2/20/2018 13:10	MB_PRO1	0 days 06:00:00	5.06	11.46	5.13
2/20/2018 13:10	MB_PRO6	0 days 06:00:00	3.88	15.25	8.43
2/20/2018 13:40	MB_SEG9	0 days 06:00:00	3.63	14.59	7.81
2/25/2018 18:50	MB_COQ3	0 days 06:00:00	14.81	18.49	10.87

Chapter 3

All application files are stored on GitHub, and can be downloaded from the following addresses:

https://github.com/leocrivels/flood_alert-DataManagement
https://github.com/leocrivels/flood_alert

The following is the main code of the progressive web application:

Map.vue

```
<template>
 <GmapMap
  :key="mapKey"
  ref="map"
  fullscreen
  :center="center"
  map-type-id="terrain"
  style="height: 100%; width: 100%"
  dark
  :options="{
   streetViewControl: false,
   zoomControl: false,
   fullscreenControl: false,
   mapTypeControl: false,
  }"
 >
  <template v-for="(floodArea, j) in floodAreasArray">
   <template v-for="(area, i) in floodArea">
    <GmapPolygon
     :key="'area-' + i + 'flood' + j"
     :path="area"
     :options="{
      fillColor: 'blue',
      strokeOpacity: 0,
     }"
    />
   </template>
  </template>

  <GmapMarker :position="center" />
  <template
   v-for="(marker, i) in Object.values(markers)"
```

```
  style="max-width: 300px"
>
  <gmap-custom-marker
    :marker="marker.coord"
    :key="'marker' + i"
    @click.native="markerClicked(marker)"
  >
    <img :src="getMarkerIcon(marker)" />
  </gmap-custom-marker>
</template>

<v-dialog
  v-model="infoDialogBool"
  style="max-width: 100%; overflow-x: hidden"
  width="280"
  height="300"
  hide-overlay
>
  <v-card>
    <v-img
      class="white--text align-end"
      height="144"
      width="260"
      :src="actualMarker.image"
    ></v-img>
  </v-card>
</v-dialog>

<v-dialog
  v-model="showGraphBool"
  style="max-width: 100%; overflow-x: hidden"
>
  <v-card style="max-width: 100%; overflow-x: hidden">
    <v-tabs v-model="tab" background-color="primary" dark>
      <v-tab> About </v-tab>
      <v-tab> R. Section </v-tab>
      <v-tab> W. Level/Time </v-tab>
    </v-tabs>
    <v-tabs-items v-model="tab">
      <v-tab-item>
        <v-card v-if="$vuetify.breakpoint.mdAndUp" class="pa-2">
          <div class="d-flex">
            <v-col cols="6">
              <v-img class="white--text" :src="actualMarker.image"></v-img>
            </v-col>
            <v-col cols="6">
              <div>
                <v-card-title
                  class="headline"
```

```
          v-text="actualMarker.description"
        ></v-card-title>

        <v-card-subtitle>
          <p>
            <strong>Description:</strong>
            {{ actualMarker.description }}
          </p></v-card-subtitle
        >
        <v-card-subtitle>
          <p>
            <strong>Threshold:</strong> {{ actualMarker.limit }} m
          </p></v-card-subtitle
        >
        <v-card-subtitle>
          <p>
            <strong>Water Level:</strong>
            {{ parseFloat(actualMarkerState.height).toFixed(2) }}m
          </p></v-card-subtitle
        >
        <v-card-subtitle>
          <p>
            <strong>Situation:</strong>
            {{ actualMarkerState.label }}
          </p></v-card-subtitle
        >
      </div>
    </v-col>
  </div>
</v-card>
<v-card v-if="$vuetify.breakpoint.smAndDown">
  <div class="d-flex">
    <v-col cols="12">
      <v-img class="white--text" :src="actualMarker.image"></v-img>
      <div class="mt-3">
        <v-card-subtitle>
          <p>
            <strong>Description:</strong>
            {{ actualMarker.description }}
          </p></v-card-subtitle
        >
        <v-card-subtitle>
          <p>
            <strong>Threshold:</strong> {{ actualMarker.limit }} m
          </p></v-card-subtitle
        >
        <v-card-subtitle>
          <p>
            <strong>Water Level:</strong>
```

```
            {{ parseFloat(actualMarkerState.height).toFixed(2) }} m
          </p></v-card-subtitle
        >
        <v-card-subtitle>
          <p>
            <strong>Situation:</strong>
            {{ actualMarkerState.label }}
          </p></v-card-subtitle
        >
      </div>
    </v-col>
  </div>
 </v-card>
</v-tab-item>
<v-tab-item>
 <v-card flat>
  <v-row
   :justify="$vuetify.breakpoint.mdAndUp ? 'center' : 'left'"
   :class="$vuetify.breakpoint.mdAndUp ? '' : 'pl-2'"
  >
   <GChart
    class="align-center"
    type="AreaChart"
    :data="channelChartData"
    :options="channelChartOptions"
   />
  </v-row>

  <v-row justify="center" align="center">
   <v-chip class="ma-2" :color="clockChipColor" text-color="black">
    <v-icon left>{{ clockChipIcon }}</v-icon>
    {{ sliderLabels[slider] }}
   </v-chip>
   <v-chip outlined>{{ clockChipLabel }} </v-chip>
  </v-row>
  <v-slider
   v-model="slider"
   class="align-center mx-4 pb-4"
   :max="sliderMax"
   min="0"
   hide-details
   @input="updateGraph()"
  >
  </v-slider>
 </v-card>
</v-tab-item>
<v-tab-item>
 <v-card flat>
  <v-container wrap>
```

```
            <v-layout wrap>
              <v-row
                :justify="$vuetify.breakpoint.mdAndUp ? 'center' : 'left'"
                :class="$vuetify.breakpoint.mdAndUp ? '' : 'pl-0'"
              >
                <GChart
                  class="align-left mx-0"
                  type="LineChart"
                  :data="timeChartData"
                  :options="timeChartOptions"
                />
              </v-row>
              <v-row>
                <v-col cols="3" sm="3" class="pa-1">
                  <v-chip color="green" small> Safe </v-chip>
                </v-col>
                <v-col cols="9" sm="8" class="pa-1">
                  <p style="font-size: 13px">
                    <strong
                      >The limit where the water is at a safe level</strong
                    >
                  </p>
                </v-col>
              </v-row>
              <v-row>
                <v-col cols="3" sm="3" class="pa-1" center>
                  <v-chip small color="red"> warning </v-chip>
                </v-col>
                <v-col cols="9" sm="8" class="pa-1">
                  <p style="font-size: 13px">
                    <strong
                      >When the water level is higher then the
                      Threshold</strong
                    >
                  </p>
                </v-col>
              </v-row>
            </v-layout>
          </v-container>
        </v-card>
      </v-tab-item>
    </v-tabs-items>
  </v-card>
</v-dialog>

<v-dialog
  v-model="aboutDialog"
  fullscreen
  style="max-width: 100%; overflow-x: hidden; backgroud: #ffffff"
```

```
>
 <v-card :height="screenHeight - 100">
  <v-layout
   style="max-width: 100%; overflow-x: hidden; backgroud: #ffffff"
   fluid
   fullscreen
   row
   align-end
   justify-center
   fill-height
  >
   <v-toolbar dark color="primary">
    <v-btn icon dark @click="aboutDialog = false">
     <v-icon>mdi-close</v-icon>
    </v-btn>
    <v-toolbar-title>About the app</v-toolbar-title>
    <v-spacer></v-spacer>
   </v-toolbar>
   <v-layout row align-end justify-center fill-height>
    <v-flex xs12 sm12 md12 lg12 xg12>
     <v-img :src="logo_app"></v-img>
    </v-flex>
    <v-flex class="about-text about-center py-4 px-4">
     <div
      v-if="$vuetify.breakpoint.xsOnly"
      class="text-xs-center subheading"
     >
      <p>
       This app was developed by the joined efforts of Federal
       University of Mato Grosso do Sul (UFMS) and Hydrology and
       Water Security Research Group (HWS).
      </p>
      <p>
       The study was supported by grants from the Ministry of
       Science, Technology, Innovation and Communication – MCTIC and
       National Council for Scientific and Technological Development
       – CNPq (grants 441289/2017-7 and 306830/2017-5) and
       Coordenação de Aperfeiçoamento de Pessoal de Nível Superior -
       Brasil – CAPES (Finance Code 001 and Capes PrInt).
      </p>
     </div>
     <div
      v-if="$vuetify.breakpoint.smAndUp"
      class="text-xs-center headline"
     >
      <p>
       This app was developed by the joined efforts of Federal
       University of Mato Grosso do Sul (UFMS) and Hydrology and
       Water Security Research Group (HWS).
```

```
          </p>
          <p>
            The study was supported by grants from the Ministry of
            Science, Technology, Innovation and Communication – MCTIC and
            National Council for Scientific and Technological Development
            – CNPq (grants 441289/2017-7 and 306830/2017-5) and
            Coordenação de Aperfeiçoamento de Pessoal de Nível Superior -
            Brasil – CAPES (Finance Code 001 and Capes PrInt).
          </p>
        </div>

        <p
          v-if="$vuetify.breakpoint.xsOnly"
          class="body-2 text-xs-center mt-4 white--text"
          style="text-decoration: underline"
        >
          Version: Alpha-0.1
        </p>
        <p
          v-if="$vuetify.breakpoint.smAndUp"
          class="body-1 text-xs-center mt-4 white--text"
          style="text-decoration: underline"
        >
          Version: Alpha-0.1
        </p>
      </v-flex>
      <v-flex xs6 sm6 md6 lg6 xg6 class="pl-6 pr-1 pb-12 mb-10">
        <v-img :src="logo_ufms"></v-img>
      </v-flex>
      <v-flex xs6 sm6 md6 lg6 xg6 class="pl-1 pr-6 pb-12 mb-10">
        <v-img :src="logo_hws"></v-img>
      </v-flex>
    </v-layout>
  </v-layout>
 </v-card>
</v-dialog>

<template v-if="loadButton">
 <v-row>
  <v-col cols="9">
   <v-select
    v-model="selectedDate"
    :items="simulationDatesAvailable"
    label="Data"
    dense
    solo
    background-color="white"
    height="4"
    class="ma-2"
```

```
          @change="changeSelectedDate()"
        ></v-select>
      </v-col>
      <v-speed-dial
        style="position: absolute"
        v-model="fab"
        large
        top
        right
        direction="bottom"
        transition="slide-y-reverse-transition"
      >
        <template v-slot:activator>
          <v-btn v-model="fab" color="blue darken-2" dark fab>
            <v-icon v-if="fab">mdi-close</v-icon>
            <v-icon v-else>menu</v-icon>
          </v-btn>
        </template>
        <v-btn fab dark small color="green" @click="aboutDialog = true">
          <v-icon>info</v-icon>
        </v-btn>
      </v-speed-dial>
    </v-row>
  </template>
 </GmapMap>
</template>

<style>
.vue-map-hidden {
 display: contents;
 height: 100%;
 width: 100%;
 position: absolute;
 top: 0px;
 left: 0px;
}

.bg-image {
 display: flex;
 flex-direction: column;
 justify-content: center;
}

.gm-style .gm-style-iw-c {
 width: 300px;
 max-width: 300px;
}
.gm-style .gm-style-iw {
 min-width: 300px;
```

```
}
.about-center {
  width: 90%;
  margin: auto;
  position: absolute;
  top: 50%;
  left: 50%;
  -webkit-transform: translate(-50%, -50%);
  -ms-transform: translate(-50%, -50%);
  transform: translate(-50%, -50%);
}

.wrapper {
  height: 100%;
}

.about-text {
  background-color: rgba(0, 0, 0, 0.3);
  color: #fff;
}
</style>

<script>
import { gmapApi } from "vue2-google-maps";
import { db } from "../utils/db";
import { GChart } from "vue-google-charts";
import GmapCustomMarker from "vue2-gmap-custom-marker";
import logo_ufms from "../assets/logo_ufms.jpg";
import logo_hws from "../assets/hws-ufms.png";
import logo_app from "../assets/logo_app.png";
import BackgroundImage from "../assets/bg_screen.png";
const polygons_table = "polygons_table_name";
const markers_table = "markers_tables_name";
export default {
  components: {
    GChart,
    "gmap-custom-marker": GmapCustomMarker,
  },
  computed: {
    google: gmapApi,
  },
  firebase: {
    polygons: db.ref(polygons_table),
  },
  mounted() {
    if (localStorage.getItem("floodSurfaces"))
      this.floodSurfaces = JSON.parse(localStorage.getItem("floodSurfaces"));
    if (localStorage.getItem("lastUpdate"))
      this.lastUpdate = JSON.parse(localStorage.getItem("lastUpdate"));
```

```
if (localStorage.getItem("markers"))
  this.markers = JSON.parse(localStorage.getItem("markers"));

db.ref(polygons_table).once("value", (snapshot) => {
  const documents = snapshot.val();
  for (const itemID in documents) {
    db.ref(polygons_table+'/' + itemID).once("value", (snapshot) => {
      const document = snapshot.val();
      if (document.properties.created > this.lastUpdate) {
        const surface = { id: itemID, properties: document.properties };
        this.floodSurfaces.push(surface);
        this.lastUpdate = document.properties.created;
      }
    });
  }
});

db.ref(markers_table).once("value", (snapshot) => {
  const documents = snapshot.val();
  this.markers = documents;
});

var min = 0;
var max = 99999999;
var selected = 0;
var selectedSurfaces = [];

for (const surface of this.floodSurfaces) {
  var ts = new Date(surface.properties.timestamp);
  if (ts >= min && ts < Date.now() && selected == 0) {
    if (ts == min) {
      selectedSurfaces.push(surface);
    } else {
      selectedSurfaces = [];
      selectedSurfaces.push(surface);
    }
    min = ts;
  } else if (ts >= Date.now() && ts <= max) {
    if (ts == max || selected == 0) {
      selectedSurfaces.push(surface);
    } else {
      selectedSurfaces = [];
      selectedSurfaces.push(surface);
    }
    max = ts;
    selected = ts;
  }
  this.simulationDatesAvailable.push(ts.toLocaleString());
}
```

```
  if (selected == 0) {
    this.selectedDate = min.toLocaleString();
  } else {
    this.selectedDate = selected.toLocaleString();
  }
  this.changeSelectedDate(this.selectedDate);

  for (const surface of selectedSurfaces) {
    this.getPolyCoordinates(surface);
  }

  this.geolocate();
  this.loadButton = true;
},
updated() {
  setInterval(this.geolocate(), 1800000);
},
data: () => ({
  backgroundImage: BackgroundImage,
  screenHeight: window.innerHeight,
  logo_hws: logo_hws,
  logo_ufms: logo_ufms,
  logo_app: logo_app,
  selectedDate: "",
  selectedTimestamp: 0,
  dateObjSelected: {},
  sliderMax: 0,
  sliderLabels: [],
  actualMarker: {},
  lastUpdate: 0,
  actualMarkerState: {},
  slider: 0,
  clockChipColor: "green",
  clockChipIcon: "done_outline",
  clockChipLabel: "Safe",
  tab: null,
  zoom: 15,
  showGraphBool: 0,
  infoDialogBool: 0,
  aboutDialog: false,
  timeChartData: [],
  channelChartData: [],
  channelChartOptions: {
    vAxis: {
      title: "Water Level (m)",
      titleTextStyle: { bold: true, fontSize: "14" },
    },
    hAxis: {
```

```
    title: "Width (m)",
    titleTextStyle: { bold: true, fontSize: "14" },
  },
  legend: { position: "top", textStyle: { bold: true, fontSize: "12" } },
  height: 350,
  width: 350,
  isStacked: true,
  forceIFrame: true,
  series: [
    { color: "black", lineWidth: 1 },
    { color: "blue", lineWidth: 0 },
  ],
},
timeChartOptions: {
  chart: {
    title: "Time x Water Level",
  },
  curveType: "function",
  crosshair: {
    color: "#000",
    trigger: "selection",
  },
  forceIFrame: true,
  vAxis: {
    title: "Water Level (m)",
    titleTextStyle: { bold: true, fontSize: "14" },
  },
  hAxis: {
    title: "Hour (h)",
    titleTextStyle: { bold: true, fontSize: "14" },
  },
  legend: {
    position: "top",
    textStyle: { bold: true, fontSize: "12" },
    maxLines: "2",
  },
  series: {
    0: {
      visibleInLegend: false,
      // Set any applicable options on the first series
    },
    1: {
      // Set the options on the second series
      color: "black",
      lineWidth: 1,
      lineDashStyle: [4, 2, 4],
      pointSize: 3,
      visibleInLegend: true,
    },
```

```
      2: {
        // Set the options on the second series
        color: "green",
        lineWidth: 2,
        pointSize: 0,
        visibleInLegend: true,
      },
      3: {
        // Set the options on the second series
        color: "red",
        lineWidth: 2,
        pointSize: 0,
        visibleInLegend: true,
      },
    },
  },
  mapKey: 0,
  polygons: [],
  simulationDatesAvailable: [],
  floodSurfaces: [],
  loadButton: false,
  fab: false,
  center: { lat: -20.50327, lng: -54.609691 },
  marker: { lat: -20.45495, lng: -54.582083 },
  markers: {},
  floodAreasArray: [],
  floodAreas: [],
}),
watch: {
  floodSurfaces: {
    handler() {
      localStorage.setItem(
        "floodSurfaces",
        JSON.stringify(this.floodSurfaces)
      );
    },
    deep: true,
  },
  markers: {
    handler() {
      localStorage.setItem("markers", JSON.stringify(this.markers));
    },
    deep: true,
  },
  lastUpdate: {
    handler() {
      localStorage.setItem("lastUpdate", JSON.stringify(this.lastUpdate));
    },
    deep: true,
```

```
  },
 },
 methods: {
  // Set the chosen simulation date on the picker and get it from firebase
  changeSelectedDate: function () {
   this.floodAreasArray = [];
   var dateAndTime = this.selectedDate.split(" ");
   var date = dateAndTime[0].split("/");
   var time = dateAndTime[1].split(":");

   this.dateObjSelected = {
    year: date[2],
    month: parseInt(date[1]) - 1,
    day: date[0],
    hour: time[0],
    minutes: time[1],
    seconds: time[2],
   };
   this.selectedTimestamp = new Date(
    date[2],
    parseInt(date[1]) - 1,
    date[0],
    time[0],
    time[1],
    time[2]
   ).getTime();

   var selectedSurfaces = [];
   for (const surface of this.floodSurfaces) {
    var ts = surface.properties.timestamp;

    if (parseInt(ts) == parseInt(this.selectedTimestamp)) {
     selectedSurfaces.push(surface);
    }
   }

   for (const surface of selectedSurfaces) {
    db.ref(polygons_table+'/' + surface.id).once("value", (snapshot) => {
     const document = snapshot.val();
     this.getPolyCoordinates(document);
    });
   }
  },
  // Convert date string to object
  getDateObj: function (dateString) {
   var dateAndTime = dateString.split(" ");
   var date = dateAndTime[0].split("/");
   var time = dateAndTime[1].split(":");
   return {
```

```
    year: date[2],
    month: parseInt(date[1]) - 1,
    day: date[0],
    hour: time[0],
    minutes: time[1],
    seconds: time[2],
  };
},

findTimestampIndex: function (array, value) {
  const position = array.findIndex(function (object) {
    return object.timestamp === value;
  });
  return position;
},
// Creates graphs of the marker info
showGraphs: function () {
  var dateObjSelected = this.dateObjSelected;
  this.sliderLabels = [];

  var hourselected = parseFloat(dateObjSelected.hour);
  var daySelectedTimestamp = new Date(
    dateObjSelected.year,
    dateObjSelected.month,
    dateObjSelected.day,
    0,
    0,
    0
  ).getTime();

  this.slider = hourselected;
  var marker = this.actualMarker;
  var timeChartData = [["Hour", "Depth", "S. Time", "Safe", "Warning"]];

  var channelChartData = [["Calha X", "Channel", "Water"]];

  for (const depth of marker.depths) {
    if (
      depth.timestamp >= daySelectedTimestamp &&
      depth.timestamp < daySelectedTimestamp + 86400000
    ) {
      var ts = new Date(parseInt(depth.timestamp));
      var time = this.getDateObj(ts.toLocaleString());
      var newData;
      if (depth.timestamp == this.selectedTimestamp) {
        timeChartData.push([
          parseInt(time.hour) + time.minutes / 60,
          parseFloat(depth.height),
          0,
```

```
        marker.limit - 0.5,
        marker.limit,
      ]);
      newData = [
        parseInt(time.hour) + time.minutes / 60,
        parseFloat(depth.height),
        parseFloat(depth.height),
        marker.limit - 0.5,
        marker.limit,
      ];
    } else {
      newData = [
        parseInt(time.hour) + time.minutes / 60,
        parseFloat(depth.height),
        null,
        marker.limit - 0.5,
        marker.limit,
      ];
    }
    timeChartData.push(newData);
    if (time.hour == hourselected) this.slider = this.sliderLabels.length;
    this.sliderLabels.push(time.hour + ":" + time.minutes);
  }
}
this.sliderMax = this.sliderLabels.length - 1;

for (const arrayXY of marker.graphArray) {
  var timeSelectedSlider = this.sliderLabels[this.slider].split(":");
  var timestampSliderSelected = new Date(
    dateObjSelected.year,
    dateObjSelected.month,
    dateObjSelected.day,
    timeSelectedSlider[0],
    timeSelectedSlider[1],
    0
  ).getTime();
  var xy = arrayXY.slice();

  var depth = marker.depths.find((obj) => {
    return parseInt(obj.timestamp) === parseInt(timestampSliderSelected);
  });
  parseFloat(depth.height) - xy[1] > 0
    ? xy.push(parseFloat(depth.height) - xy[1])
    : xy.push(0);
  channelChartData.push(xy);
}
this.changeClockChipColor(timestampSliderSelected);

this.timeChartData = timeChartData;
```

```
  if (this.$vuetify.breakpoint.lgAndUp) {
    this.timeChartOptions.height = 700;
    this.timeChartOptions.width = 850;
    this.channelChartOptions.height = 700;
    this.channelChartOptions.width = 800;
  } else if (this.$vuetify.breakpoint.mdOnly) {
    this.timeChartOptions.height = 500;
    this.timeChartOptions.width = 650;
    this.channelChartOptions.height = 500;
    this.channelChartOptions.width = 600;
  } else if (this.$vuetify.breakpoint.smAndDown) {
    this.timeChartOptions.height = 300;
    this.timeChartOptions.width = 400;
    this.channelChartOptions.height = 300;
    this.channelChartOptions.width = 350;
  }

  this.channelChartData = channelChartData;
  this.showGraphBool = 1;
},
// updates the channel form graph with new water level when using the slider
updateGraph: function () {
  var channelChartData = [["Calha X", "Channel", "Water"]];
  var marker = this.actualMarker;
  var dateObjSelected = this.dateObjSelected;
  for (const arrayXY of marker.graphArray) {
    var timeSelectedSlider = this.sliderLabels[this.slider].split(":");
    var timestampSliderSelected = new Date(
      dateObjSelected.year,
      dateObjSelected.month,
      dateObjSelected.day,
      timeSelectedSlider[0],
      timeSelectedSlider[1],
      0
    ).getTime();
    var xy = arrayXY.slice();

    var depth = marker.depths.find((obj) => {
      return parseInt(obj.timestamp) === parseInt(timestampSliderSelected);
    });

    parseFloat(depth.height) - xy[1] > 0
      ? xy.push(parseFloat(depth.height) - xy[1])
      : xy.push(0);
    channelChartData.push(xy);
  }
  this.changeClockChipColor(timestampSliderSelected);

  this.channelChartData = channelChartData;
```

```
},
// Change the color, icon and label of the chip in the slider
// according to the level state
changeClockChipColor: function (timestamp) {
  var state = this.checkLevelState(this.actualMarker, timestamp);
  this.clockChipColor = state.color;
  this.clockChipIcon = state.icon;
  this.clockChipLabel = state.label;
},
// Check the level state in a marker
checkLevelState: function (marker, timestamp) {
  var state = {
    label: "",
    icon: "",
    color: "",
    height: 0,
  };
  var depth = marker.depths.find((obj) => {
    return parseInt(obj.timestamp) === parseInt(timestamp);
  });
  if (!depth) {
    state.color = "blue";
    state.icon = "warning";
    state.label = "No Information";
    state.height = 0;
    return state;
  }
  if (depth.height > marker.limit) {
    state.color = "red";
    state.icon = "warning";
    state.label = "Danger";
    state.height = depth.height;
  } else if (
    depth.height <= marker.limit &&
    depth.height >= marker.limit - 0.5
  ) {
    state.color = "yellow";
    state.icon = "error_outline";
    state.label = "Warning";
    state.height = depth.height;
  } else if (depth.height < marker.limit - 0.5) {
    state.color = "green";
    state.icon = "done_outline";
    state.label = "Safe";
    state.height = depth.height;
  }
  return state;
},
// Get the marker icon url according to its level state
```

```
getMarkerIcon: function (marker) {
  var state = this.checkLevelState(marker, this.selectedTimestamp);
  var color = state.color;
  return "http://maps.google.com/mapfiles/ms/icons/" + color + "-dot.png";
},
// Updates the user location
geolocate: function () {
  navigator.geolocation.getCurrentPosition((position) => {
    this.center = {
      lat: position.coords.latitude,
      lng: position.coords.longitude,
    };
  });
},
// Get the polygon vertices coordinates
getPolyCoordinates(floodSurfaces) {
  var coordsArray;
  var item;
  var item2;
  var floodAreas = [];

  for (coordsArray in floodSurfaces.geometries) {
    for (item in floodSurfaces.geometries[coordsArray].coordinates) {
      var geometries = [];
      for (item2 in floodSurfaces.geometries[coordsArray].coordinates[
        item
      ]) {
        geometries.push({
          lng:
            floodSurfaces.geometries[coordsArray].coordinates[item][
              item2
            ][0],
          lat:
            floodSurfaces.geometries[coordsArray].coordinates[item][
              item2
            ][1],
        });
      }
      floodAreas.push(geometries);
    }
  }
  this.floodAreasArray.push(floodAreas);
},
// Changes the selected marker
markerClicked: function (marker) {
  this.actualMarker = marker;
  this.actualMarkerState = this.checkLevelState(
    marker,
    this.selectedTimestamp
```

```
      );
      this.showGraphs();
    },
  },
};
</script>
```

Send_to_db_app.py (Pytho application for sending data to firebase)

```
from tkinter import *
from tkinter import filedialog
from tkinter import messagebox
from tkinter import ttk
import pyrebase
import json
import rasterio
from rasterio.mask import mask
from rasterio import features
import pprint
import numpy as np
import sys
from rasterio.enums import Resampling
import gdal, ogr, os, osr, errno
import csv
import time
import datetime
from functools import partial
import json
import csv
from datetime import datetime, timedelta
import requests
import requests_ftp
from google.cloud import storage

now = datetime.now()
backup_foldername = 'YOUR:/BACKUP/DIRECTORY/' + now.strftime("%Y-%m-%d")

def clickSelectFolder(folderEntry):
    direc = filedialog.askdirectory()
    folderEntry.set(direc)

#Get the forecast from cptec and creates a CSV
def createForecastCSV(folderEntry):
    if folderEntry.get() != '' and os.path.exists(os.path.dirname(folderEntry.get())):
        dateTimeObj = datetime.now()
        dateTimeObj = dateTimeObj - timedelta(hours=int(dateTimeObj.strftime("%H")))
        dayString = dateTimeObj.strftime("%d")
```

```
        monthString = dateTimeObj.strftime("%m")
        yearString = dateTimeObj.strftime("%Y")
        url = 'http://ftp1.cptec.inpe.br/modelos/tempo/WRF/ams_05km/recortes/grh/json/' + year
String + '/' + monthString + '/' + dayString + '/00/225.json'
        requests_ftp.monkeypatch_session()
        response = requests.get(url)
        print(response)
        data = response.text
        print(data)
        weather = json.loads(data)

        hora = int(dateTimeObj.strftime("%H"))
        print(str(hora))
        print(str(dateTimeObj))
        timestampStr = dateTimeObj.strftime("%d%b%Y %H")

        print('Current Timestamp : ', timestampStr)

        fileOutput = folderEntry.get()+'/forecast.csv'
        outputFile = open(fileOutput, 'w') #load csv file
        with open(fileOutput, 'w', newline='') as outputFile:
            output = csv.writer(outputFile, delimiter=',', quotechar='"', quoting=csv.QUOTE_MIN
IMAL)
            datasets = weather["datasets"][0]
            data = datasets["data"] #load json content
            outputFile.write("B,,PROSA\n")
            outputFile.write("C,UTC,PRECIP-INC\n")
            outputFile.write("E,,1HOUR\n")
            outputFile.write("F,,OBS\n")
            outputFile.write("Units,,MM\n")
            outputFile.write("Type,,PER-CUM\n")

            for i,row in enumerate(data):
                print(str(hora + i))
                outputFile.write(str(i+1) + "," + timestampStr + "00" +', '+ str(row["prec"]))
                outputFile.write('\n')
                dateTimeObj = dateTimeObj + timedelta(hours=1)
                timestampStr = dateTimeObj.strftime("%d%b%Y %H")

    elif folderEntry.get() == '':
        messagebox.showinfo('Error', 'Please Select the Destination Folder!')
    elif not os.path.exists(os.path.dirname(folderEntry.get())):
        messagebox.showinfo('Error', 'Destination Folder Doesn\'t Exist!')

#Downsample the raster
def downsampling( g, hires_data, factor ):
    """This function downsamples, using the **mode**, the 2D array
    `hires_data`. The datatype is assumed byte in this case, and
    you might want to change that. The output files are given by
```

```
    `fname_out`, and we downsample by a factor of 100 and 300. The
    initial GDAL dataset is `g` (this is where the data are coming
    from, and we use that to fish out the resolution, geotransform,
    etc.).

    NOTE that this is fairly specialised a function, and you might
    want to have more flexiblity by adding options to deal with
    the aggregation procedure in `gdal.RegenerateOverviews`, the
    resolutions of the aggregations you want, the datatypes, etc.
    """
    # Create an in-memory GDAL dataset to store the full resolution
    # dataset...

    total_obs = g.RasterCount
    drv = gdal.GetDriverByName( "MEM" )
    dst_ds = drv.Create("", g.RasterXSize, g.RasterYSize, 1, gdal.GDT_UInt16 )
    dst_ds.SetGeoTransform( g.GetGeoTransform())

    srs = osr.SpatialReference()
    srs.ImportFromEPSG(32721)

    dst_ds.SetProjection ( srs.ExportToWkt() )
    proj = osr.SpatialReference(wkt=g.GetProjection())

    dst_ds.GetRasterBand(1).WriteArray( hires_data.astype(float)*100 )

    geoT = g.GetGeoTransform()
    drv1 = gdal.GetDriverByName( "GTiff" )

    resampled_dir = backup_foldername + "/raster/"

    if not os.path.exists(os.path.dirname(resampled_dir)):
        try:
            os.makedirs(os.path.dirname(resampled_dir))
        except OSError as exc: # Guard against race condition
            if exc.errno != errno.EEXIST:
                raise

    resampled_filename =  resampled_dir + now.strftime("%Y-%m-%d_%H%M%S") + ".tif"

    resampled = drv1.Create( resampled_filename , int(g.RasterXSize/factor), int(g.RasterYSiz
e/factor), 1, gdal.GDT_UInt16 )

    this_geoT = ( geoT[0], geoT[1]*factor, geoT[2], geoT[3], geoT[4], geoT[5]*factor )
    resampled.SetGeoTransform( this_geoT )
    resampled.SetProjection (srs.ExportToWkt())

    gdal.RegenerateOverviews ( dst_ds.GetRasterBand(1), [resampled.GetRasterBand(1)],'aver
age' )
```

```
    resampled.GetRasterBand(1).SetNoDataValue ( 0 )

    return resampled_filename

#Makes the geojson of the raster's shape polygon
def makePolyGeojson(filename) :
    now = datetime.now()
    geoteste = ''
    orig_stdout = sys.stdout
    dateString = filename[filename.find('(')+1 : filename.find(')')]

    jsonBackUpName = backup_foldername + '/json/' + now.strftime("%Y-%m-
%d_%H%M%S")+'.json'
    if not os.path.exists(os.path.dirname(jsonBackUpName)):
        try:
            os.makedirs(os.path.dirname(jsonBackUpName))
        except OSError as exc: # Guard against race condition
            if exc.errno != errno.EEXIST:
                raise

    f = open(jsonBackUpName, 'w')
    print(filename)
    with rasterio.open(filename) as src:
        print(
            """{    "type": "GeometryCollection",
    "geometries": ["""
        )
        geoteste = geoteste +"""{    "type": "GeometryCollection",
    "geometries": ["""


        mask = src.dataset_mask()

        for geom, val in rasterio.features.shapes(
                mask, transform=src.transform):

            # Transform shapes from the dataset's own coordinate
            # reference system to CRS84 (EPSG:4326).
            geom = rasterio.warp.transform_geom(
                src.crs, 'EPSG:4326', geom, precision=5)

            # Print GeoJSON shapes to stdout.
            if val > 0 :
                pprint.pprint(geom)
                geoteste = geoteste + json.dumps(geom)
                geoteste = geoteste + "\n,"
                lastline = f.tell()
                print(',')
```

```
        f.seek(lastline)
        """],
        "period": {
           "begin": + str(time.time()*1000) + ,
           "end": + str((time.time()+3*3600)*1000) +}
           }"""
        print("""],
        "properties": {timestamp": """ + str(time.mktime(datetime.datetime.strptime(dateString,
"%d%b%Y %H %M %S").timetuple())) + """}
           }"""
        )

        geoteste = geoteste[:-1]
        geoteste = geoteste + """],
        "properties": {timestamp": """ + str(time.mktime(datetime.datetime.strptime(dateString,
"%d%b%Y %H %M %S").timetuple())) + "}"
        geoteste = geoteste +"""

           }"""

    sys.stdout = orig_stdout
    f.close()
    return geoteste

config = {
  "apiKey": "YOR_API_KEY",
  "authDomain": "YOUR_AUTHDOMAIN",
  "databaseURL": "YOUR_DATABASE_URL",
  "storageBucket": "YOUR_STORAGEBUCKET",
  "serviceAccount": "YOUR_SERVICEACCOUNT_JSON"
}
firebase = pyrebase.initialize_app(config)

window = Tk()

window.title('Flood Alert Data')

window.geometry('720x200')
style = ttk.Style()

tab_control = ttk.Notebook(window)

tab_areas = ttk.Frame(tab_control)

tab_markers = ttk.Frame(tab_control)

tab_forecast = ttk.Frame(tab_control)
```

```
tab_control.add(tab_areas, text='Areas')

tab_control.add(tab_markers, text='Markers')

tab_control.add(tab_forecast, text='Forecast')

lbl = Label(tab_areas, text="Select the flood surface raster:", justify=LEFT,font=("Arial Bold
", 24))

lbl.grid(column=0, row=0)

fileEntry = StringVar()

downsampling_factor = StringVar()
downsampling_factor.set('3')

#send the raster shape to firebase
def sendClicked(raster):
    if downsampling_factor.get() != '' and os.path.exists(os.path.dirname(raster.get())):
        db = firebase.database()

        resampled_filename = ''
        with rasterio.open(raster.get()) as src:
            print(src.crs)
            resampled_filename = downsampling( gdal.Open(raster.get()), np.array(src.read(1)), i
nt(downsampling_factor.get()) )

        geoteste = makePolyGeojson(resampled_filename)

        db.child("polygons").push(json.loads(geoteste))

        messagebox.showinfo('Success', 'Data sent to server!')
    elif downsampling_factor.get() == '':
        messagebox.showinfo('Error', 'Missing Downsampling Factor!')
    elif not os.path.exists(os.path.dirname(raster.get())):
        messagebox.showinfo('Error', 'Missing flood surface raster!')

fileDir = Entry(tab_areas,width=40, font=("Arial", 18), textvariable=fileEntry)
fileDir.grid(column=0, row=1)

lbl2 = Label(tab_areas, text="Downsampling Factor:", justify=LEFT,font=("Arial Bold", 24))
lbl2.grid(column=0, row=2)
factorBlock = Entry(tab_areas,width=10, font=("Arial", 18), textvariable=downsampling_fact
or)
factorBlock.grid(column=0, row=3)

def clickSelectFile(entry):
    direc = filedialog.askopenfilename(filetypes = [('Image Files', ['.tiff', '.tif'])])
    entry.set(direc)
```

```
def clickSelectImage(entry):
    direc = filedialog.askopenfilename(filetypes = [('Image Files', ['.png', '.jpg'])])
    entry.set(direc)

def clickSelectCSV(entry):
    direc = filedialog.askopenfilename(filetypes = [('Image Files', ['.csv'])])
    entry.set(direc)

lbl3 = Label(tab_markers, text="Create Marker", justify=CENTER,font=("Arial Bold", 24))
lbl3.grid(column=1, row=0)

#Upload the marker image to firebasestorage
def uploadToCloudStorage (path) :
    os.environ["GOOGLE_APPLICATION_CREDENTIALS"]="YOUR_APPLICATION_C
REDENTIALS"
    client = storage.Client()
    bucket = client.get_bucket('YOUR_FIREBASE_BUCKET')
    # posting to firebase storage
    imageBlob = bucket.blob("/")
    separatePath = path.split('/')
    name = separatePath[-1]
    imagePath = path
    imageBlob = bucket.blob(name)
    imageBlob.upload_from_filename(imagePath)

    return 'https://firebasestorage.googleapis.com/v0/b/'+'YOUR_APPLICATIONSTORAGE_
URL'+'/o/'+name+'?alt=media'

#Get a channel form and its limit from a CSV
def setArrayGraphFromCSV(path,marker):
    maioresElev = [0,0]
    menorElev = 9999
    i = 0
    array = []
    with open(path, mode='r') as infile:
        reader = csv.reader(infile)
        next(reader)
        for row in reader:
            array.append(row)
            if(float(row[1]) > maioresElev[i%2]):
                i+=1
                maioresElev[i%2] = float(row[1])

            if(float(row[1]) < menorElev):
                menorElev = float(row[1])

    if (maioresElev[0] > maioresElev[1]):
        marker["limit"] = maioresElev[0]
```

```
    else:
        marker["limit"] = maioresElev[1]
    marker["graphArray"] = array

#Send a marker info to firebase
def sendMarker (markerStrings):
    marker = {
        "coord" : {
            "lat": markerStrings["lat"].get(),
            "long": markerStrings["long"].get()
        },
        "description": markerStrings["description"].get(),
        "image": "",
        "limit": 0,
        "interval": 60,
        "graphArray": [],
        "depths": []
    }

    if marker["coord"]["lat"] != '' and marker["coord"]["long"] != ''\
    and marker["description"]!= '' and os.path.exists(os.path.dirname(markerStrings["csvDir"].
get()))\
    and os.path.exists(os.path.dirname(markerStrings["imgDir"].get())):

        marker['image'] = uploadToCloudStorage(markerStrings["imgDir"].get())
        print(marker['image'])
        setArrayGraphFromCSV(markerStrings["csvDir"].get(),marker)

        db = firebase.database()
        db.child("markers").push(marker)

        messagebox.showinfo('Success', 'Data sent to server!')
    else:
        messagebox.showinfo('Error', 'Please Fill All Variables')


for i in range(1) :
    marker = {
        "lat": StringVar(),
        "long": StringVar(),
        "csvDir": StringVar(),
        "description": StringVar(),
        "imgDir": StringVar()
    }
    lbl4 = Label(tab_markers, text="Lat:", justify=LEFT,font=("Arial Bold", 24))
    lbl4.grid(column=0, row=(i*2)+1)

    markerLatBlock = Entry(tab_markers,width=40, font=("Arial", 18), textvariable=marker["l
at"])
```

```
    markerLatBlock.grid(column=1, row=(i*2)+1)

    lbl5 = Label(tab_markers, text="Lng:", justify=LEFT,font=("Arial Bold", 24))
    lbl5.grid(column=0, row=(i*2)+2)

    markerLngBlock = Entry(tab_markers,width=40, font=("Arial", 18), textvariable=marker["
long"])
    markerLngBlock.grid(column=1, row=(i*2)+2)

    lbl6 = Label(tab_markers, text="CSV:", justify=LEFT,font=("Arial Bold", 24))
    lbl6.grid(column=0, row=(i*2)+3)

    markercsvBlock = Entry(tab_markers,width=40, font=("Arial", 18), textvariable=marker["c
svDir"])
    markercsvBlock.grid(column=1, row=(i*2)+3)
    btncsvSelect = Button(tab_markers, text="Choose File", bg="grey", fg="black", command
=partial(clickSelectCSV,marker["csvDir"]))
    btncsvSelect.grid(column=2, row=(i*2)+3)

    lbl7 = Label(tab_markers, text="Description:", justify=LEFT,font=("Arial Bold", 24))
    lbl7.grid(column=0, row=(i*2)+4)

    markerDescBlock = Entry(tab_markers,width=40, font=("Arial", 18), textvariable=marker[
"description"])
    markerDescBlock.grid(column=1, row=(i*2)+4)

    lbl8 = Label(tab_markers, text="Image:", justify=LEFT,font=("Arial Bold", 24))
    lbl8.grid(column=0, row=(i*2)+5)

    markerImgBlock = Entry(tab_markers,width=40, font=("Arial", 18), textvariable=marker["
imgDir"])
    markerImgBlock.grid(column=1, row=(i*2)+5)
    btnImgSelect = Button(tab_markers, text="Choose File", bg="grey", fg="black", command
=partial(clickSelectImage,marker["imgDir"]))
    btnImgSelect.grid(column=2, row=(i*2)+5)

    btnImgSelect = Button(tab_markers, text="Create", bg="grey", fg="black", command=parti
al(sendMarker,marker))
    btnImgSelect.grid(column=2, row=(i*2)+6)

def buildForecastTab():
    lbl = Label(tab_forecast,text="Select Destination Folder:", justify=LEFT,font=("Arial Bold
", 24))

    lbl.grid(column=0, row=0)

    folderEntry = StringVar()
    folderDir = Entry(tab_forecast,width=40, font=("Arial", 18), textvariable=folderEntry)
    folderDir.grid(column=0, row=1)
```

```
    btnSelect = Button(tab_forecast,text="Choose Folder", bg="honeydew3", fg="black", com
mand=partial(clickSelectFolder,folderEntry))

    btnSelect.grid(column=1, row=1)

    btn = Button(tab_forecast,text="Create", bg="DarkOliveGreen2", fg="black", command=p
artial(createForecastCSV, folderEntry))
    btn.grid(column=1, row=2)

buildForecastTab()

btnSelect = Button(tab_areas, text="Choose File", bg="grey", fg="black", command=partial(c
lickSelectFile,fileEntry))

btnSelect.grid(column=1, row=1)

btn = Button(tab_areas, text="Send to app", bg="grey", fg="black", command=partial(sendCli
cked,fileEntry))

btn.grid(column=1, row=7)

tab_control.pack(expand=1, fill='both')
window.mainloop()
```